

DISSERTATION

submitted to the
Combined Faculties for the Natural Sciences and for Mathematics
of the Ruperto-Carola University of Heidelberg, Germany
for the degree of
Doctor of Natural Sciences

Put forward by
[Valentin Kasper](#)

Born in: Pforzheim

Oral examination: 05.02.2016

Lattice Gauge Theory and Cold Atoms Out of Equilibrium

Referees: Prof. Dr. Jürgen Berges
Priv.-Doz. Dr. Jörg Evers

Within the framework of this thesis, the following articles were published in refereed journals or are available on pre-print servers:

- (i) V. Kasper, F. Hebenstreit, and J. Berges, [Phys. Rev. D 90, 025016 \(2014\)](#).
- (ii) V. Kasper, F. Hebenstreit, M. Oberthaler, and J. Berges, [arXiv:1506.01238, \(2015\)](#).
- (iii) T. Schweigler, V. Kasper, S. Erne, B. Rauer, T. Langen, T. Gasenzer, J. Berges, and J. Schmiedmayer, [arXiv:1505.03126, \(2015\)](#).

Gittereichtheorie und kalte Atome außerhalb des Gleichgewichts

Abstract

In dieser Arbeit untersuchen wir die Quantensimulation von Gittereichtheorien durch Experimente mit kalten Atomen. Wir machen einen expliziten Vorschlag für eine $(1+1)$ -dimensionale $U(1)$ Gittereichtheorie. Ausgehend von einem Gas, bestehend aus fermionischen und bosonischen Atomen, ändern wir die Geometrie und manipulieren die Wechselwirkungen so, dass wir ein eindimensionales System und lokale Eichinvarianz erhalten. Ein weiterer wichtiger Aspekt dieses Vorschlags ist das explizite Nutzen von hochbesetzten bosonischen Zuständen, um die Physik starker Felder in der Quantenelektrodynamik greifbar zu machen. Basierend auf dem Funktionalintegral, präsentieren wir eine Methode, um $U(1)$ und $SU(N)$ Eichfelder außerhalb des Gleichgewichts, welche mit Materiefeldern wechselwirken, theoretisch zu behandeln. Wir zeigen, dass unter bestimmten Voraussetzungen die Quantentheorie akkurat auf ein klassisches statistisches Ensemble abgebildet werden kann. Wir nutzen diese Möglichkeit, um die Aussichten zu evaluieren, Phänomene der Hochenergiephysik, wie Schwinger-Paarproduktion und Stringbreaking, in zukünftigen Experimenten mit kalten Atomen zu beobachten.

Lattice Gauge Theory and Cold Atoms Out of Equilibrium

Abstract

In this thesis we theoretically investigate the quantum simulation of lattice gauge theories for cold atom experiments. We give an explicit proposal to study a $(1+1)$ -dimensional $U(1)$ lattice gauge theory. Starting with a bosonic and a fermionic atomic gas we tune the geometry and engineer the interactions such that we end up with a one-dimensional system obeying the principle of local gauge invariance. A further important aspect of this proposal is the explicit use of highly occupied bosonic states in order to make the investigation of strong field quantum electrodynamics feasible. In addition, we present an approach based on the functional integral in order to theoretically treat $U(1)$ and $SU(N)$ gauge fields interacting with matter out of equilibrium. We show that under specific conditions the quantum theory can be accurately mapped onto a classical statistical ensemble. Further, exploiting this possibility, we study the prospect to observe intricate high energy phenomena like Schwinger pair-production and string breaking in such future cold atom experiments.

Contents

Abstract	ii
1 Introduction	1
2 Fundamentals of Lattice Gauge Theory	6
2.1 Abelian Gauge Theories	6
2.2 Non-Abelian Gauge Theories	11
2.3 Discretized Gauge Theories	13
2.4 Hamiltonian Formulation of QED	15
2.5 Abelian Quantum Link Models	19
3 Lattice Gauge Theories with Cold Atoms	21
3.1 The Schwinger Model	21
3.2 Experimental Realization	23
3.2.1 One-Dimensional Staggered Geometry	24
3.2.2 Angular Momentum Conservation	27
3.2.3 Bosonic Intra-species Interactions	30
3.2.4 Fermionic Intra-species Interaction Term	31
3.2.5 Inter-species Interaction Term	32
3.3 Cold-Atom QED Hamiltonian	36
3.4 Initial State and Gauss's Law	38
4 Lattice Gauge Theories Out of Equilibrium	41
4.1 Real-time Lattice Gauge Theory	41
4.1.1 U(1) Gauge Theory	47
4.1.2 SU(N) Gauge Theory	53
4.2 Diagrammatics	57
4.2.1 Classical and Quantum Vertices	57
4.2.2 Classality Condition	60
4.3 Real-time Simulation of Quantum Electrodynamics	62
4.3.1 Lattice Action	63
4.3.2 Equations of Motion	64
4.3.3 Numerical Algorithm	66
4.3.4 Initial Conditions	66

4.4	Fermion Production in Three Dimensions	68
4.4.1	Schwinger Mechanism	68
4.4.2	Back-reaction and Plasma Oscillations	71
5	Strong Field QED with Cold Atoms	75
5.1	Kogut-Susskind and the Cold Atoms	77
5.2	Classical-Statistical Approach with Cold Atoms	78
5.3	Pair Production with Cold Atoms	80
5.4	String Breaking	85
5.5	Correlation Functions of the Schwinger Model	90
6	Conclusion and Outlook	94
	Appendices	99
A	Overlap Integrals	99
B	Mode Functions for Fermions	103
C	Mode Functions for Gauge Fields	106
D	Fermionic Observables	110
E	Continuum Results for the Schwinger effect	113
	Bibliography	115
	Acknowledgements	123

Chapter 1

Introduction

Gauge theories belong to some of the most beautiful mathematical models describing nature. They emerge in strongly correlated systems in condensed matter physics [1] and they are central for the formulation of the dynamics of the Standard Model of particle physics [2]. The most prominent example of an Abelian gauge theory is the photon coupled to electrons and positrons in quantum electrodynamics [3–5].

On the theoretical side, lattice gauge theory provides a unified framework to construct the aforementioned theories on a discretized space. Moreover, in thermal equilibrium, these quantum theories can be mapped onto classical statistics problem. In the absence of a sign problem the statistical theory can then be efficiently simulated by Monte Carlo techniques [6]. However, despite the significant knowledge gained from lattice gauge theories in equilibrium, there remain fundamental open questions.

In particular the out-of-equilibrium dynamics of these quantum field theories are one of the most active research fields of contemporary theoretical and experimental physics [7, 8]. In fact, deep questions regarding non-equilibrium dynamics appear at various length scales ranging from the early universe dynamics and heavy ion collisions to cold-atom systems. Standard Monte Carlo techniques cannot resolve the difficult situation given by these generic non-equilibrium problems since they suffer from an inherent non-positive definite measure. Therefore, the study of the

real-time behavior of gauge fields interacting with matter remains particularly elusive, but is necessary to understand the thermalization process of these non-trivial theories [9].

This is not only a theoretical, but also an experimental challenge. In quantum electrodynamics the creation of particles from the vacuum in an external electric field has been investigated since the work of Sauter [10–12], but it has not yet been directly observed in an experiment. This non-perturbative quantum phenomenon is exponentially suppressed unless the field strength exceeds a critical size, which is given by an electric field $E \sim M^2/e \sim 10^{18} \text{V/m}$ for quantum electrodynamics (QED) with electron mass M and electric charge e . The new experimental laser facilities, like the Extreme Light Infrastructure (ELI) [13], will make a large step towards the observation of Schwinger pair-production, however, the direct observation stays a challenging subject.

Moreover, strong non-Abelian gauge fields are also able to produce particle anti-particle pairs. In particular during a nuclear collisions at high energy, color fields dominantly contribute to the dynamics of the Quark Gluon Plasma. The initial state is usually described by the Color Glass Condensate characterized by field strengths of the order $1/g$, where g is the running gauge coupling [14] of quantum chromodynamics. Since the coupling is small at these scales, the probability for quark pair production is expected to be enhanced. However, the experimental accessibility of heavy-ion collisions at the initial stages is highly difficult and a formidable task.

One possibility to overcome the theoretical and experimental obstacles is the usage of quantum simulators being tailor-made machines based on quantum mechanical principles. They can then be employed to solve very complex and hard problems [15]. Specifically, in order to address the challenges given by lattice gauge theories in condensed matter and elementary particle physics, cold-atom experiments provide the outstanding possibility to study these non-trivial theories relevant for vastly different scales. Atomic, molecular and optical physics deliver the suitable tools to

engineer Hamiltonians of these complex theories and make the realization of quantum simulators possible [16].

We illustrate the idea of quantum simulation by considering again the critical field strength $E_c = M^2/e$ of Schwinger-pair production. It is determined by the electron/positron mass M and the absolute value of the electric charge e . However, the pair production itself is controlled by the dimensionless ratio E/E_c for an applied electric field E . This implies that different physical systems with very different characteristic scales can be exploited to show the same phenomenons, when considering dimensionless quantities. Therefore, one has to transfer all the essential properties of the original theory, such as the dimensionality, the statistics of the particles, and the symmetries, to the cold-atom system.

In the case of lattice gauge theories the implementation of gauge invariance in the atomic setup is a very demanding task [17–19]. Nevertheless, once achieved this will deliver a new way to answer the fundamental questions in heavy-ion collision experiments or in strongly correlated materials.

The purpose of this thesis is twofold. In the first part we present an explicit theoretical proposal of a quantum simulator realizing a lattice gauge theory, whereas the second part investigates and discusses the theoretical treatment of Abelian and non-Abelian lattice gauge theories coupled to matter.

Concerning the implementation of lattice gauge theories in cold-atom systems many proposals choose quantum link models [20] as a starting point. Quantum links constitute a particular class of lattice gauge theories with local finite Hilbert spaces. Therefore, a realization with atomic systems is expected to be easier. However, the original lattice gauge theory of interest is Wilson’s lattice gauge theory using an infinite dimensional representation corresponding to quantum electrodynamics or quantum chromodynamics.

We will exploit this fact and aim to a realization of the infinite dimensional Hilbert space of quantum electrodynamics. The one-dimensional $U(1)$ gauge theory is special in the sense, that its structure is simpler in comparison to higher spatial dimensions. This facilitates the Hamiltonian tremendously. Hence, we will focus in the following on the conceptually important example of quantum electrodynamics in one spatial dimension [21, 22].

We consider as a starting point a cold-atom experiment providing us with an ultra-cold gas of bosonic and fermionic atoms. Finally, we have to manipulate this system such that the system is described by a lattice gauge theory. In cold-atom systems one is able to reduce the dimension of the system under consideration. Using a tight radial confinement and imposing an optical lattice one can already model a one dimensional discretized quantum field theory. In order to obtain a lattice gauge theory we further have to reduce and tune the interactions. Angular momentum conserving atomic scattering processes will play a crucial role in the construction. In the end, the engineered Hamiltonian will respect the $U(1)$ gauge invariance [23]. This deductive bottom-up approach allows us to make a direct connection between the original microscopic system and the parameters of the lattice gauge theory.

In order to ensure that the experiment virtually realizes a lattice gauge system, theoretical predictions building upon local gauge invariance are necessary. Therefore, this thesis investigates the real-time dynamics of $U(1)$ and $SU(N)$ gauge theories coupled to fermions on a lattice. Despite the fact that the full quantum problem is very difficult to solve [24], a large class of non-equilibrium problems can be approximated by a classical-statistical ensemble [25–29]. Choosing the functional integral as the starting point we derive the classical-statistical approximation and clarify the genuine quantum contributions [30–34].

This non-perturbative simulation method is applied to study the non-equilibrium dynamics of Schwinger pair production and string breaking. In particular, we will clarify the difference between Wilson’s formulation

of lattice gauge theories and the corresponding quantum link models. We will study the dynamics of these models in a yet unexplored parameter regime and give bounds for the dimensionality of the local Hilbert space in order to observe quantum electrodynamics [35, 36]. The aim of this thesis is to contribute to a deeper understanding of the non-equilibrium dynamics of lattice gauge theories from an experimental and a theoretical perspective.

Chapter 2

Fundamentals of Lattice Gauge Theory

In this chapter, we give a brief introduction to gauge theories and in particular to lattice gauge theories. We will formulate a gauge invariant action and the Hamiltonian of U(1) gauge theories. These two objects will be the starting point for the later chapters. The Hamiltonian is suited to study the quantum simulation of lattice gauge theories, whereas the action will reappear when we use the functional integral formulation. Further, we will introduce quantum link models and connect them to Wilson's formulation of lattice gauge theory. For later purposes we comment on non-Abelian gauge theories and their corresponding discretization. As far as theoretical calculations and arguments are concerned we use units with $\hbar = c = 1$. However, when modeling real systems, we will reintroduce \hbar and c .

2.1 Abelian Gauge Theories

We consider a complex valued matter field $\psi(t, \mathbf{x})$ at the space-time point (t, \mathbf{x}) and define a gauge transformation of the matter field as

$$\psi(t, \mathbf{x})' = V(t, \mathbf{x})\psi(t, \mathbf{x}), \quad (2.1)$$

where $V(t, \mathbf{x})$ is an element of the fundamental representation of $U(1)$, i.e. $V(t, \mathbf{x}) = e^{i\alpha(t, \mathbf{x})}$ with $\alpha(t, \mathbf{x})$ being a real number. Moreover, since we wish to study the propagation from one space-time point to another we compare $\psi(t_1, \mathbf{x}_1)$ and $\psi(t_2, \mathbf{x}_2)$. Therefore, we consider the difference $\psi(t_2, \mathbf{x}_2) - \psi(t_1, \mathbf{x}_1)$ as a measure for the change of the matter field. However, since we are able to gauge transform each space-time point separately, this quantity is not gauge invariant. In order to get a more sensible quantity comparing two space-time points, we introduce the parallel transporter $U(t_2, \mathbf{x}_2; t_1, \mathbf{x}_1)$. This object is an element of $U(1)$ connecting space-time point (t_1, \mathbf{x}_1) to space-time point (t_2, \mathbf{x}_2) . It has the following transformation property

$$U(t_2, \mathbf{x}_2; t_1, \mathbf{x}_1)' = V(t_2, \mathbf{x}_2)U(t_2, \mathbf{x}_2; t_1, \mathbf{x}_1)V^*(t_1, \mathbf{x}_1). \quad (2.2)$$

Now, we are able to compare the matter fields at two space-time points by moving the field ψ employing the parallel transporter from (t_1, \mathbf{x}_1) to (t_2, \mathbf{x}_2) . This leads to the difference

$$\psi(t_2, \mathbf{x}_2) - U(t_2, \mathbf{x}_2; t_1, \mathbf{x}_1)\psi(t_1, \mathbf{x}_1). \quad (2.3)$$

Performing a gauge transformation yields

$$\begin{aligned} & [\psi(t_2, \mathbf{x}_2) - U(t_2, \mathbf{x}_2; t_1, \mathbf{x}_1)\psi(t_1, \mathbf{x}_1)]' \\ &= V(t_2, \mathbf{x}_2) [\psi(t_2, \mathbf{x}_2) - U(t_2, \mathbf{x}_2; t_1, \mathbf{x}_1)\psi(t_1, \mathbf{x}_1)]. \end{aligned} \quad (2.4)$$

This quantity is now determined up to a single gauge transformation. By taking an infinitesimal distance, we can define the covariant derivatives in the time and space direction in the following manner:

$$D_t\psi(t, \mathbf{x}) \equiv \lim_{\varepsilon \rightarrow 0} \frac{1}{\varepsilon} [\psi(t + \varepsilon, \mathbf{x}) - U(t + \varepsilon, \mathbf{x}; t, \mathbf{x})\psi(t, \mathbf{x})], \quad (2.5)$$

$$\mathbf{n} \cdot \mathbf{D} \psi(t, \mathbf{x}) \equiv \lim_{\varepsilon \rightarrow 0} \frac{1}{\varepsilon} [\psi(t, \mathbf{x} + \varepsilon \mathbf{n}) - U(t, \mathbf{x} + \varepsilon \mathbf{n}; t, \mathbf{x})\psi(t, \mathbf{x})], \quad (2.6)$$

where \mathbf{n} is a unit vector in the spatial direction and we introduced the vector $\mathbf{D} = (D_1, D_2, D_3)$. By definition the covariant derivatives will

also transform like the difference in (2.4). Now, we consider the parallel transporter linking two infinitesimally separated space-time points. We will transport along the time direction and the spatial direction

$$U(t + \varepsilon, \mathbf{x}; t, \mathbf{x}) = 1 + ig\phi(t, \mathbf{x})\varepsilon + \dots, \quad (2.7)$$

$$U(t, \mathbf{x} + \varepsilon\mathbf{n}; t, \mathbf{x}) = 1 - ig\mathbf{n} \cdot \mathbf{A}(t, \mathbf{x})\varepsilon + \dots, \quad (2.8)$$

where we used $U(t, \mathbf{x}; t, \mathbf{x}) = 1$ and we introduced the gauge field four vector $(A_\mu) = (\phi, -\mathbf{A})$ with $\mu \in \{0, 1, 2, 3\}$. The gauge coupling is denoted by g . Repeating the infinitesimal transformation we get an expression for the parallel transporter

$$U(t_2, \mathbf{x}_2; t_1, \mathbf{x}_1) = \text{P exp} \left(ig \int_\gamma dx^\mu A_\mu \right), \quad (2.9)$$

where γ is the path connecting the points $x_1 = (t_1, \mathbf{x}_1)$ and $x_2 = (t_2, \mathbf{x}_2)$ and P denotes path-ordering. In the following, we will use the abbreviation $U(x_1; x_2) \equiv U(t_1, \mathbf{x}_1; t_2, \mathbf{x}_2)$. We further use (2.8) in order to express the covariant derivative in time and spatial direction as

$$D_t\psi(t, \mathbf{x}) = [\partial_t - ig\phi(t, \mathbf{x})] \psi(t, \mathbf{x}), \quad (2.10)$$

$$\mathbf{D}\psi(t, \mathbf{x}) = [\nabla + ig\mathbf{A}(t, \mathbf{x})] \psi(t, \mathbf{x}). \quad (2.11)$$

The transformation law for the parallel transporter in equation (2.2) determines also the transformation law of A_μ . Consider the gauge transformation $V(t, \mathbf{x}) = 1 + i\alpha(t, \mathbf{x}) + \dots$ and insert this into (2.2) for an infinitesimal parallel transporter (2.8). This results in

$$\phi(t, \mathbf{x})' = \phi(t, \mathbf{x}) + g^{-1}\partial_t\alpha(t, \mathbf{x}), \quad (2.12)$$

$$\mathbf{A}(t, \mathbf{x})' = \mathbf{A}(t, \mathbf{x}) - g^{-1}\nabla\alpha(t, \mathbf{x}). \quad (2.13)$$

Now, we couple the gauge field to matter. Therefore, we write down an action containing the covariant derivatives, which act on the complex field

$\psi(t, \mathbf{x})$. The final expression for the action is

$$S_M = \int dt \int d^3\mathbf{x} \left[\psi^* i D_t \psi - \frac{1}{2M} (\mathbf{D}\psi) \cdot (\mathbf{D}\psi) \right]. \quad (2.14)$$

Note that the first order time derivative renders this model non-relativistic invariant. The classical equation of motion is given by varying the action with respect to $\psi(t, \mathbf{x})$, i.e. $\frac{\delta S}{\delta \psi(t, \mathbf{x})} = 0$, leading to

$$i D_t \psi(t, \mathbf{x}) + \frac{1}{2M} \mathbf{D} \cdot \mathbf{D} \psi(t, \mathbf{x}) = 0. \quad (2.15)$$

This equation (2.15) only determines the dynamics of the matter $\psi(t, \mathbf{x})$, but the gauge field is external. In order to get a dynamical gauge field as well, one has to construct a gauge invariant object solely depending on A_μ . Therefore, we consider the commutator $[D_\mu, D_\nu] = D_\mu D_\nu - D_\nu D_\mu$ acting on the matter field $\psi(t, \mathbf{x})$, where we introduced the four vector notation of the covariant derivative $D_\mu = \partial_\mu - igA_\mu$. The commutator acting on the matter-field $\psi(x)$ leads to the expression

$$[D_\mu, D_\nu] \psi(x) = -ig F_{\mu\nu}(x) \psi(x), \quad (2.16)$$

where the field strength tensor is defined by

$$F_{\mu\nu}(x) \equiv \partial_\mu A_\nu(x) - \partial_\nu A_\mu(x). \quad (2.17)$$

We note that an infinitesimal Wilson loop [37] immediately leads to the above definition of $F_{\mu\nu}(x)$. In order to determine the transformation properties of $F_{\mu\nu}$ we consider an explicit gauge transformation

$$[D_\mu', D_\nu'] \psi(x)' = -ig F_{\mu\nu}(x)' \psi(x)' \quad (2.18)$$

and this leads to

$$V(x) [D_\mu, D_\nu] \psi(x) = -ig F_{\mu\nu}(x)' V(x) \psi(x). \quad (2.19)$$

From the last equation we conclude the transformation property of the field strength tensor

$$F_{\mu\nu}(x)' = V(x)F_{\mu\nu}(x)V^*(x) = F_{\mu\nu}(x). \quad (2.20)$$

This derivation of the transformation properties is cumbersome for the Abelian case, but becomes convenient for the non-Abelian case. In order to make the gauge field dynamical we consider the action

$$S_G = -\frac{1}{4} \int dt \int d^3\mathbf{x} F_{\mu\nu}F^{\mu\nu}. \quad (2.21)$$

By varying the action S_G with respect to the gauge field A_μ we get the equation of motion

$$\partial_\mu F^{\mu\nu} = 0. \quad (2.22)$$

This leads to classical electrodynamics given by the homogeneous Maxwell equations

$$\begin{aligned} \nabla \cdot \mathbf{E}(t, \mathbf{x}) &= 0, & \nabla \cdot \mathbf{B}(t, \mathbf{x}) &= 0, \\ \nabla \times \mathbf{E}(t, \mathbf{x}) + \partial_t \mathbf{B}(t, \mathbf{x}) &= 0, & \nabla \times \mathbf{B}(t, \mathbf{x}) &= \partial_t \mathbf{E}(t, \mathbf{x}), \end{aligned} \quad (2.23)$$

governing the dynamics of the electric field $\mathbf{E}(t, \mathbf{x})$ and the magnetic field $\mathbf{B}(t, \mathbf{x})$. The potentials are connected to the electric and magnetic field via

$$\mathbf{E}(t, \mathbf{x}) = -\nabla\phi(t, \mathbf{x}) + \partial_t \mathbf{A}(t, \mathbf{x}), \quad \mathbf{B}(t, \mathbf{x}) = \nabla \times \mathbf{A}(t, \mathbf{x}). \quad (2.24)$$

Then the total action is given by the sum of (2.14) and (2.21):

$$S = S_G + S_M, \quad (2.25)$$

describing a dynamical gauge field A_μ coupled to a matter field ψ .

2.2 Non-Abelian Gauge Theories

Since we will investigate SU(N) gauge fields in this thesis, we briefly introduce non-Abelian gauge theories. Using the parallel transporter we can generalize the notions of Abelian gauge theories in a straightforward way to the non-Abelian case. Therefore, we consider multiple matter fields ψ_m with $m = 1, \dots, N$. In equation (2.13) the matter field is locally transformed by a phase, whereas in a non-Abelian theory it is a local unitary transformation of the matter field

$$\psi_m(x)' = V_{mn}(x)\psi_n(x), \quad (2.26)$$

where $V_{mn}(x)$ is an unitary matrix and an element of the fundamental representation of SU(N). This means we can write $V(x) = \exp[i\alpha_a(x)t^a]$ with $a = 1, \dots, N^2 - 1$ and the t^a are the generators of SU(N) fulfilling the Lie-algebra

$$[t^a, t^b] = if^{abc}t^c. \quad (2.27)$$

The f^{abc} are the structure constants of SU(N) and we will use the standard normalization

$$\text{tr} [t^a, t^b] = \frac{1}{2} \delta_{ab}. \quad (2.28)$$

We will frequently call $a \in \{1, \dots, N^2 - 1\}$ the adjoint gauge index. We can immediately generalize the parallel transporter to the non-Abelian case by taking $U(x_2, x_1) \in \text{SU}(N)$. Then we introduce the non-Abelian parallel transporter as

$$U(x_2, x_1) = \text{P exp} \left(ig \int_{\gamma} dx^{\mu} A_{\mu} \right), \quad (2.29)$$

where A_{μ} is a linear combination of the generators $A_{\mu} = t^a A_{\mu}^a$. Comparing this to (2.9) shows the formulation in terms of parallel transporter

makes the generalization from Abelian to non-Abelian gauge groups immediate. The gauge transformation of the parallel transporter is by construction

$$U(x_2, x_1)' = V(x_2)U(x_2, x_1)V^\dagger(x_1), \quad (2.30)$$

where we suppressed the gauge indices. The same reasoning as in the Abelian case leads to the covariant derivative

$$(D_\mu \Psi)_m = \partial_\mu \Psi_m - igA_\mu^c(t^c)_{mn}\Psi_n, \quad (2.31)$$

where Ψ is a vector containing the fields ψ_m . Then the action of the matter field Ψ coupled to a non-Abelian gauge field is given by

$$S_M = \int dt \int d^3\mathbf{x} \left[\Psi^\dagger \cdot iD_t \Psi - \frac{1}{2M} (\mathbf{D}\Psi) \cdot (\mathbf{D}\Psi) \right]. \quad (2.32)$$

As before we can introduce a field strength tensor as

$$[D_\mu, D_\nu] = (-ig)F_{\mu\nu}. \quad (2.33)$$

Note this object can again be expanded in terms of the generators, i.e. $F_{\mu\nu} = F_{\mu\nu}^a t^a$. The components are given by

$$F_{\mu\nu}^a = \partial_\mu A_\nu^a - \partial_\nu A_\mu^a + gf^{abc} A_\mu^b A_\nu^c. \quad (2.34)$$

Thus the pure gauge part is determined by the following expression

$$S_G = -\frac{1}{2} \int dt \int d^3\mathbf{x} \text{Tr} F_{\mu\nu} F^{\mu\nu}, \quad (2.35)$$

where Tr is the trace with respect to the generators.

2.3 Discretized Gauge Theories

We will see that the formulation of an action in terms of parallel transporters makes the gauge invariant discretization on a space-time lattice straightforward. First, we will discuss the discretization of Abelian gauge theories and generalize the discussion later to the non-Abelian case. Consider a four dimensional space-time lattice with $x = (a_T n_0, a_S \mathbf{n})$ and $n = (n_0, \mathbf{n}) \in \mathbb{Z}^4$. The matter fields on the lattice are still complex numbers and are given by

$$\psi_n \equiv \psi(a_T n_0, a_S \mathbf{n}). \quad (2.36)$$

The transformation property of the matter field is still

$$\psi'_n = V_n \psi_n, \quad (2.37)$$

with V_n being an element of $U(1)$ and it has support on the space-time point n . The parallel transporter $U(x_2, x_1)$ linking the two space-time points on this lattice is separated by a lattice spacing in temporal direction (a_T) or in spatial direction (a_S) and it is given by

$$U_{\mu,n} \equiv U(x + \hat{\mu}; x), \quad (2.38)$$

where $\hat{\mu}$ is a unit vector in the μ direction

$$\hat{0} = a_T(1, \mathbf{0}), \quad (2.39)$$

$$\hat{i} = a_S(0, \mathbf{e}_i), \quad i \in \{1, 2, 3\}. \quad (2.40)$$

The object $U_{\mu,n}$ is frequently called the link variable. They are located between the lattice sites n and $n + \hat{\mu}$ and points in the direction of $\hat{\mu}$. The transformation properties are analog to the continuum

$$U'_{\mu,n} = V_{n+\mu} U_{\mu,n} V_n^*. \quad (2.41)$$

For link variables pointing in the direction of $-\hat{\mu}$, we use the definition

$$U_{-\mu,n} \equiv U_{\mu,n-\hat{\mu}}^\dagger. \quad (2.42)$$

Because of the transformation properties of the parallel transporter we can immediately write down a discretized gauge invariant action for an external gauge field coupled to matter

$$S_M = -t \sum_{n,\mu} [\psi_n^* U_{\mu,n} \psi_{n+\hat{\mu}} + \psi_{n+\hat{\mu}}^* U_{\mu,n}^* \psi_n] + M \sum_n \psi_n^* \psi_n, \quad (2.43)$$

where t determines the strength of the kinetic term and M is called the mass parameter [38]. In order to make the gauge field dynamical we construct a quantity which consists purely out of the links and forms a plaquette $n \rightarrow n + \hat{\mu} \rightarrow n + \hat{\nu} + \hat{\mu} \rightarrow n + \hat{\nu} \rightarrow n$ leading to

$$U_{\mu\nu,n} \equiv U_{\mu,n} U_{\nu,n+\hat{\mu}} U_{\mu,n+\hat{\nu}}^\dagger U_{\nu,n}^\dagger. \quad (2.44)$$

This is the discrete version of the smallest, aforementioned Wilson loop. We will call $U_{\mu\nu,n}$ the plaquette and frequently use the shorthand notation U_\square . In order to keep the notation simple we take the action to be Euclidean. It is then given by

$$S_G = \frac{1}{g^2} \sum_n \sum_{\mu < \nu} \text{Re}(1 - U_{\mu\nu,n}) \quad (2.45)$$

or using the short hand notation

$$S_G = \frac{1}{g^2} \sum_\square \left[1 - \frac{1}{2}(U_\square + U_\square^*) \right]. \quad (2.46)$$

The total action in Euclidean time is

$$S = S_G + S_M. \quad (2.47)$$

We will consider the discretization procedure involving non-Abelian gauge theories and we will focus on the important case of the $SU(N)$ gauge group,

but the discussion can be easily applied to other Lie groups. The matter fields on the lattice have to transform with respect to the following rule

$$\psi'_{a,n} = V_{n,ab} \psi_{n,b} . \quad (2.48)$$

For the SU(N) non-Abelian gauge group the link is given by

$$U_{\mu,n} = \exp(igaA_{\mu,n}) . \quad (2.49)$$

For simplicity we assume the same lattice spacing $a \equiv a_S = a_T$ in the spatial and temporal direction. The vector potential again can be expanded in terms of the generators of SU(N), i.e. $A_{\mu,n} = A_{\mu,n}^a t^a$, and we denoted the gauge coupling by g . Then the pure gauge part of this non-Abelian lattice gauge theory in Euclidean time is given by

$$S_G = \frac{2}{g^2} \sum_{\square} \text{Tr} \left[\mathbb{1} - \frac{1}{2}(U_{\square} + U_{\square}^{\dagger}) \right] , \quad (2.50)$$

where the sum is performed over all elementary plaquettes. The prefactors in S_G have been chosen such that the correct naive continuum limit is obtained when using the standard normalization of the generators t^a .

2.4 Hamiltonian Formulation of QED

In this section, we quantize electrodynamics coupled to fermionic matter on a lattice. In particular we will connect the previous discussion to the Hamiltonian formalism. We set the stage by writing down the Lagrangian density of quantum electrodynamics for continuous space-time:

$$\mathcal{L} = \bar{\psi}(i\gamma^{\mu}D_{\mu} - M)\psi - \frac{1}{4}F^{\mu\nu}F_{\mu\nu} . \quad (2.51)$$

The fermionic fields are given by $\psi(x)$ and $\bar{\psi}(x) = \psi^\dagger(x)\gamma^0$ where the γ 's are Dirac matrices and fulfill the Clifford algebra. Next, we have to determine the canonical variables and determine a gauge invariant Hamiltonian. Therefore, we briefly outline the quantization of the pure gauge part in the Hamiltonian formalism [39] and then generalize it to the lattice. We choose the temporal axial gauge $A_0 = 0$. Then the dynamical degrees of freedom are the spatial components A_i and the canonical momentum is given by the electric field

$$E_i \equiv \frac{\partial \mathcal{L}}{\partial(\partial_0 A_i)}. \quad (2.52)$$

The canonical commutator relation is

$$[A_i(t, \mathbf{x}), E_j(t, \mathbf{y})] = i\delta_{i,j}\delta(\mathbf{x} - \mathbf{y}). \quad (2.53)$$

On the lattice this commutator becomes

$$[A_{i,m}, E_{j,n}] = i\delta_{m,n}\delta_{i,j}. \quad (2.54)$$

Note that n and m are now defined on a spatial lattice meaning $n = (n_1, n_2, n_3)$ and $m = (m_1, m_2, m_3)$. The spatial link variable

$$U_{j,n} = \exp(iga_S A_{j,n}) \quad (2.55)$$

is determined by the gauge field $A_{j,n}$ with $j \in \{1, 2, 3\}$. Using the Baker-Campbell-Hausdorff identity [40] one gets the commutator relationships between the electric field and the link:

$$[E_{i,m}, U_{j,n}] = ga_S U_{i,m} \delta_{i,j} \delta_{m,n}, \quad (2.56)$$

$$[E_{i,m}, U_{j,n}^\dagger] = -ga_S U_{i,m}^\dagger \delta_{i,j} \delta_{m,n}. \quad (2.57)$$

In order to simplify the following discussion we absorb the factors ga_S in the gauge field A_μ . Then the commutators simplify to

$$[E_{i,m}, U_{j,n}] = U_{i,m} \delta_{i,j} \delta_{m,n}, \quad (2.58)$$

$$[E_{i,m}, U_{j,n}^\dagger] = -U_{i,m}^\dagger \delta_{i,j} \delta_{m,n}. \quad (2.59)$$

Since the matter fields live now on a spatial lattice, they are denoted by an operator ψ_n . Further, they fulfill canonical anti-commutator relationships

$$\{\psi_m, \psi_n^\dagger\} = \delta_{m,n}. \quad (2.60)$$

The operator representing a local gauge transformation at all space points is denoted by $V = \prod_n V_n$, where the V_n are all representations of $U(1)$. The matter fields and the parallel transporter have to transform like

$$V \psi_n V^\dagger = \Omega_n \psi_n, \quad (2.61)$$

$$V \psi_n^\dagger V^\dagger = \psi_n^\dagger \Omega_n^*, \quad (2.62)$$

$$V U_{n,i} V^\dagger = \Omega_n U_{n,i} \Omega_{n+\hat{i}}^*, \quad (2.63)$$

where the $\Omega_n = e^{i\alpha_n}$ are elements of the fundamental representation of $U(1)$. Since the Hamiltonian should be gauge invariant, we demand

$$V H V^\dagger = H. \quad (2.64)$$

Further the operator V can be written as

$$V = \prod_n \exp(i\alpha_n G_n), \quad (2.65)$$

where α_n is the local phase and G_n is the generator of the transformation. If one considers an infinitesimal gauge transformation at one lattice site n , i.e. $V = 1 + i\alpha_n G_n + \dots$, we will obtain the following relation

$$[H, G_n] = 0 \quad (2.66)$$

from (2.64). An explicit form of the Gauss's law operator is given by:

$$G_n = \sum_i (E_{i,n} - E_{-i,n}) - \rho_n, \quad (2.67)$$

where we introduced the charge density as

$$\rho_n = \psi_n^\dagger \psi_n \quad (2.68)$$

and the abbreviation

$$E_{-i,n} \equiv E_{i,n-\hat{i}}. \quad (2.69)$$

Note that one can always add a constant to the charge density without changing the transformation properties, see chapter 3 for a detailed discussion. We can write down a gauge invariant Hamiltonian [41] for quantum electrodynamics

$$\begin{aligned} H = & -t \sum_{i,n} s_{i,n} (\psi_n^\dagger U_{i,n} \psi_{n+\hat{i}} + \psi_{n+\hat{i}}^\dagger U_{i,n}^\dagger \psi_n) \\ & + M \sum_n s_n \psi_n^\dagger \psi_n + \frac{g^2}{2} \sum_{i,n} E_{i,n}^2 - \frac{1}{4g^2} \sum_{\square} (U_{\square} + U_{\square}^\dagger), \end{aligned} \quad (2.70)$$

where we introduced the sign factors $s_{1,n} = 1$, $s_{2,n} = (-1)^{n_1}$ and $s_{3,n} = (-1)^{n_1+n_2}$ and $s_n = (-1)^{n_1+n_2+n_3}$. We remark that the summation is with respect to all spatial plaquettes. This is the Kogut-Susskind Hamiltonian employing the staggered fermion discretization of quantum electrodynamics in temporal axial gauge [22]. We define the physical part of the Hilbert space via

$$V_n |\text{phys}\rangle = |\text{phys}\rangle \quad (2.71)$$

or using an infinitesimal transformation we get

$$G_n |\text{phys}\rangle = 0. \quad (2.72)$$

All the other states which do not fulfill this relation are gauge variant.

2.5 Abelian Quantum Link Models

Quantum link models [20] are another way to implement local gauge invariance on the lattice using a finite dimensional local Hilbert space. In order to make contact with Abelian quantum link model we remind ourselves of the $SU(2)$ algebra [42] of angular momentum operators

$$[L_i, L_j] = i\varepsilon_{ijk}L_k \quad (2.73)$$

with $i, j, k \in \{1, 2, 3\}$. Introducing raising and lowering operators we get

$$L_+ = L_x + iL_y, \quad L_- = L_x - iL_y. \quad (2.74)$$

The raising and lowering operators obey the following algebra

$$[L_z, L_+] = L_+, \quad (2.75)$$

$$[L_z, L_-] = -L_-. \quad (2.76)$$

A direct comparison of these commutators with the commutators of link and field (2.56) and (2.57) motivate the following substitution rule

$$U_{i,n} \rightarrow L_{+,i,n}, \quad (2.77)$$

$$U_{i,n}^\dagger \rightarrow L_{-,i,n}, \quad (2.78)$$

$$E_{i,n} \rightarrow L_{z,i,n}. \quad (2.79)$$

Note that the spins now live also on the links denoted by the lattice point n and the direction i . The new Hamiltonian is then given by

$$\begin{aligned} H = & -t \sum_{i,n} s_{i,n} (\psi_n^\dagger L_{+,i,n} \psi_{n+\hat{i}} + \psi_{n+\hat{i}}^\dagger L_{-,i,n} \psi_n) \\ & + M \sum_n s_n \psi_n^\dagger \psi_n + \frac{g^2}{2} \sum_{i,m} L_{z,i,m}^2 - \frac{1}{4g^2} \sum_{\square} (L_{\square} + L_{\square}^\dagger), \quad (2.80) \end{aligned}$$

where we introduced the plaquette term as

$$L_{ij,n} \equiv L_{+,i,n+\hat{i}} L_{+,j,n+\hat{i}+\hat{j}} L_{+,i,n+\hat{j}}^\dagger L_{+,j,n}^\dagger \quad (2.81)$$

and its abbreviation L_\square . The Gauss's law operator is now

$$G_n = \sum_i (L_{z,i,n} - L_{z,-i,n}) - \rho_n, \quad (2.82)$$

where the density is $\rho_n = \psi_n^\dagger \psi_n$ and we introduced

$$L_{z,-i,n} \equiv L_{z,i,n-\hat{i}}. \quad (2.83)$$

Note that G_n commutes again with H given in (2.80). We define the physical part of the Hilbert space via

$$G_n |\text{phys}\rangle = 0. \quad (2.84)$$

The main difference between the Abelian lattice gauge theory in section 2.4 and the quantum link models is the dimensionality of the Hilbert space. Note that the algebra

$$[U_{i,m}, U_{j,n}] = 0, \quad (2.85)$$

$$[E_{i,m}, U_{j,n}] = \delta_{m,n} \delta_{i,j} U_{i,m} \quad (2.86)$$

has only a representation on a infinite dimensional Hilbert space. On the other hand the canonical commutator relations of the angular momentum imply that the underlying Hilbert-space is finite dimensional. The dimension is given by $2\ell + 1$ with ℓ being the set consisting of positive half- and integer numbers: $\ell = 0, \frac{1}{2}, 1, \frac{3}{2}, \dots$. Formally one can recover the Hamiltonian (2.70) from the Hamiltonian (2.80) by sending ℓ to infinity and a proper rescaling of the coupling constants.

Chapter 3

Lattice Gauge Theories with Cold Atoms

In this chapter, we give an explicit proposal for an experiment realizing a $U(1)$ gauge theory coupled to fermionic matter in $(1 + 1)$ dimensions. The starting point is a gas of fermionic and bosonic atoms. By using optical potentials we reduce the system from three spatial dimensions to one spatial dimension. Further, we introduce another optical potential to engrave a lattice structure in the remaining longitudinal direction. Next, we will distribute the fermions such that we get a staggered fermion structure. We will investigate angular momentum conserving scattering processes and by choosing an appropriate external magnetic field we select particular interaction terms. This selection in combination with the localized nature of the bosons and fermions leads to a gauge invariant model system. Note that we will emphasize the experimental perspective in this section.

3.1 The Schwinger Model

Numerical studies of $(1 + 1)$ -dimensional QED, the massive Schwinger model, are typically based on a lattice discretization of the continuum model. We employ the staggered fermion discretization introduced in chapter 2 according to which the Dirac spinor is decomposed in such a

way that particle and antiparticle components reside on neighboring lattice sites. The Hamiltonian [21, 22] of the theory is given by

$$H_{\text{KS}} = \frac{a_S}{2} \sum_n E_n^2 + M \sum_n (-1)^n \psi_n^\dagger \psi_n - \frac{i}{2a_S} \sum_n (\psi_n^\dagger U_n \psi_{n+1} - h.c.) , \quad (3.1)$$

where a_S denotes the lattice spacing and M the fermion mass. Here, the staggered fermion field operator ψ_n , which resides on lattice sites n , fulfills the canonical anti-commutation relation $\{\psi_n, \psi_m^\dagger\} = \delta_{n,m}$. The link operator U_n and electric field operator E_n act between neighboring lattice sites n and $n + 1$ and obey the commutation relations

$$[U_n, U_m^\dagger] = 0 , \quad (3.2a)$$

$$[E_n, U_m] = ga_S \delta_{n,m} U_m , \quad (3.2b)$$

where g denotes the gauge coupling. We emphasize again that this algebra necessarily entails an infinite dimensional local Hilbert space. Being a U(1) gauge theory, the Gauss's law operator $G_n = E_n - E_{n-1} - \rho_n$ generates local gauge transformations and commutes with the Hamiltonian $[H_{\text{KS}}, G_n] = 0$, see section 3.4 for details.

Recently, the prospect of constructing quantum simulators for gauge theories has boosted the interest in these models as their implementation in atomic systems is supposed to be possible [19]. We perform the substitution for E_n and U_n , i.e. $E_n \rightarrow gL_{z,n}$ and the link operators are determined by $U_n \rightarrow [\ell(\ell + 1)]^{-1/2} L_{+,n}$ and $U_n^\dagger \rightarrow [\ell(\ell + 1)]^{-1/2} L_{-,n}$. The raising and lowering operator are $L_{\pm,n} = L_{x,n} \pm iL_{y,n}$ and ℓ denotes the spin size.

This leads to a quantum link model, which is still gauge invariant

$$H_{\text{QL}} = \frac{g^2 a_S}{2} \sum_n L_{z,n}^2 + M \sum_n (-1)^n \psi_n^\dagger \psi_n - \frac{i}{2a_S \sqrt{\ell(\ell+1)}} \sum_n (\psi_n^\dagger L_{n,+} \psi_{n+1} - h.c.) . \quad (3.3)$$

It is this one-dimensional Hamiltonian which has become an active playground [43]. As already mentioned, the finite dimensional representation of the angular momentum algebra makes its implementation in systems of ultra-cold atoms feasible.

3.2 Experimental Realization

Our starting point for the realization of the U(1) gauge theory coupled to fermionic matter in a cold atom experiment is a genuine interacting gas of fermionic and bosonic atoms [44]. The bosons $\phi_\alpha(\mathbf{x})$ and fermions $\psi_\alpha(\mathbf{x})$ fulfill the canonical commutator and anti-commutator relations, respectively

$$[\phi_\alpha(\mathbf{x}_1), \phi_\beta^\dagger(\mathbf{x}_2)] = \delta_{\alpha,\beta} \delta(\mathbf{x}_1 - \mathbf{x}_2) , \quad (3.4a)$$

$$\{\psi_\alpha(\mathbf{x}_1), \psi_\beta^\dagger(\mathbf{x}_2)\} = \delta_{\alpha,\beta} \delta(\mathbf{x}_1 - \mathbf{x}_2) . \quad (3.4b)$$

Here, the Greek labels denote magnetic hyperfine states of the atoms. The particles are confined by external potentials and interact via inter- and intra-species scattering processes. The corresponding Hamiltonian consists of three parts: $H = H_T + H_V + H_I$. The kinetic part describes the movement of the atoms

$$H_T = \frac{\hbar^2}{2M_b} \int d^3\mathbf{x} \sum_\alpha |\nabla \phi_\alpha(\mathbf{x})|^2 + \frac{\hbar^2}{2M_f} \int d^3\mathbf{x} \sum_\alpha |\nabla \psi_\alpha(\mathbf{x})|^2 , \quad (3.5)$$

where M_b is the mass of the bosonic atoms and M_f is the mass of the fermionic atoms. The potential energy contribution is determined by the external potentials

$$H_V = \int d^3\mathbf{x} \sum_{\alpha} V_{\alpha}^b(\mathbf{x}) \phi_{\alpha}^{\dagger}(\mathbf{x}) \phi_{\alpha}(\mathbf{x}) + \int d^3\mathbf{x} \sum_{\alpha} V_{\alpha}^f(\mathbf{x}) \psi_{\alpha}^{\dagger}(\mathbf{x}) \psi_{\alpha}(\mathbf{x}), \quad (3.6)$$

whereas the atomic scattering processes [45] are described by

$$H_I = \int d^3\mathbf{x} \sum_{\alpha\beta\gamma\delta} \frac{g_{\alpha\beta\gamma\delta}^b}{2} \phi_{\alpha}^{\dagger}(\mathbf{x}) \phi_{\beta}^{\dagger}(\mathbf{x}) \phi_{\delta}(\mathbf{x}) \phi_{\gamma}(\mathbf{x}) + \int d^3\mathbf{x} \sum_{\alpha\beta\gamma\delta} \frac{g_{\alpha\beta\gamma\delta}^f}{2} \psi_{\alpha}^{\dagger}(\mathbf{x}) \psi_{\beta}^{\dagger}(\mathbf{x}) \psi_{\delta}(\mathbf{x}) \psi_{\gamma}(\mathbf{x}) + \int d^3\mathbf{x} \sum_{\alpha\beta\gamma\delta} \frac{g_{\alpha\beta\gamma\delta}^{bf}}{2} \psi_{\alpha}^{\dagger}(\mathbf{x}) \phi_{\beta}^{\dagger}(\mathbf{x}) \phi_{\delta}(\mathbf{x}) \psi_{\gamma}(\mathbf{x}). \quad (3.7)$$

The coupling constants are determined by the scattering lengths of the inter- and intra-species scattering processes. Throughout this work, we use indices to denote purely bosonic terms by b , fermionic terms by f and boson-fermion interactions by bf .

3.2.1 One-Dimensional Staggered Geometry

The basic ingredient for realizing a one-dimensional (1D) lattice structure with lattice constant a is an optical lattice with tight radial confinement. Employing a laser frequency which is blue detuned for fermions and red detuned for bosons allows for positioning a mesoscopic bosonic gas on the links between the fermionic lattice sites, cf. Fig. 3.1a. In fact, the potential energy contributions (3.6) can be split into an axial and radial part

$$V_{\alpha}^s(\mathbf{x}) = V_{\parallel\alpha}^s(x) + V_{\perp\alpha}^s(r), \quad (3.8)$$

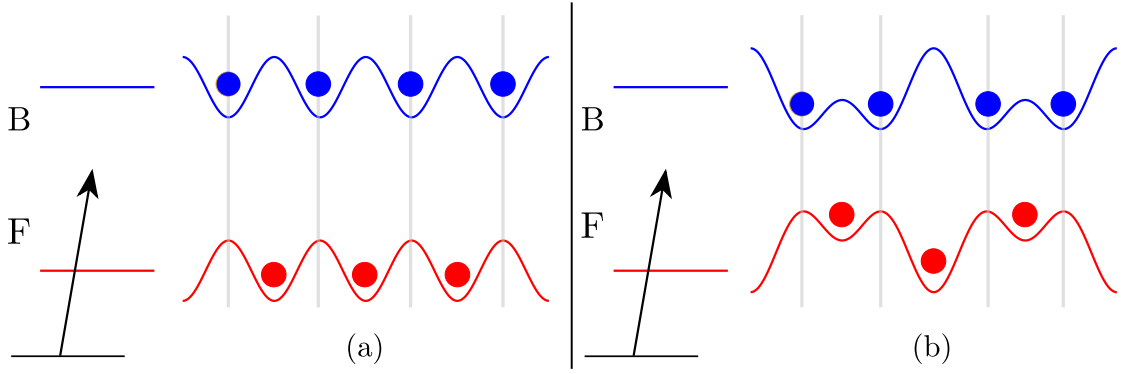


FIGURE 3.1: Realization of the staggered lattice structure. The black arrow indicates the off-resonant laser. (a) Blue/red detuning for fermions/bosons generates phase-shifted optical potentials for bosons and fermions with a lattice period a . (b) The superposition of the lattice with period a by a super-lattice of period $2a$ generates the staggered structure for the fermions.

with $s \in \{b, f\}$ and $r = \sqrt{y^2 + z^2}$. Choosing a sufficient tight radial confinement effectively renders the three-dimensional system to a one-dimensional one. We denote the dimensionally reduced operators as

$$\phi_\alpha(\mathbf{x}) = \varphi_b(y)\varphi_b(z)\phi_\alpha(x), \quad (3.9a)$$

$$\psi_\alpha(\mathbf{x}) = \varphi_f(y)\varphi_f(z)\psi_\alpha(x), \quad (3.9b)$$

where $\varphi_s(y)$, $\varphi_s(z)$ denote the ground state wave functions in the y and z directions, respectively. We assume that these states are independent of the magnetic quantum number.

To generate a staggered structure for the fermions, the original optical lattice with period a needs to be superimposed by an optical super-lattice with period $2a$, cf. Fig. 3.1b. Disregarding the effect of an overall confinement in the longitudinal direction, the axial part of the potential is then given by

$$V_{\parallel\alpha}^s(x) = V_{1,\alpha}^s \cos^2(kx) + V_{2,\alpha}^s \sin^2(2kx), \quad (3.10)$$

where we introduced $k = \pi/a$. The values of the amplitudes $V_{i,\alpha}^s$ and $i = \{1, 2\}$, are determined by the ac-Stark shift of the corresponding magnetic substates α . As already noted in [23], such a construction is spin-independent and clearly distinct from the spin dependent proposal in [43].

We note that the potential barrier between adjacent bosons is decreased by generating the staggered structure for the fermions. An appropriate choice of the amplitudes of the lasers building the super-lattice leads to a double-well structure, which inhibits tunneling of bosons between neighboring sites [46].

In the following, it is useful to switch to a representation in terms of localized Wannier functions. To this end, we first consider the bosonic degrees of freedom. By tuning of the laser amplitude we may choose $V_{i,\alpha}^b$ such that we obtain two Wannier functions which are sufficiently localized in the left or right minimum of the elementary cell. The corresponding expansion of the bosonic field operator reads

$$\phi_\alpha(x) = \sum_{n,p} w_{\alpha,np}^b(x) \phi_{\alpha,np}, \quad (3.11)$$

where n labels the elementary cells and $p = \{L, R\}$ denotes the left-right minimum in the elementary cell, respectively. We comment on the Wannier functions in Appendix A. The determination of $V_{i,\alpha}^b$ also fixes the fermionic contributions $V_{i,\alpha}^f$. In analogy to the bosons, we may select Wannier functions localized in the two minima of the elementary cell. We expand the fermionic field operators like the bosonic field operators leading to $\psi_\alpha(x) = \sum_{n,p} w_{\alpha,np}^f(x) \psi_{\alpha,np}$. Moreover, the structure of the super-lattice suggests the definition

$$\psi_{2n,\alpha} \equiv \psi_{\alpha,nL}, \quad \psi_{2n+1,\alpha} \equiv \psi_{\alpha,nR}, \quad (3.12a)$$

$$\phi_{2n,\alpha} \equiv \phi_{\alpha,nL}, \quad \phi_{2n+1,\alpha} \equiv \phi_{\alpha,nR}, \quad (3.12b)$$

with n numbering the elementary cells in the optical lattice. We note that the kinetic energy contributions (3.5) vanish, due to the fact that the Wannier functions corresponding to the different minima in the optical lattice do not have sizable overlap.

3.2.2 Angular Momentum Conservation

In the previous section, we showed how the potential energy (3.6) can be used to generate the staggered lattice structure. Moreover, we have seen that the kinetic energy (3.5) vanishes due to the localization of the Wannier functions at the potential minima. To finally generate dynamics in the cold atom system, which mimics the Schwinger model, we have to tune the interaction Hamiltonian (3.7), such that effectively only the desired gauge invariant terms survive. To this end, we have to investigate the interaction terms in more detail and establish the connection between the various scattering lengths and coupling constants $g_{\alpha\beta\gamma\delta}^r$ with $r = \{b, f, bf\}$. First, we discuss the construction in free space and take into account the lattice later.

We suppose that the inter-species interactions of bosons and fermions as well as the intra-species interactions between bosons and fermions are local and conserve angular momentum. Specifically, we consider bosons with spin $f_b = 1$ and fermions with spin $f_f = 1/2$. Therefore, the two-particle potentials are given by

$$V^r(\mathbf{x}_1, \mathbf{x}_2) = \delta(\mathbf{x}_1 - \mathbf{x}_2) \sum_{\mathcal{F}_r} g_{r, \mathcal{F}_r} \mathbf{P}_{f_1, f_2, \mathcal{F}_r}, \quad (3.13)$$

where the total spin can take the values $\mathcal{F}_b \in \{0, 2\}$, $\mathcal{F}_f \in \{0, 1\}$ and $\mathcal{F}_{bf} \in \{1/2, 3/2\}$. The interaction strengths are related to the s-wave scattering lengths via

$$g_{r, \mathcal{F}_r} = \frac{4\pi\hbar^2 a_{r, \mathcal{F}_r}}{M_r}, \quad (3.14)$$

where M_r denotes the reduced mass. Note that $\mathcal{F}_b = 1$ is not possible due to Bose symmetry [45]. In general, the projector $\mathbf{P}_{f_1, f_2, \mathcal{F}}$ for two particles with individual spins f_1 and f_2 onto the subspace with total spin \mathcal{F} can

be written as

$$\mathbf{P}_{f_1, f_2, \mathcal{F}} = \sum_M |f_1, f_2; \mathcal{F}, M\rangle \langle f_1, f_2; \mathcal{F}, M|, \quad (3.15)$$

where $M = \{-\mathcal{F}, -\mathcal{F} + 1, \dots, \mathcal{F} - 1, \mathcal{F}\}$ are the possible magnetic quantum numbers. Writing the interaction potential in second quantized form, we may relate the interaction constants according to

$$\begin{aligned} g_{\alpha\beta\gamma\delta}^r &= \sum_{\mathcal{F}_r} \sum_M g_{r, \mathcal{F}_r} \langle f_1; \alpha; f_2; \beta | f_1, f_2; \mathcal{F}_r, M \rangle \\ &\times \langle f_1, f_2; \mathcal{F}_r, M | f_1; \gamma; f_2; \delta \rangle. \end{aligned} \quad (3.16)$$

Here, $\langle f_1; \alpha; f_2; \beta | f_1, f_2; \mathcal{F}_r, M \rangle$ are the Clebsch-Gordan coefficients for coupling the individual spins f_1 and f_2 to the total spin \mathcal{F}_r . Specifically, we have $f_1 = f_2 = 1$ for boson-boson interactions ($r = b$), $f_1 = f_2 = 1/2$ for fermion-fermion interaction ($r = f$) and $f_1 = 1/2, f_2 = 1$ for the boson-fermion interaction ($r = bf$).

As in the previous section, we again reduce the three-dimensional system to one spatial dimension and expand the field operators in terms of Wannier functions. Using a compact notation, where $\mathbf{n} = (n_1, n_2, n_3, n_4)$ denotes the site indices and $\boldsymbol{\mu} = (\alpha, \beta, \gamma, \delta)$ the magnetic quantum numbers, we have

$$\begin{aligned} H_I &= \frac{1}{2} \sum_{\mathbf{n}, \boldsymbol{\mu}} U_{\mathbf{n}}^b g_{\boldsymbol{\mu}}^b \phi_{n_1\alpha}^\dagger \phi_{n_2\beta}^\dagger \phi_{n_4\delta} \phi_{n_3\gamma} \\ &+ \frac{1}{2} \sum_{\mathbf{n}, \boldsymbol{\mu}} U_{\mathbf{n}}^f g_{\boldsymbol{\mu}}^f \psi_{n_1\alpha}^\dagger \psi_{n_2\beta}^\dagger \psi_{n_4\delta} \psi_{n_3\gamma} \\ &+ \frac{1}{2} \sum_{\mathbf{n}, \boldsymbol{\mu}} U_{\mathbf{n}}^{bf} g_{\boldsymbol{\mu}}^{bf} \psi_{n_1\alpha}^\dagger \phi_{n_2\beta}^\dagger \phi_{n_4\delta} \psi_{n_3\gamma}. \end{aligned} \quad (3.17)$$

The coupling constants $U_{\mathbf{n}}^r$ are determined by the dimensional reduction and the overlap integrals of Wannier functions, see Appendix A. Note we also assumed that all functions used to determine $U_{\mathbf{n}}^r$ are $\boldsymbol{\mu}$ independent.

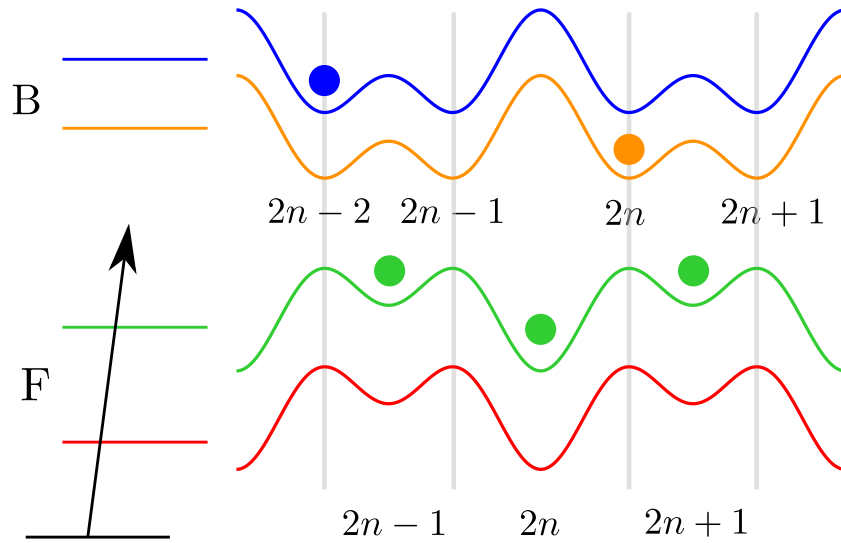


FIGURE 3.2: The application of a B -field splits the super-lattice for the individual magnetic substates of the bosons and fermions.

Based on this interaction Hamiltonian, we see that a plethora of possible interaction terms are generated. In order to realize the Hamiltonian (3.3), however, we have to guarantee that only a small number of terms contributes. To this end, we use the fact that an appropriate B -field and external dressing [47] allows for a selection of a smaller number of interaction terms whereas all other contributions are suppressed. We emphasize that this selection is achieved by the unequal shift of the bosonic and fermionic energy levels, as depicted in Fig. 3.2. Most notably, this procedure results in the bosonic spin exchange with a simultaneous fermion hopping (cf. Fig. 3.3) which corresponds to the gauge invariant interaction term in (3.3). We note that this selection process does not exclude elastic scattering terms, i.e. scattering processes without changing the individual spins of the atoms.

Finally, we assume that all bosonic states are prepared in the $\alpha_b \in \{-1, 0\}$ sectors whereas the fermionic degrees of freedom are generated in the staggered configuration with $\alpha_f = 1/2$ on even sites and $\alpha_f = -1/2$ on odd sites. As a consequence, interactions including the $\alpha_b = 1$ sector, which would be allowed in principle, are suppressed during the whole time evolution. We further elaborate on this issue in the following sections.

3.2.3 Bosonic Intra-species Interactions

In this section, we discuss the intra-species interaction terms of bosons in more detail. Owing to localization, only on-site interaction terms of bosons contribute, i.e. $U_{\mathbf{n}}^b \neq 0$ only, if all values n_i in \mathbf{n} are the same. Accordingly, the bosonic interaction term is given by

$$H_I^b = \frac{1}{2} \sum_{\mathbf{n}, \mu} U_{\mathbf{n}}^b g_{\mu}^b \phi_{n\alpha}^{\dagger} \phi_{n\beta}^{\dagger} \phi_{n\beta} \phi_{n\alpha}, \quad (3.18)$$

with $\mathbf{n} = (n, n, n, n)$ and $\alpha_b, \beta_b \in \{-1, 0\}$. Again, we note that we disregard terms containing the magnetic substates $\alpha_b = 1$ which are excluded by the spin conservation if initialized accordingly. Denoting the bosonic degrees of freedom according to $b_n \equiv \phi_{n,0}$ and $d_n \equiv \phi_{n,-1}$, the interaction term (3.18) is written as

$$H_I^b = \frac{1}{2} \sum_n (g_b b_n^{\dagger} b_n^{\dagger} b_n b_n + g_d d_n^{\dagger} d_n^{\dagger} d_n d_n + g_{bd} b_n^{\dagger} d_n^{\dagger} d_n b_n), \quad (3.19)$$

where the coupling constants result from (3.16) and are

$$g_b = U_{\mathbf{n}}^b \left(\frac{g_{b,0}}{3} + \frac{2g_{b,2}}{3} \right), \quad (3.20a)$$

$$g_d = U_{\mathbf{n}}^b g_{b,2}, \quad (3.20b)$$

$$g_{bd} = 2U_{\mathbf{n}}^b g_{b,2}. \quad (3.20c)$$

In addition, we assumed that the overlap integrals $U_{\mathbf{n}}^b$ are the same in all terms. In fact, the bosons b_n and d_n can be understood as Schwinger bosons

$$L_{+,n} = b_n^{\dagger} d_n, \quad L_{-,n} = d_n^{\dagger} b_n, \quad (3.21a)$$

$$L_{z,n} = \frac{1}{2}(b_n^{\dagger} b_n - d_n^{\dagger} d_n), \quad (3.21b)$$

which constitute a representation [48] of the angular momentum algebra

$$[L_{i,n}, L_{j,m}] = i\delta_{n,m} \epsilon_{ijk} L_{k,n} \quad (3.22)$$

with $L_{\pm,n} = L_{x,n} \pm iL_{y,n}$. As the hopping of bosons between neighboring sites $n \rightarrow n \pm 1$ is suppressed, the constraint $2\ell = b_n^\dagger b_n + d_n^\dagger d_n$ is exactly fulfilled. For later convenience, we introduce

$$\frac{g^2 a_S}{2} \equiv \frac{1}{2}(g_b + g_d - g_{bd}), \quad (3.23a)$$

$$\Delta_{b,0} \equiv \frac{1}{2}(2\ell - 1)(g_b - g_d) \quad (3.23b)$$

and further relabel the bosonic degrees of freedom to distinguish between even and odd sites. For even sites we employ the same definition as above, $b_{2n} \equiv \phi_{2n,0}$ and $d_{2n} \equiv \phi_{2n,-1}$, whereas we interchange their roles on odd sites, i.e. $b_{2n+1} \equiv \phi_{2n+1,-1}$ and $d_{2n+1} \equiv \phi_{2n+1,0}$. Accordingly, on even sites we still have (3.21) whereas on odd sites the role of the raising and lowering operators are interchanged and the z -component of the angular momentum changes sign. Using this convention, the bosonic intra-species interaction Hamiltonian is given by

$$H_I^b = \frac{g^2 a_S}{2} \sum_n L_{z,n}^2 + \Delta_{b,0} \sum_n (-1)^n L_{z,n}, \quad (3.24)$$

where we disregarded an irrelevant constant which only depends on ℓ .

3.2.4 Fermionic Intra-species Interaction Term

In this section, we discuss the intra-species interaction terms of fermions in more detail. Again, only on-site interaction terms contribute due to their localization such that $U_{\mathbf{n}}^f \neq 0$ only if all values of n_i in \mathbf{n} are the same. Taking into account the Clebsch-Gordon coefficients, the corresponding interaction term can be reduced according to

$$H_I^f = \sum_n U_{\mathbf{n}}^f g_{f,0} \psi_{n,1/2}^\dagger \psi_{n,-1/2}^\dagger \psi_{n,-1/2} \psi_{n,1/2}, \quad (3.25)$$

with $\mathbf{n} = (n, n, n, n)$. In general, this four-fermion interaction term does contribute non-trivially to the dynamics. This contribution can also be

written as a density-density interaction between $\alpha_f = -1/2$ and $\alpha_f = 1/2$ particles

$$H_I^f = U_{\mathbf{n}}^f g_{f,0} \left(\sum_{n,\text{even}} \rho_{n,1/2} \rho_{n,-1/2} + \sum_{n,\text{odd}} \rho_{n,-1/2} \rho_{n,1/2} \right), \quad (3.26)$$

with density operators $\rho_{n,\pm 1/2} = \psi_{n,\pm 1/2}^\dagger \psi_{n,\pm 1/2}$. Restricting ourselves, however, to the staggered initial state $|\Psi\rangle$ with only $\alpha_f = 1/2$ particles on even sites and only $\alpha_f = -1/2$ particles on odd sites. We immediately see that $H_I^f |\Psi\rangle = 0$. This implies that this four-fermion interaction does not contribute to the time evolution due to an appropriate initial-state preparation.

3.2.5 Inter-species Interaction Term

Regarding the fermion-boson scattering contributions to the Hamiltonian, we have to consider both the spin exchange process as well as elastic scattering processes. According to the interaction selection described above, the spin exchange term involving the correlated hopping of fermions and

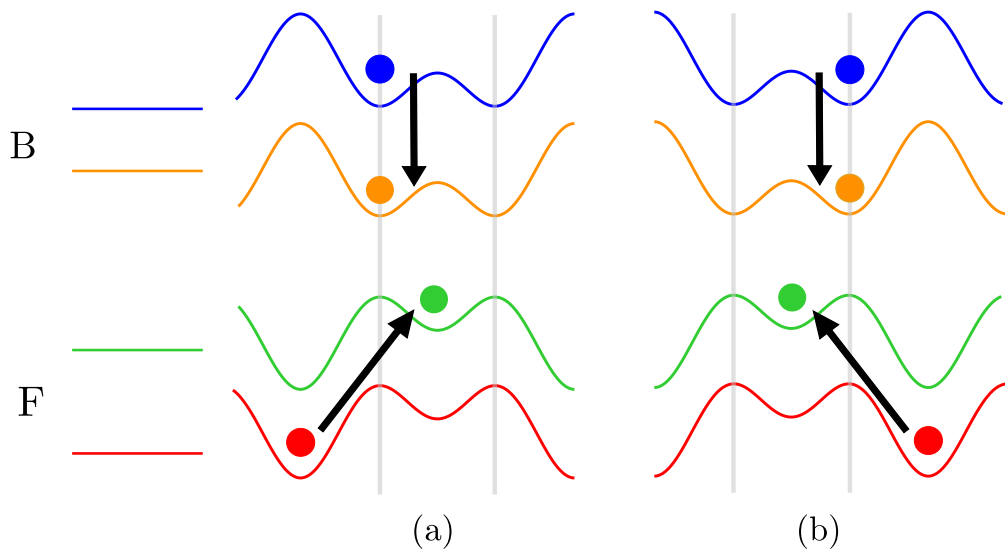


FIGURE 3.3: The selection of the interaction results in a correlated bosonic spin exchange plus a fermionic hopping. This is also known as interaction induced hopping. Note that the inverse process is allowed as well.

bosons is given by

$$H_{I_{se}}^{bf} = \frac{1}{2} \sum_n U_{\mathbf{n}}^{bf} g_{\boldsymbol{\mu}}^{bf} (\psi_{2n,\alpha}^\dagger \phi_{2n,\beta}^\dagger \phi_{2n,\delta} \psi_{2n+1,\gamma} + \psi_{2n,\alpha}^\dagger \phi_{2n-1,\beta}^\dagger \phi_{2n-1,\delta} \psi_{2n-1,\gamma} + h.c.) , \quad (3.27)$$

with $\boldsymbol{\mu} = (\alpha, \beta, \gamma, \delta) = (-1/2, 0, 1/2, -1)$. The first term corresponds to Fig. 3.3a, whereas the second term is shown in Fig. 3.3b. According to equation (3.16), the coupling constant for this specific scattering process is given by

$$g_{\boldsymbol{\mu}}^{bf} = \frac{\sqrt{2}}{3} (g_{bf,3/2} - g_{bf,1/2}) . \quad (3.28)$$

We emphasize that the spin exchange term does not change the staggered occupation of fermions such that the four-fermion term (3.25) still does not contribute. We anticipate that this applies to the elastic scattering terms as well. Accordingly, the scattering properties of the fermions are completely determined by their parity (even/odd sites) and we may drop the spin label completely. This motivates to define $\psi_{2n} \equiv \psi_{2n,-1/2}$ and $\psi_{2n+1} \equiv \psi_{2n+1,1/2}$.

Employing the Schwinger boson representation and taking into account that the overlap integral $U_{\mathbf{n}}^{bf}$ does not depend on the specific lattice site n , the spin exchange Hamiltonian can be written as

$$H_{I_{se}}^{bf} = \frac{1}{2a_S \sqrt{\ell(\ell+1)}} \sum_n (\psi_n^\dagger L_{+,n} \psi_{n+1} + h.c.) , \quad (3.29)$$

where we introduced $[a_S \sqrt{\ell(\ell+1)}]^{-1} = U_{\mathbf{n}}^{bf} g_{\boldsymbol{\mu}}^{bf}$.

The elastic scattering processes, on the other hand, are given by

$$\begin{aligned}
H_{I_{el}}^{bf} &= \frac{1}{2} \sum_{n\beta} U_{\mathbf{n}}^{bf} g_{\boldsymbol{\mu}}^{bf} \psi_{2n}^{\dagger} \phi_{2n,\beta}^{\dagger} \phi_{2n,\beta} \psi_{2n} \\
&+ \frac{1}{2} \sum_{n\beta} U_{\mathbf{n}}^{bf} g_{\boldsymbol{\mu}}^{bf} \psi_{2n}^{\dagger} \phi_{2n-1,\beta}^{\dagger} \phi_{2n-1,\beta} \psi_{2n} \\
&+ \frac{1}{2} \sum_{n\beta} U_{\mathbf{n}}^{bf} g_{\boldsymbol{\mu}}^{bf} \psi_{2n+1}^{\dagger} \phi_{2n,\beta}^{\dagger} \phi_{2n,\beta} \psi_{2n+1} \\
&+ \frac{1}{2} \sum_{n\beta} U_{\mathbf{n}}^{bf} g_{\boldsymbol{\mu}}^{bf} \psi_{2n+1}^{\dagger} \phi_{2n+1,\beta}^{\dagger} \phi_{2n+1,\beta} \psi_{2n+1}, \quad (3.30)
\end{aligned}$$

where $\beta \in \{-1, 0\}$. We note again that the coupling constants $g_{\boldsymbol{\mu}}^{bf}$ still depend on the magnetic substates and are hence not identical for all terms. Moreover, we observe that each $U_{\mathbf{n}}^{bf}$ is independent of n , however, identical for the first and second line (further denoted by $U_{\mathbf{n}1}^{bf}$) as well as identical for the third and fourth line (further denoted by $U_{\mathbf{n}3}^{bf}$), cf. Appendix A. The first term in (3.30) for which $\boldsymbol{\mu} = (-1/2, \beta, -1/2, \beta)$, we obtain

$$\begin{aligned}
H_{I_{el,1}}^{bf} &= \frac{g_{bf,3/2}}{2} \sum_n U_{\mathbf{n}1}^{bf} \psi_{2n}^{\dagger} d_{2n}^{\dagger} d_{2n} \psi_{2n} \\
&+ \frac{g_{bf,1/2} + 2g_{bf,3/2}}{6} \sum_n U_{\mathbf{n}1}^{bf} \psi_{2n}^{\dagger} b_{2n}^{\dagger} b_{2n} \psi_{2n}, \quad (3.31)
\end{aligned}$$

where we used (3.16) again. The second term in (3.30) is the same as the first one upon replacing $b_{2n} \rightarrow d_{2n-1}$ and $d_{2n} \rightarrow b_{2n-1}$. The third term in (3.30) is different, because of $\boldsymbol{\mu} = (1/2, \beta, 1/2, \beta)$ and corresponds to the different fermionic parity

$$\begin{aligned}
H_{I_{el,3}}^{bf} &= \frac{2g_{bf,1/2} + g_{bf,3/2}}{6} \sum_n U_{\mathbf{n}3}^{bf} \psi_{2n+1}^{\dagger} d_{2n}^{\dagger} d_{2n} \psi_{2n+1} \\
&+ \frac{g_{bf,1/2} + 2g_{bf,3/2}}{6} \sum_n U_{\mathbf{n}3}^{bf} \psi_{2n+1}^{\dagger} b_{2n}^{\dagger} b_{2n} \psi_{2n+1}. \quad (3.32)
\end{aligned}$$

The fourth term in (3.30) is again the same as the third one upon replacing $b_{2n} \rightarrow d_{2n+1}$ and $d_{2n} \rightarrow b_{2n+1}$. Employing again the Schwinger boson

representation $b_{2n}^\dagger b_{2n} = \ell + L_{z,2n}$ and $d_{2n}^\dagger d_{2n} = \ell - L_{z,2n}$, the first term (3.31) can be written as

$$\begin{aligned} H_{I_{el},1}^{bf} &= \frac{g_{bf,1/2} + 5g_{bf,3/2}}{6} \ell \sum_n U_{\mathbf{n}1}^{bf} \psi_{2n}^\dagger \psi_{2n} \\ &+ \frac{g_{bf,1/2} - g_{bf,3/2}}{6} \sum_n U_{\mathbf{n}1}^{bf} L_{z,2n} \psi_{2n}^\dagger \psi_{2n}. \end{aligned} \quad (3.33)$$

The third term (3.32) can be expressed as

$$\begin{aligned} H_{I_{el},3}^{bf} &= \frac{g_{bf,1/2} + g_{bf,3/2}}{2} \ell \sum_n U_{\mathbf{n}3}^{bf} \psi_{2n+1}^\dagger \psi_{2n+1} \\ &- \frac{g_{bf,1/2} - g_{bf,3/2}}{6} \sum_n U_{\mathbf{n}3}^{bf} L_{z,2n} \psi_{2n+1}^\dagger \psi_{2n+1}, \end{aligned} \quad (3.34)$$

and similar expressions are also obtained for the second and fourth line by replacing $L_{z,2n} \rightarrow -L_{z,2n\mp 1}$. We emphasize that both $U_{\mathbf{n}1}^{bf} \neq U_{\mathbf{n}3}^{bf}$ and $g_{bf,1/2} \neq g_{bf,3/2}$. Combining the first and second line leads to

$$\begin{aligned} H_{I_{el},1,2}^{bf} &= \frac{g_{bf,1/2} + 5g_{bf,3/2}}{3} \ell \sum_n U_{\mathbf{n}1}^{bf} \psi_{2n}^\dagger \psi_{2n} \\ &+ \frac{g_{bf,1/2} + 5g_{bf,3/2}}{6} \sum_n U_{\mathbf{n}1}^{bf} \psi_{2n}^\dagger \psi_{2n} (L_{z,2n} - L_{z,2n-1}) \end{aligned} \quad (3.35)$$

and combining the third and fourth line is given by

$$\begin{aligned} H_{I_{el},3,4}^{bf} &= (g_{bf,1/2} + g_{bf,3/2}) \ell \sum_n U_{\mathbf{n}3}^{bf} \psi_{2n+1}^\dagger \psi_{2n+1} \\ &+ \frac{g_{bf,1/2} - g_{bf,3/2}}{6} \sum_n U_{\mathbf{n}3}^{bf} \psi_{2n+1}^\dagger \psi_{2n+1} (L_{z,2n+1} - L_{z,2n}). \end{aligned} \quad (3.36)$$

We perform the substitution

$$L_{z,n} - L_{z,n-1} = G_n + \psi_n^\dagger \psi_n, \quad (3.37)$$

where G_n is Gauss's law operator. When acting on physical states every term containing G_n cancels out, see section 3.4 for a detailed discussion

of Gauss's law. Using the anti-commutator relationships shows that the $H_{I_{el},1,2}^{bf} + H_{I_{el},3,4}^{bf}$ is a bilinear in the fermionic operators, i.e. a sum of $\psi_n^\dagger \psi_n$ with only parity dependent prefactors. This shows that the elastic scattering terms only contribute to the potential energy of the fermions.

3.3 Cold-Atom QED Hamiltonian

Summing up all contributions, the cold-atom QED Hamiltonian takes the form

$$\begin{aligned}
H = & \frac{g^2 a_S}{2} \sum_n L_{z,n}^2 + \Delta_{b,0} \sum_n (-1)^n L_{z,n} \\
& + \frac{1}{2a_S \sqrt{\ell(\ell+1)}} \sum_n (\psi_n^\dagger L_{+,n} \psi_{n+1} + h.c.) \\
& + \sum_n (V_n^f \psi_n^\dagger \psi_n + V_n^b b_n^\dagger b_n + V_n^d d_n^\dagger d_n) . \tag{3.38}
\end{aligned}$$

The terms in the last line include the potential energy contributions, in particular the energy due to the trapping of the atoms as well as due to the elastic scattering terms. We emphasize that the fermionic contribution V_n^f depends on the parity of n . Introducing the energy difference Δ_f according to $V_{2n}^f = V_0^f - \Delta_f/2$ and $V_{2n+1}^f = V_0^f + \Delta_f/2$, the fermionic contribution to the potential energy is given by

$$H_V^f = V_0^f \sum_n \psi_n^\dagger \psi_n - \frac{\Delta_f}{2} \sum_n (-1)^n \psi_n^\dagger \psi_n . \tag{3.39}$$

Since the total particle number of the fermions is conserved, the first term does not contribute to the dynamics and can thus be disregarded. The bosonic potential term is treated in a similar fashion. Defining $\Delta_{b,1}$ according to $V_n^b = V_0^b + (-1)^n \Delta_{b,1}/2$ and $V_n^d = V_0^b - (-1)^n \Delta_{b,1}/2$ and using $L_{z,n} = (b_n^\dagger b_n - d_n^\dagger d_n)/2$ leads us to

$$H_V^b = \Delta_{b,1} \sum_n (-1)^n L_{z,n} , \tag{3.40}$$

where we disregarded an irrelevant constant term. Adding the second contribution in (3.38) and defining $\Delta_b \equiv \Delta_{b,0} + \Delta_{b,1}$, we obtain

$$H_V^b + \Delta_{b,0} \sum_n (-1)^n L_{z,n} = \Delta_b \sum_n (-1)^n L_{z,n} . \quad (3.41)$$

Comparison of the cold-atom QED Hamiltonian with the target Hamiltonian (3.3) then shows that we still have an undesired contribution linear in $L_{z,n}$. However, this term does not contribute if we transform the Hamiltonian into the rotating frame or interaction picture. To this end, we split the cold-atom QED Hamiltonian $H = H_0 + H_1$ into two parts

$$H_0 = \Delta_b \sum_n (-1)^n \left(L_{z,n} - \frac{1}{2} \psi_n^\dagger \psi_n \right) , \quad (3.42a)$$

$$H_1 = \frac{g^2 a_S}{2} \sum_n L_{z,n}^2 + M \sum_n (-1)^n \psi_n^\dagger \psi_n \\ + \frac{1}{2a_S \sqrt{\ell(\ell+1)}} \sum_n (\psi_n^\dagger L_{+,n} \psi_{n+1} + h.c.) , \quad (3.42b)$$

where we introduced the mass parameter according to

$$M = \frac{\Delta_b - \Delta_f}{2} . \quad (3.43)$$

Upon acting with the unitary transformation $U(t) = \exp(-iH_0 t)$, we get the new Hamiltonian $H'_1 = U^\dagger(t) H_1 U(t)$. Performing the canonical transformation $\psi_n \rightarrow (-i)^n \psi_n$ we can finally identify the Hamiltonian H'_1 with

$$H_{\text{QL}} = \frac{g^2 a_S}{2} \sum_n L_{z,n}^2 + M \sum_n (-1)^n \psi_n^\dagger \psi_n \\ - \frac{i}{2a_S \sqrt{\ell(\ell+1)}} \sum_n (\psi_n^\dagger L_{+,n} \psi_{n+1} - h.c.) . \quad (3.44)$$

This is the quantum link Hamiltonian in (3.3). We note again that we have to take the limit $\ell \rightarrow \infty$ in order to recover the Hamiltonian formulation of the Wilson's lattice gauge theory corresponding to (3.1).

3.4 Initial State and Gauss's Law

After discussing the necessary steps for realizing the Hamiltonian (3.44) in a cold atom system, we briefly discuss the initial state and Gauss's law in more detail. To study the real-time dynamics of fermions coupled to strong gauge fields, represented by two-component coherent bosonic samples, the system is supposed to be initialized in eigenstates of both the free bosonic and fermionic theories

$$H_{b,0} = \frac{g^2 a_S}{2} \sum_n L_{z,n}^2, \quad (3.45a)$$

$$H_{f,0} = -\frac{i}{2a_S} \sum_n [\psi_n^\dagger \psi_{n+1} - h.c.] + M \sum_n (-1)^n \psi_n^\dagger \psi_n. \quad (3.45b)$$

To initiate the dynamic evolution, the system is then instantaneously quenched to an interacting field theory governed by the Hamiltonian (3.44). The bosonic samples are prepared in an excited eigenstate of $H_{b,0}$, determined by the number of bosonic atoms on each site $2\ell = b_n^\dagger b_n + d_n^\dagger d_n$ and the eigenvalue of the operator $L_{z,n} = (b_n^\dagger b_n - d_n^\dagger d_n)/2$. The initial value of the bosonic species imbalance drives the non-trivial real-time evolution of the coupled system after the quench.

The fermions, on the other hand, are supposed to be initialized in the ground state of the Hamiltonian $H_{f,0}$. Owing to the fact that the free Hamiltonian is quadratic, the dispersion relation can be determined analytically. Given an optical lattice with N elementary cells, i.e. $2N$ lattice sites, the dispersion relation is given by two bands $\pm\omega_k$ with

$$\omega_k = \sqrt{M^2 + p_k^2} \quad (3.46)$$

and $p_k = \frac{1}{a_S} \sin(\frac{\pi k}{N})$ as well as $k \in \{0, \dots, N-1\}$. The corresponding mode function expansion of the fermionic field operator reads

$$\psi_n = \frac{1}{\sqrt{2N}} \sum_k e^{\frac{i\pi kn}{N}} \left(\frac{M + (-1)^n (\omega_k - p_k)}{\sqrt{2\omega_k (\omega_k - p_k)}} A_k - \frac{M - (-1)^n (\omega_k + p_k)}{\sqrt{2\omega_k (\omega_k + p_k)}} B_k^\dagger \right), \quad (3.47)$$

and the momentum space creation/annihilation operators are defined with respect to the zero-particle state $|0\rangle$ according to $A_k |0\rangle = B_k |0\rangle = 0$. The Dirac vacuum state corresponds to a N -particle state where the negative energy band is occupied and the positive energy band is empty

$$|GS\rangle_D = \prod_k B_k^\dagger |0\rangle. \quad (3.48)$$

Due to the fact that the ground state is supposed to carry no charge, $\rho_n |GS\rangle = 0$, the charge operator for the staggered Dirac vacuum needs to be defined according to

$$\rho_n^{(D)} = \psi_n^\dagger \psi_n - \frac{1}{2N} \sum_k \frac{\omega_k - (-1)^n M}{\omega_k}. \quad (3.49)$$

The experimental realization of the Dirac vacuum, corresponding to a highly correlated fermionic initial state, is intricate but possible in principle [49]. After performing the quench, the theory becomes a U(1) gauge theory with the Gauss's law operator defined according to

$$G_n = L_{z,n} - L_{z,n-1} - \rho_n^{(D)}. \quad (3.50)$$

The Gauss's law operator commutes with the Hamiltonian, $[G_n, H] = 0$, and is the generator of local gauge transformations.

Finally, we note that the realization of the Dirac vacuum state is an important ingredient for simulating quantum electrodynamics. On the other

hand, there are also other possible initial states which have been investigated in the past [43]. In these cases, the quench to the interacting field theory has been performed from the heavy mass limit initial state $Ma_S \gg 1$, which is obtained by disregarding the free hopping term in (3.45b). In this case, the dispersion relation becomes flat and degenerate, $\omega_n = (-1)^n M$, and the ground state in the N -particle sector corresponds to a state where the odd sites are occupied

$$|GS\rangle_M = \prod_n \psi_{2n+1}^\dagger |0\rangle, \quad (3.51)$$

with $\psi_n |0\rangle = 0$. The charge operator is defined according to

$$\rho_n^{(M)} = \psi_n^\dagger \psi_n - \frac{1 - (-1)^n}{2}, \quad (3.52)$$

which immediately follows from (3.49) by replacing $\omega_k \rightarrow M$ corresponding to the heavy mass limit.

Chapter 4

Lattice Gauge Theories Out of Equilibrium

In this chapter, we investigate the real-time dynamics of Abelian $U(1)$ and non-Abelian $SU(N)$ gauge theories coupled to fermionic matter. Standard importance sampling is not a reliable technique for real-time lattice gauge theories. However, for a large class of time-dependent quantum mechanical problems, the system can be described by a classical-statistical ensemble. The quantum corrections included in this approach are analyzed via a diagrammatic representation depicted in a series expansion. This method is non-perturbative and is applied to pair production in $(3 + 1)$ -dimensional quantum electrodynamics. There are known analytical results for constant background field, which are modified, if the back-reaction of the produced fermion pairs on the gauge fields is included.

4.1 Real-time Lattice Gauge Theory

The quantum mechanical problem posed by strong gauge fields coupled to fermions is an important theoretical question. In particular the Schwinger mechanism describes the situation, where the electron-positron pairs are produced from an electric field [10–12]. The critical field strength is given

by $E_c \sim M^2/g \sim 10^{18}V/m$ for quantum electrodynamics (QED) with electron mass M and gauge coupling g . Pair production appears as well in quantum chromodynamics (QCD). During a nuclear collision at high energies, the strong color fields will influence the dynamics of the Quark-Gluon plasma. Considering the Color-Glass condensate, its characteristic field strengths are of the order of $1/g$, where g is the running coupling [14]. In such a situation, the quark pair production should be enhanced. A similar question can also be asked in scalar field theories coupled to fermions, where one can show the importance of fluctuations for the production of fermions [50].

The Pauli principle does not allow two fermions to occupy the same state. Hence, their quantum nature is very important. A decent theoretical treatment should include this particular feature of the fermions, when we study the dynamics of such theories. It is well known that a quantum theory in equilibrium in d spatial dimensions can be described by a classical-statistical mechanics problem in $(d+1)$ spatial dimensions. Nevertheless, the production of fermions by strong fields or fluctuations is generically not an equilibrium problem and the Euclidean formulation cannot describe such situations. In particular, there is no feasible general approach for non-equilibrium problems.

However, a large class of physical problems can be mapped on a classical-statistical ensemble [25–29]. The agreement between a quantum field theoretic approach using resummation techniques and the corresponding classical-statistical theories [30–34] was explicitly shown for scalar quantum field theories coupled to fermionic matter [50, 51]. There exist already derivations of the classical-statistical approximations for purely scalar field theories and pure gauge field theories. The classical-statistical theory can also be connected to kinetic theories [52–54]. The relation between kinetic theory and the classical-statistical lattice simulations for gauge theories was investigated in [55–57].

We will study the real-time dynamics of $U(1)$ and $SU(N)$ gauge theories coupled to fermionic matter on a discrete space-time lattice. The starting point is the functional integral of the full quantum theory. Then we will outline the classical-statistical approximation of the functional integral. From there we can give arguments concerning the validity of this approach. The quantum corrections included in this description can be interpreted by a corresponding diagrammatic representation of an underlying series expansion. This non-perturbative approach will then be applied to electron-positron production in QED in three spatial dimensions. This extends the study of previous one-dimensional results [58]. The analytic expression for a constant background field can be used as a benchmark for the early time behavior. However, we establish the necessity to include the back-reaction of the produced fermion-pairs on the gauge fields.

The functional integral on the closed time path is the starting point to handle real-time quantum field theories. The closed time path or Keldysh contour [59, 60] is depicted in Fig. 4.1. It begins at time t_0 and continues towards a final time along the real axis. Then the contour propagates backwards to the initial time t_0 . We discretize space-time on a four dimensional hypercubic lattice

$$\Lambda = \{(n_0, \mathbf{n}) \mid n_0 \in 0, \dots, 2N_T; n_i \in 0, \dots, N_i - 1\}, \quad (4.1)$$

with $\mathbf{n} = (n_1, n_2, n_3)$ and $i \in \{1, 2, 3\}$. The vector $\hat{\mu}$ points along the time contour if $\mu = 0$ and is directed along the spatial coordinate axes for $\mu \in \{1, 2, 3\}$. Note that we consider an isotropic spatial lattice with spacings $a_i = a_S$. The number of lattice points is given by $N_i = N_S$ for $i \in \{1, 2, 3\}$. If we discretize the time contour, this leads to

$$t_C(n_0) = \begin{cases} t_0 + a_T n_0, & 0 \leq n_0 \leq N_T \\ t_F - a_T (n_0 - N_T), & N_T + 1 \leq n_0 \leq 2N_T. \end{cases} \quad (4.2)$$

Here the final time $t_F = t_0 + a_T N_T$ denotes an arbitrary late time and n_0 is a non-negative integer. We define the lattice spacing in the temporal

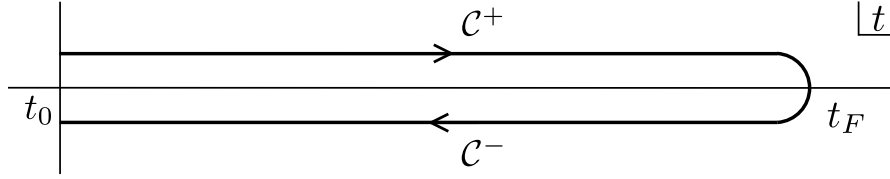


FIGURE 4.1: Graphical representation of the real-time Schwinger-Keldysh contour where C_+ denotes the forward branch and C_- is the backward branch.

direction as

$$a_0 \equiv \text{sgn}_{\mathcal{C}} a_T, \quad (4.3)$$

where $\text{sgn}_{\mathcal{C}}$ is $+1$ on the forward branch ($0 \leq n_0 \leq N_T$) and -1 on the backward branch ($N_T + 1 \leq n_0 \leq 2N_T$) of the closed time path.

We consider the Wilsonian action on a Minkowskian lattice [61, 62]. In particular the pure gauge part is given by

$$\begin{aligned} S_G[U] &= \frac{2}{g_0^2} \sum_{n \in \Lambda} \frac{a_S}{a_0} \sum_i \text{Re tr} (\mathbb{1} - U_{0i,n}) \\ &\quad - \frac{2}{g_S^2} \sum_{n \in \Lambda} \frac{a_0}{a_S} \sum_{\substack{i,j \\ i < j}} \text{Re tr} (\mathbb{1} - U_{ij,n}), \end{aligned} \quad (4.4)$$

where the gauge invariant plaquette term appears

$$U_{\mu\nu,n} = U_{\mu,n} U_{\nu,n+\hat{\mu}} U_{\mu,n+\hat{\nu}}^\dagger U_{\nu,n}^\dagger. \quad (4.5)$$

Each link variable $U_{\mu,n}$ is located between the lattice sites n and $n + \hat{\mu}$ and points in the direction of $\hat{\mu}$. In contrast to chapter 2 we also discretize the time direction and have links in the temporal direction. If the link points in the $-\hat{\mu}$ direction, we use the definition

$$U_{-\mu,n} \equiv U_{\mu,n-\hat{\mu}}^\dagger. \quad (4.6)$$

To simplify the following considerations we set $g_0 = g_S = g$. We use the standard normalization $\text{tr} [t^a, t^b] = 1/2 \delta_{ab}$ of the $SU(N)$ generators t^a , with the adjoint gauge index $a \in \{1, \dots, N^2 - 1\}$. Then the prefactors in

S_G can be chosen such that we obtain the correct naive continuum limit. Note that for the U(1) gauge theory the overall factor 2 has to be replaced by 1.

For the fermions we consider the naive discretization for simplicity

$$S_F[\bar{\psi}, \psi, U] = S_{if} - M \sum_{n \in \Lambda} a_0 a_S^3 \bar{\psi}_n \psi_n + \frac{i}{2} \sum_{\substack{n \in \Lambda \\ n_0 \neq 0, 2N_T}} \frac{a_0 a_S^3}{a_\mu} \bar{\psi}_n \gamma^\mu [U_{\mu, n} \psi_{n+\hat{\mu}} - U_{-\mu, n} \psi_{n-\hat{\mu}}] \quad (4.7)$$

and treat the issue of fermion doublers in Sec. 4.3. We employ the central difference discretization for the fermions. The term S_{if} containing the initial and final contributions of the fermionic fields is given by

$$S_{if} = i \frac{a_0 a_S^3}{a_\mu} \bar{\psi}_0 \gamma^\mu [U_{\mu, 0} \psi_{0+\hat{\mu}} - \psi_0] + i \frac{a_0 a_S^3}{a_\mu} \bar{\psi}_{2N_T} \gamma^\mu [\psi_{2N_T} - U_{-\mu, 2N_T} \psi_{2N_T-1}]. \quad (4.8)$$

The initial state is given by a density matrix $\rho(t_0)$ and can be in thermal equilibrium or describe non-equilibrium situations. An expectation value of a general observable $O(U, \bar{\psi}, \psi)$ can be calculated from the functional integral according to

$$\langle O(U, \bar{\psi}, \psi) \rangle = \int [dU] \int [d\bar{\psi} d\psi] \rho(t_0) \times O(U, \bar{\psi}, \psi) \exp(iS_G + iS_F). \quad (4.9)$$

The action $S_G + S_F$ contains the gauge and fermion degrees of freedom. Moreover, we introduce the abbreviations

$$\int [dU] = \prod_{\substack{n \in \Lambda \\ \mu}} \int dU_{\mu, n}, \quad (4.10a)$$

$$\int [d\bar{\psi} d\psi] = \prod_{n \in \Lambda} \int d\bar{\psi}_n d\psi_n. \quad (4.10b)$$

Note that the initial state $\rho(t_0)$ depends on $U_{\mu,n}$, $\bar{\psi}_n$ and ψ_n with time $n_0 \in \{0, 2N_T\}$.

The evolution of the density matrix can be expressed by a functional integral on the closed time path

$$Z_C = \int [dU] \int [d\bar{\psi} d\psi] \rho(t_0) \exp(iS_G + iS_F). \quad (4.11)$$

This expression is normalized to one, because the contributions of the forward and backward branch of the Schwinger-Keldysh contour cancel, if there are no source terms, i.e. $Z_C = 1$. This expression will be frequently called the partition function. Using the closed time path the normalization is always included when we compute observables like (4.9). By introducing source terms we can construct a generating functional for correlation functions from (4.11). For a pedagogical introduction to nonequilibrium generating functionals in quantum field theory see [63]. In the following discussion, we will not take the effect of source terms into account, in order to keep the notation simple. The manipulations on the integrand of the functional integral in (4.11) always implicitly assumes the presence of sources, or a direct insertion of the observables. If we wish to obtain the corresponding expectation values, we can take derivatives with respect to the sources.

We observe that the complex factor $\sim \exp(iS_G + iS_F)$ in the partition function (4.11) does not allow the efficient use of standard importance sampling techniques. Hence, we will describe an alternative method to approximate non-equilibrium problems and discuss its range of validity in Sec. 4.2. We focus on quadratic fermionic actions and note that a similar approach is useful for theories with non-Gaussian fermion interaction terms. This leads to the introduction of composite fields via a Hubbard-Stratonovich transformation.

4.1.1 U(1) Gauge Theory

In the following, we will motivate the classical-statistical approximation for quantum electrodynamics. We will parametrize the link variables $U_{\mu,n}$ in terms of the gauge fields $A_{\mu,n}$, whereas the simulations will be performed directly in terms of the link variables

$$U_{\mu,n} = \exp (i g a_{\mu} A_{\mu,n}) . \quad (4.12)$$

The numerical algorithm will be given in Sec. 4.3. The functional integral representation then reads

$$Z_C = \int [dA] \int [d\bar{\psi} d\psi] \rho(t_0) \exp (i S_G + i S_F) . \quad (4.13)$$

We observe that the parametrization of the Haar measure in terms of gauge fields can lead to non-trivial contributions to the exponent in the functional integral [64]. This issue becomes crucial for SU(N) gauge theories and will be discussed in Sec. 4.1.2. However, in the U(1) gauge theory, the Haar measure is trivial and will not change the action in the functional integral. Moreover, we will assume a Gaussian initial density matrix for the fermionic fields, i.e.

$$\rho(t_0) = \exp \left[- \sum_{n,m \in \Lambda} a_0 a_S^3 a_0 a_S^3 \bar{\psi}_n (\mathcal{K}^{-1})_{nm} \psi_m \right] \rho_G(A) , \quad (4.14)$$

where the matrix \mathcal{K}^{-1} only contributes at $n_0, m_0 \in \{0, 2N_T\}$. In addition, one can include a dependency on the initial gauge fields. If one wishes to introduce correlated initial states, one can consider an additional imaginary time branch [65]. Note that the pure gauge part $\rho_G(A)$ is only dependent on the initial field configuration $A_{\mu,n}$ with $n_0 \in \{0, 2N_T\}$. Such an initial state assures that the fermionic fields build a quadratic form in the

action

$$S_{FQ}[A] = \sum_{n,m \in \Lambda} \bar{\psi}_n i \Delta_C[A]_{nm}^{-1} \psi_m \quad (4.15)$$

of the functional integral (4.13). The inverse fermion propagator is given by $i \Delta_C[A]^{-1}$. This object has support on the Schwinger-Keldysh contour and depends on the gauge field A . The fermionic fields appear at most quadratic in the exponent, hence we are able to integrate them out

$$Z_C = \int [dA] \rho_G(A) \exp(\text{Tr} \log \Delta_C[A]^{-1} + i S_G) . \quad (4.16)$$

This procedure introduces a non-local effective interaction mediated by the fermionic degrees of freedom given by $\text{Tr} \log \Delta_C[A]^{-1}$, where the trace involves Dirac as well as space-time indices on the contour.

We label the gauge fields on the forward/backward branch of the contour by $+/-$ and perform the following transformation

$$A_{\mu,n}^+ = \bar{A}_{\mu,n} + \frac{1}{2} \tilde{A}_{\mu,n} , \quad (4.17a)$$

$$A_{\mu,n}^- = \bar{A}_{\mu,\bar{n}} - \frac{1}{2} \tilde{A}_{\mu,\bar{n}} , \quad (4.17b)$$

with $\bar{n} = (2N_T - 1 - n_0, \mathbf{n})$. We call \bar{A} the classical field and \tilde{A} the quantum field. Using the new coordinates we rewrite the partition function as

$$Z_C = \int [d\bar{A}] [d\tilde{A}] \rho_G(A) \exp(\text{Tr} \log \Delta_C[A]^{-1} + i S_G[A]) . \quad (4.18)$$

The part of the action $S_G[A]$ containing only gauge fields is

$$S_G[A] = -\frac{1}{4} \sum_{n \in \Lambda} a_0 a_S^3 F_{\mu\nu,n}[A] F_n^{\mu\nu}[A] , \quad (4.19)$$

when we expand in the lattice spacing and neglect higher order corrections. The field strength tensor $F_n^{\mu\nu}$ is determined by

$$F_{\mu\nu,n}[A] = \partial_\mu A_{\nu,n} - \partial_\nu A_{\mu,n}. \quad (4.20)$$

We reformulate the action in the new coordinates \bar{A} and \tilde{A} leading to

$$S_G[\bar{A}, \tilde{A}] = a_T a_S^3 \sum_{n \in \Lambda^+} \tilde{A}_{\nu,n} \partial_\mu F_n^{\mu\nu}[\bar{A}]. \quad (4.21)$$

It is crucial that this part of the action is linear in \tilde{A} . The forward branch is denoted by Λ^+ and $F_n^{\mu\nu}[\bar{A}]$ is the field strength tensor determined by the classical field.

We also expand $\text{Tr} \log \Delta_C[A]^{-1}$ in (4.18) to linear order in the quantum field \tilde{A} . This is then given by

$$\text{Tr} \log \Delta_C^{-1}[A] = \text{Tr} \log \Delta_C^{-1}[\bar{A}] + \frac{ig}{2} \text{Tr} \{ \Delta_C[\bar{A}] \text{sgn}_C \tilde{A} \} + \dots, \quad (4.22)$$

where $\Delta_C[\bar{A}]$ is the fermion propagator in the background of the classical field \bar{A} with $\tilde{A} = 0$ and we use the notation $\tilde{A} \equiv \gamma^\mu \tilde{A}_\mu$. We observe that the leading term of the expansion (4.22) will not contribute in the functional integral. The reasoning is as follows: The quantum field \tilde{A} does not appear in this expression. Hence the contributions of the + branch is canceled by the same contribution of the – branch resulting in

$$e^{\text{Tr} \log \Delta_C^{-1}[\bar{A}]} = \det \Delta_C^{-1}[\bar{A}] = 1. \quad (4.23)$$

As a consequence we set this term to one for the following calculations.

Considering the linear order, the \tilde{A} contributions are given by

$$\frac{ig}{2} \text{Tr} \{ \Delta_C[\bar{A}] \text{sgn}_C \tilde{A} \} = -ia_T a_S^3 \sum_{n \in \Lambda^+} \bar{j}_n^\nu \tilde{A}_{\nu,n}, \quad (4.24)$$

where the fermion current is determined by

$$\bar{j}_n^\nu = \frac{g}{2} \text{tr} \{ \langle [\bar{\psi}_n, \psi_n] \rangle_{\bar{A}} \gamma^\nu \}. \quad (4.25)$$

The trace over the Dirac indices is denoted by tr and the commutator expectation value in the presence of the classical field \bar{A} is denoted by $\langle [\bar{\psi}_n, \psi_n] \rangle_{\bar{A}}$. We will now give a detailed derivation of this expression and how to determine $\langle [\bar{\psi}_n, \psi_n] \rangle_{\bar{A}}$.

We rewrite the second term in (4.22) and use a continuum notation. Note that the inverse propagator is given by

$$i\Delta_{\mathcal{C}}^{-1}[\bar{A}] \equiv \left(i\cancel{\partial}_x - g\cancel{A}(x) - M \right) \delta_{\mathcal{C}}(x, y), \quad (4.26)$$

where we neglected higher terms in the lattice spacing and $\delta_{\mathcal{C}}(x, y)$ is the delta function on the time contour. Using the subscript \mathcal{C} we highlight that the closed time path is implicitly included in this continuum notation. With this in mind the propagator is

$$\left(i\cancel{\partial}_x - g\cancel{A}(x) - M \right) \Delta_{\mathcal{C}}(x, y) = i\delta_{\mathcal{C}}(x, y). \quad (4.27)$$

We connect the contour-ordered correlation functions and the propagator through the relation

$$\Delta_{\mathcal{C}}(x, y) = \langle T_{\mathcal{C}} \psi(x) \bar{\psi}(y) \rangle_{\bar{A}}, \quad (4.28)$$

where $T_{\mathcal{C}}$ is the time ordering along the Keldysh contour. We indicate via $\langle \cdots \rangle_{\bar{A}}$ that the correlation functions have to be calculated by (4.27) for a given classical field \bar{A} background. The propagator can be rewritten in the following manner

$$\Delta_{\mathcal{C}}(x, y) = \theta_{\mathcal{C}}(x_0, y_0) \Delta^>(x, y) + \theta_{\mathcal{C}}(y_0, x_0) \Delta^<(x, y), \quad (4.29)$$

where $\theta_C(x_0, y_0)$ is the Heaviside function on the closed time path [66]. The individual components of the closed time path propagator are

$$\Delta^>(x, y) = \langle \psi(x) \bar{\psi}(y) \rangle_{\bar{A}}, \quad (4.30a)$$

$$\Delta^<(x, y) = - \langle \bar{\psi}(y) \psi(x) \rangle_{\bar{A}}. \quad (4.30b)$$

Evaluating the trace in (4.24) leads to

$$\text{Tr}\{\Delta_C[\bar{A}] \text{sgn}_C \tilde{A}\} = \text{tr} \int_{t_0}^{t_F} \int_{\mathbf{x}} [\Delta^>(x, x) + \Delta^<(x, x)] \tilde{A}(x). \quad (4.31)$$

Again tr denotes the trace over Dirac indices. Further, we used the relation

$$\theta_C(x_0, y_0) + \theta_C(y_0, x_0) = 1. \quad (4.32)$$

For the fermionic fields the Keldysh propagator is determined by

$$\Delta^K(x, y) \equiv \Delta^>(x, y) + \Delta^<(x, y) = \langle [\psi(x), \bar{\psi}(y)] \rangle_{\bar{A}} \quad (4.33)$$

and has to obey

$$\left(i\partial_x - g\tilde{A}(x) - M \right) \Delta^K(x, y) = 0. \quad (4.34)$$

In addition, the equation (4.31) can be reformulated as:

$$\text{Tr}\{\Delta_C[\bar{A}] \text{sgn}_C \tilde{A}\} = \text{tr} \int_{t_0}^{t_F} \int_{\mathbf{x}} \Delta^K(x, x) \tilde{A}(x). \quad (4.35)$$

It is worth emphasizing that the term on the right hand side of the last equation is related to the current

$$\bar{j}^\nu(x) = -\frac{g}{2} \text{tr} \{ \Delta^K(x, x) \gamma^\nu \} \quad (4.36)$$

determined by the fermionic field coupled to \tilde{A} [67]. The trace tr is taken with respect to the Dirac indices. Consequently, the partition function employing the expansion of $\text{Tr} \log \Delta_C^{-1}[A]$ to linear order in the quantum

field \tilde{A} is

$$Z_C^{\text{cl}} = \int [d\bar{A}][d\tilde{A}] \rho_G(A) \times \exp \left\{ ia_{TAS} \sum_{n \in \Lambda^+} \tilde{A}_{\nu,n} (\partial_\mu F_n^{\mu\nu}[\bar{A}] - \bar{j}_n^\nu) \right\}. \quad (4.37)$$

We will explain the physical interpretation of this approximation in more detail in Sec. 4.2. This partition function is the classical-statistical description of the original quantum field theory. In order to evaluate this functional integral, we integrate out the quantum field \tilde{A} . In addition we perform a Fourier transformation of the initial state $\rho_G(A)$ with respect to \tilde{A} . This results in the Wigner transform

$$\rho_G(A) = \int d\Pi_{\mathbf{0}} \rho_W(\bar{A}_{\mathbf{0}}, \Pi_{\mathbf{0}}) \exp \left(i \sum_{\mathbf{n}} a_S^3 \Pi_{\mathbf{0}}^\mu \tilde{A}_{\mu,\mathbf{0}} \right), \quad (4.38)$$

where we introduced the notation $\mathbf{0} = (0, \mathbf{n})$. Note that the momentum $\Pi_{\mathbf{0}}$ is the conjugate variable of the classical field $\bar{A}_{\mathbf{0}}$ at the initial time step. Performing the integration with respect to \tilde{A} results in

$$Z_C^{\text{cl}} = \int [d\bar{A}] \int d\Pi_{\mathbf{0}} \rho_W(\bar{A}_{\mathbf{0}}, \Pi_{\mathbf{0}}) \delta[\partial F[\bar{A}] - \bar{j}]. \quad (4.39)$$

We observe that the argument of the delta function is given by the classical equation of motion

$$\partial_\mu \bar{F}_n^{\mu\nu} = \frac{g}{2} \text{tr} \left\{ \langle [\bar{\psi}_n, \psi_n] \rangle_{\bar{A}} \gamma^\nu \right\}. \quad (4.40)$$

The Wigner function ρ_W determines the statistical initial conditions for the classical equation of motion. The observables are determined by averaging with respect to the ensemble produced by numerically solving the classical field equations and choosing stochastic initial conditions according to

$$\langle O[\bar{A}] \rangle = \int [d\bar{A}] \int d\Pi_{\mathbf{0}} \rho_W(\bar{A}_{\mathbf{0}}, \Pi_{\mathbf{0}}) O[\bar{A}] \delta[\partial F[\bar{A}] - \bar{j}]. \quad (4.41)$$

As a technical remark we note, that changing variables introduces a Jacobian in the functional integral. However, this can be taken to be constant in the following discussion, for details see [53].

4.1.2 SU(N) Gauge Theory

Now we will motivate the classical-statistical approximation for SU(N) gauge theory coupled to fermionic matter. This will proceed along similar lines as for the U(1) case. Hence, it is not necessary to repeat the entire derivation, however, we will emphasize where differences appear.

In non-Abelian gauge theories the fermions carry a color index and have to transform with respect to the fundamental representation of the SU(N) gauge group. The link variables $U_{n,\mu}$ will be given by $A_{\mu,n} = t^a A_{\mu,n}^a$, where the t^a are the generators of the SU(N) gauge group. This leads us to

$$U_{\mu,n} = \exp(iga_{\mu}A_{\mu,n}) . \quad (4.42)$$

Note that for the non-Abelian case an explicit parametrization of the Haar measure introduces new contributions to the functional integral [64]. The partition function is now

$$Z_C = \int [dA] \int [d\bar{\psi} d\psi] \rho(t_0) \exp(iS_G + iS_F - S_M) \quad (4.43)$$

with the standard gauge and fermion actions $S_G + S_F$ and the term

$$S_M = -\frac{1}{2} \sum_{\substack{n \in \Lambda \\ \mu}} \text{tr} \log [1 + N(A_{\mu,n})] . \quad (4.44)$$

The trace is performed with respect to the adjoint gauge indices and we introduced the expression

$$N(A_{\mu,n}) = 2 \sum_{l=1}^{\infty} \frac{(-1)^l}{(2l+2)!} (ga_{\mu}A_{\mu,n})^{2l} . \quad (4.45)$$

We will arrive again at the classical-statistical approximation of the quantum theory, when we expand the exponent appearing in equation (4.43) in powers of the quantum field \tilde{A} .

First, we investigate the contribution from S_M . The linear term in \tilde{A} vanishes and the remaining zeroth order term will be interpreted as the functional integral measure of the classical field as $\int [d\bar{A}] \exp(-S_M[\bar{A}])$. We see this by starting from the explicit expression for the Haar measure of SU(N) gauge theories given by (4.44) and (4.45). Now, we expand S_M in the quantum field \tilde{A} resulting in

$$\begin{aligned} S_M &= -\frac{1}{2} \sum_{\substack{n \in \Lambda \\ \mu}} \text{tr} \log[1 + N(A_{\mu,n})] \\ &= -\frac{1}{2} \sum_{\substack{n \in \Lambda \\ \mu}} \text{tr} \log(1 + N(\bar{A}_{\mu,n})) \\ &\quad - \frac{1}{2} \sum_{\substack{n \in \Lambda \\ \mu}} B^a(\bar{A}_{\mu,n}) \text{sgn}_{\mathcal{C}} \tilde{A}_{\mu,n}^a + \dots, \end{aligned} \quad (4.46)$$

where we used the abbreviation $A = \bar{A} + \frac{1}{2} \text{sgn}_{\mathcal{C}} \tilde{A}$. Note that $B^a(\bar{A}_{\mu,n})$ is given by the first order term of the logarithm when expanding with respect to \tilde{A} and evaluate it at $\tilde{A} = 0$. We note that this is a local function of the classical field \bar{A} . We observe that $B^a(\bar{A}_{\mu,n})$ has the same value on the forward and backward branch. This is in contrast to the term $\text{sgn}_{\mathcal{C}}$, which changes sign. Therefore, we conclude that the first order term vanishes. After establishing the fact that the linear terms in the response/quantum field leads to the classical equations of motion, the Haar measure will not deliver any quantum contributions to this order.

The zeroth order term is the Haar measure of the classical field in the functional integral, i.e.

$$\int [d\bar{A}] \exp(-S_M[\bar{A}]) = \int [d\bar{U}]. \quad (4.47)$$

This will appear naturally in the definition of the expectation value of observables given in (4.9). Note that the pure gauge part of the action S_G can be written as

$$S_G[A] = -\frac{1}{2} \sum_{n \in \Lambda} a_0 a_S^3 \operatorname{tr} \{ F_{\mu\nu,n}[A] F_n^{\mu\nu}[A] \} \quad (4.48)$$

up to higher orders in the lattice spacing. The field strength for non-Abelian gauge theories is given by $F_{\mu\nu,n} = t^a F_{\mu\nu,n}^a$ with

$$F_{\mu\nu,n}^a[A] = \partial_\mu A_{\nu,n}^a - \partial_\nu A_{\mu,n}^a - gf^{abc} A_{\mu,n}^b A_{\nu,n}^c. \quad (4.49)$$

The trace sums with respect to the adjoint gauge indices. The numbers f^{abc} are the structure constants of the $SU(N)$ gauge group. We will express this theory in terms of the classical fields \bar{A} and quantum fields \tilde{A} . This results in three parts: a free part S_1 , an interacting part S_2 being linear in \tilde{A} , and an interacting part S_3 , which contains all parts not being linear in the gauge field \tilde{A} . Hence, we get

$$S_G[\bar{A}, \tilde{A}] = S_1 + S_2 + S_3. \quad (4.50)$$

The individual expressions are determined by

$$S_1 = \sum_{n_1} \tilde{A}_{\nu,n_1}^a \partial_\mu [\partial^\mu \bar{A}_{n_1}^{\nu,a} - \partial^\nu \bar{A}_{n_1}^{\mu,a}], \quad (4.51a)$$

$$S_2 = \frac{1}{2} \sum_{n_1 n_2 n_3} V_{\mu\nu\rho}^{(3)abc}(n_1, n_2, n_3) \tilde{A}_{n_1}^{\mu,a} \bar{A}_{n_2}^{\nu,b} \bar{A}_{n_3}^{\rho,c} \\ + \frac{1}{6} \sum_{n_1 n_2 n_3 n_4} V_{\mu\nu\rho\sigma}^{(4)abcd}(n_1, n_2, n_3, n_4) \tilde{A}_{n_1}^{\mu,a} \bar{A}_{n_2}^{\nu,b} \bar{A}_{n_3}^{\rho,c} \bar{A}_{n_4}^{\sigma,d}, \quad (4.51b)$$

$$S_3 = \frac{1}{6} \sum_{n_1 n_2 n_3} V_{\mu\nu\rho}^{(3)abc}(n_1, n_2, n_3) \tilde{A}_{n_1}^{\mu,a} \tilde{A}_{n_2}^{\nu,b} \tilde{A}_{n_3}^{\rho,c} \\ + \frac{1}{8} \sum_{n_1 n_2 n_3 n_4} V_{\mu\nu\rho\sigma}^{(4)abcd}(n_1, n_2, n_3, n_4) \tilde{A}_{n_1}^{\mu,a} \tilde{A}_{n_2}^{\nu,b} \tilde{A}_{n_3}^{\rho,c} \bar{A}_{n_4}^{\sigma,d}. \quad (4.51c)$$

In the last expression we suppressed the lattice spacings in order to simplify the notation. The symmetrized three- and four-point vertices of the

gauge theory are denoted by $V^{(3)}$ and $V^{(4)}$ and are given in terms of \bar{A} and \tilde{A} . We will provide the continuum expressions for the vertex of the three gluon interaction

$$\begin{aligned}
V_{\mu\nu\rho}^{(3)abc}(x_1, x_2, x_3) = & \\
& gf^{abc}\eta_{\mu\nu}(\delta_{x_2,x_3}\partial_\rho^{x_1}\delta_{x_1,x_2} - \delta_{x_1,x_3}\partial_\rho^{x_2}\delta_{x_2,x_1}) \\
& + gf^{abc}\eta_{\mu\rho}(\delta_{x_1,x_2}\partial_\nu^{x_3}\delta_{x_3,x_1} - \delta_{x_2,x_3}\partial_\nu^{x_1}\delta_{x_1,x_3}) \\
& + gf^{abc}\eta_{\nu\rho}(\delta_{x_1,x_3}\partial_\mu^{x_2}\delta_{x_2,x_1} - \delta_{x_1,x_2}\partial_\mu^{x_3}\delta_{x_3,x_1}), \quad (4.52)
\end{aligned}$$

and the vertex of the four gluon interaction

$$\begin{aligned}
V_{\mu\nu\rho\sigma}^{(4)abc}(x_1, x_2, x_3, x_4) = & \delta_{x,y}\delta_{x,w}\delta_{x,z} \\
& \times \left[-\frac{1}{4}g^2 f^{abe} f^{cde} (\eta_{\rho\mu}\eta_{\sigma\nu} - \eta_{\mu\sigma}\eta_{\nu\rho}) \right. \\
& \quad - \frac{1}{4}g^2 f^{ace} f^{bde} (\eta_{\mu\nu}\eta_{\sigma\rho} - \eta_{\mu\sigma}\eta_{\nu\rho}) \\
& \quad \left. - \frac{1}{4}g^2 f^{ade} f^{cbe} (\eta_{\mu\rho}\eta_{\sigma\nu} - \eta_{\mu\nu}\eta_{\rho\sigma}) \right]. \quad (4.53)
\end{aligned}$$

of the SU(N) gauge theory. The Minkowski metric is given by $\eta = \text{diag}(1, -1, -1, -1)$. There are also expressions for the vertices without moving to a continuum notation for $V^{(3)}$ and $V^{(4)}$ and can be found in [37].

Finally, we wish to obtain the classical-statistical approximation of the partition function. Therefore, we neglect the contribution S_3 including the non-linear terms in the quantum field \tilde{A} . Note that the fermionic contribution to the action can again be integrated out. The fermions lead once more to $\text{Tr} \log \Delta_c^{-1}[A]$ and which is then expanded in the quantum field \tilde{A} . We observe once again, that the linear term in \tilde{A} is proportional to the fermion current. This physical quantity is determined by

$$\bar{j}^{a,\nu}(x) = \frac{g}{2} \text{tr} \left\{ \langle [\bar{\psi}_n, \psi_n] \rangle_{\bar{A}} \gamma^\nu t^a \right\} \quad (4.54)$$

and is dependent on the gauge indices. The trace is with respect to the

Dirac and fundamental gauge indices. At this point the remainder of the derivation will follow the Abelian U(1) case. We conclude that the partition function for the SU(N) gauge theory interacting with fermionic matter in the classical-statistical approximation is expressed in a similar way as (4.39). It is expected that the equation of motion is now determined by the classical Yang-Mills equation

$$\partial_\mu \bar{F}_n^{\mu\nu,a} + g f^{abc} A_{\mu,n}^b \bar{F}_n^{\mu\nu,c} = \frac{g}{2} \text{tr} \left\{ \langle [\bar{\psi}_n, \psi_n] \rangle_{\bar{A}} \gamma^\nu t^a \right\}. \quad (4.55)$$

4.2 Diagrammatics

After obtaining the classical-statistical approximation for the underlying U(1) and SU(N) gauge theories coupled to fermionic matter we will give a diagrammatic analysis.

4.2.1 Classical and Quantum Vertices

$$\text{Tr} \log \Delta_c^{-1}[A] = g \text{ (diagram)} + g^2 \text{ (diagram)} + g^3 \text{ (diagram)} + g^4 \text{ (diagram)} + \dots$$

FIGURE 4.2: Diagrammatic representation of $\text{Tr} \log \Delta_c^{-1}[A]$ as given in (4.56), with numerical prefactors being omitted. The fermion lines here denote free propagators $\Delta_c[0]$.

Starting from the expression (4.16) of the Abelian U(1) gauge theory where the fermions have been integrated out we consider the following expansion

$$\text{Tr} \log \Delta_c^{-1}[A] = - \sum_{m=1}^{\infty} \frac{(ig)^m}{m} \text{Tr}(\Delta_c[0] A)^m. \quad (4.56)$$

Note that this expression neglects constant contributions [68]. We represent this expansion in diagrams given in Fig. 4.2 showing the correspondence of the m -th term with the m -th diagram. If we express each term in the expansion (4.56) in terms of the classical field \bar{A} and the quantum field \tilde{A} , the photon lines in Fig. 4.2 will be replaced by the classical contribution \bar{A} or quantum contribution \tilde{A} , respectively. The essence of this

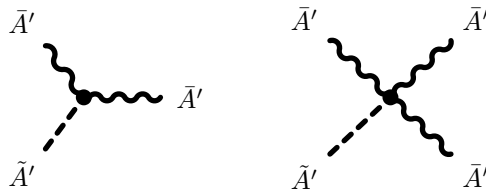


FIGURE 4.3: The classical vertices S_2 of the SU(N) gauge theory, which are independent of the coupling g in terms of the rescaled fields \bar{A}' and \tilde{A}' .

expansion becomes obvious when we rescale the fields as

$$\bar{A} = g^{-1} \bar{A}', \quad (4.57a)$$

$$\tilde{A} = g \tilde{A}'. \quad (4.57b)$$

Note that the Abelian U(1) gauge action (4.21) is invariant with respect to such a transformation since it contains one classical and one quantum field. This is also true for the free part S_1 in the SU(N) gauge action (4.51). All these contributions do not depend on the coupling g . However, in a non-Abelian gauge theory, we have to take into account the self-interactions as they are present in S_2 and S_3 . The contribution of S_2 is independent of g , which can be seen after rescaling the fields as it is shown in Fig. 4.3. All coupling-independent non-linear parts will contribute to the classical vertices. Complementary, the contribution of S_3 is a quantum vertex since it is proportional to g^4 using the rescaled fields, cf. Fig. 4.4. Performing the classical-statistical approximation of pure gauge theories we neglect S_3 because it only contains non-linear terms in \tilde{A} . After rescaling (4.57) an explicit coupling dependence is not present anymore in the classical gauge dynamics. However, the coupling will enter in the initial conditions.

Considering fermions, we observe that the rescaling of the field will still lead to a coupling dependence due to the quantum nature of the fermions. The expansion of $\text{Tr} \log \Delta_c^{-1}[A]$ in the coupling using rescaled fields leads to the expression

$$\begin{aligned} \text{Tr} \log \Delta_c^{-1}[A] &= \text{Tr} \log \Delta_c^{-1}[g^{-1}\bar{A}'] \\ &+ g^2 \frac{i}{2} \text{Tr} \{ \Delta_c[g^{-1}\bar{A}'] \text{sgn}_c \tilde{A}' \} + \mathcal{O}(g^4) + \dots \end{aligned} \quad (4.58)$$

Such an expansion in the coupling g becomes more feasible by connecting it to the expansion in the rescaled quantum field \tilde{A}' . The first term $\text{Tr} \log \Delta_c^{-1}[g^{-1}\bar{A}']$ will vanish due to the normalization given in (4.23). The second term is proportional to g^2 . However, this term also contains all diagrams with only classical fields \bar{A}' except for one quantum field \tilde{A}' and is the diagrammatic interpretation of (4.24). All the terms being proportional to g^4 contain two quantum fields \tilde{A}' , the terms containing g^6 involve three quantum fields \tilde{A}' , and so on. The explicit diagrammatic representation is given in Fig. 4.5. We emphasize that the contributions proportional to g^2 in the rescaled fields contain an infinite number of terms.

We remind ourselves, that the classical-statistical approximation neglects all terms in (4.58) containing more than one quantum field \tilde{A}' . On the other hand, this shows that the classical-statistical approximation is exact to order g^2 in the coupling constant. Hence, we conclude that the classical-statistical approximation should be valid as long $g \ll 1$. The restriction to weak couplings is important. However, we note that a theory can be strongly correlated despite small couplings, e.g. in the presence of large

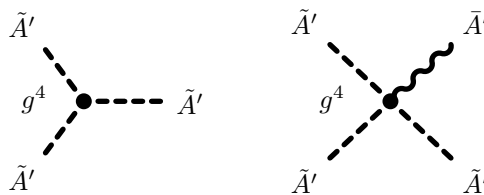


FIGURE 4.4: The quantum vertices S_3 of the non-Abelian gauge theory, which are of order g^4 in terms of the rescaled fields \bar{A}' and \tilde{A}' .

$$\text{Tr log } \Delta_C^{-1}[A] = g^2 \left[\begin{array}{c} \text{---} \bigcirc \text{---} + \text{---} \bigcirc \text{---} \text{---} + \text{---} \bigcirc \text{---} \text{---} \text{---} + \text{---} \square \text{---} \text{---} \text{---} + \dots \end{array} \right] \\ + g^4 \left[\begin{array}{c} \text{---} \bigcirc \text{---} \text{---} + \text{---} \bigcirc \text{---} \text{---} \text{---} \text{---} + \text{---} \square \text{---} \text{---} \text{---} \text{---} + \text{---} \square \text{---} \text{---} \text{---} \text{---} + \dots \end{array} \right] + \dots$$

FIGURE 4.5: Diagrammatic representation of Fig. 4.2 in terms of the rescaled field \bar{A}' and \tilde{A}' . The term proportional to g^2 corresponds to the coupling of \tilde{A}' to the fermion current (4.24). All higher order terms $\mathcal{O}(g^4)$ are neglected in the classical-statistical approximation.

fields or occupation numbers. In particular, the classical-statistical approximation can be used to discuss the corresponding non-perturbative physics in QED, or also QCD out of equilibrium, if the gauge coupling is small enough. A detailed discussion of the situations, where one expects the classical-statistical description to be valid, is discussed in the next section.

4.2.2 Classicality Condition

For small couplings $g \ll 1$, which are required by the classical-statistical approximation, we can describe large classical fields $\bar{A} \sim \mathcal{O}(1/g)$ if we rescale as in (4.57). The initial value problems, which we discuss in this thesis, implement this conditions in the initial state. In particular we will consider (Coulomb gauge) Gaussian initial conditions for the discrete Fourier transformed gauge fields

$$\bar{A}_{i,(0,\mathbf{n})} \equiv \mathcal{A}_i + \frac{1}{V} \sum_{\mathbf{q} \in \tilde{\Lambda}^*} e^{i\mathbf{q} \cdot \mathbf{x}_n} \bar{A}_{i,\mathbf{q}}. \quad (4.59)$$

For details we refer to Appendix C. We introduce the following notation for the coherent fields

$$\langle \bar{A}_{i,(0,\mathbf{n})} \rangle = \mathcal{A}_i, \quad (4.60a)$$

where we used $\langle \bar{A}_{i,\mathbf{q}} \rangle = 0$, and the connected two-point correlation function is given as

$$\langle \bar{A}_{i,\mathbf{q}} \bar{A}_{j,\mathbf{q}} \rangle = \frac{V}{\omega_{\mathbf{q}}} \left(\frac{1}{2} + n_{\mathbf{q}} \right) \mathcal{P}_{ij}. \quad (4.61a)$$

In addition one has to fix the expectation values of the first-order time derivatives of the field. Note that $n_{\mathbf{q}}$ delivers the initial occupation number of frequency $\omega_{\mathbf{q}}$. The transverse projector is denoted by \mathcal{P}_{ij} . If we consider quantum fluctuations, the occupation number will be given by $n_{\mathbf{q}} = 0$. However, we can still get a valid classical-statistical description if we consider a large initial coherent field

$$\mathcal{A}_i \sim \mathcal{O}(1/g). \quad (4.62)$$

In particular this is relevant for the initial conditions of the Schwinger pair production. This will be considered in Sec. 4.3.

On the other hand, if we describe small coherent fields, but consider large initial occupation numbers

$$1 \ll n_{\mathbf{q}} \lesssim \mathcal{O}(1/g^2), \quad (4.63)$$

for characteristic momenta \mathbf{q} , this will still lead to an accurate description of the underlying quantum dynamics. Considering the time evolution of large coherent fields or high occupation numbers one has to monitor its behavior in order to ensure the validity of the classical-statistical simulations. We will stop the time-evolution as soon as the characteristic time-dependent occupation numbers become of order one.

It is highly important that the late-time evolution leading to thermal equilibrium, involving characteristic occupancies of order one at the typical

momenta given by the temperature, cannot be described by the classical-statistical approach. It should be clear that a classical-statistical approximation will suffer from Rayleigh-Jeans divergencies, if the theory is not regularized by an ultraviolet cutoff. However, this is no restriction, if we use the classical-statistical approximation at sufficiently early times and respect the classicality conditions: Given a finite ultraviolet cutoff Λ of a lattice regularized theory, the dynamics should be dominated by the large coherent fields or the large occupations given the coupling constant was chosen sufficiently small. The large field and the large occupation numbers should not be present close to the UV-cutoff. In such a situation the results are insensitive to modifications in the ultraviolet cutoff scale. This insensitivity indicates the applicability of the classical-statistical approximation. This has been explained in detail for a scalar field theory [69].

Note that such a classicality condition restricts the bosonic sector and the analysis is analog to the scalar field theory studies of [30, 33]. Another way to state the classicality condition is that the anti-commutator expectation values, such as $|\langle \bar{A} \bar{A} \rangle|$, for typical bosonic field modes dominate in comparison to the commutators $|\langle \tilde{A} \bar{A} - \bar{A} \tilde{A} \rangle|$. We emphasize that there is one factor of the quantum field \tilde{A} more than in the corresponding anti-commutator. This will allow for a discussion of the classicality condition without referring to occupation numbers. Nevertheless, occupation numbers are often not problematic in practice since we check them at rather high momenta, where we expect that gauge fixed quantities are acceptable when using perturbation theory [63].

4.3 Real-time Simulation of Quantum Electrodynamics

This section gives an explicit algorithm, how the classical-statistical approximation can be solved. Generally speaking we have to numerically solve an initial value problem on a space-time lattice. Indicated in Sec. 4.1.1, these numerical calculations will be performed using the link

variables $U_{\mu,n}$ instead of the gauge fields $A_{\mu,n}$. Because we are mainly interested in the Schwinger pair production we will restrict ourselves to U(1) gauge theory coupled to fermions. The generalization to SU(N) gauge theory follows along the very same lines and was already employed in [70].

4.3.1 Lattice Action

We reconsider the Wilsonian action on a real-time lattice (4.4). For a U(1) gauge theory this can be written as

$$S_G [U] = \frac{1}{g^2} \sum_{n \in \Lambda^+} \sum_i \frac{a^4}{a_0^2 a_i^2} \text{Re Tr} (1 - U_{0i,n}) - \frac{1}{g^2} \sum_{n \in \Lambda^+} \sum_{\substack{i,j \\ i < j}} \frac{a^4}{a_i^2 a_j^2} \text{Re Tr} (1 - U_{ij,n}), \quad (4.64)$$

where we introduced the notation $a^4 \equiv a_0 a_1 a_2 a_3$. Since we allow anisotropic lattices we will distinguish between the different a_i with $i \in \{1, 2, 3\}$. It is clear from our discussion in Sec. 4.1 that we only have to consider the forward branch of the Schwinger-Keldysh contour. The spatial and temporal plaquettes correspond to the electric and the magnetic field and are defined as

$$E_{i,n} = \frac{1}{g a_0 a_i} \text{Im} U_{0i,n}, \quad (4.65a)$$

$$B_{i,n} = -\frac{1}{2g a_j a_k} \epsilon_{ijk} \text{Im} U_{ij,n}. \quad (4.65b)$$

Note that we will consider a central derivative discretization as outlined in (4.7) for the fermionic fields. The fermion doubling problem, which naturally arises in a lattice formulation of fermions [71], can be circumvented in several different ways [72–75]. We will use Wilson fermions, since they

can be used in a theory without any chiral symmetry:

$$S_F[\psi, \bar{\psi}, U] = a^4 \sum_{n \in \Lambda^+} \bar{\psi}_n \left[i\gamma^\mu \frac{U_{\mu,n}\psi_{n+\hat{\mu}} - U_{-\mu,n}\psi_{n-\hat{\mu}}}{2a_\mu} - M\psi_n + \sum_i \frac{U_{i,n}\psi_{n+\hat{i}} - 2\psi_n + U_{-i,n}\psi_{n-\hat{i}}}{2a_i} \right]. \quad (4.66)$$

The last contribution is present due to the discretized second derivative term and vanishes in the naive continuum limit $a_i \rightarrow 0$. The Wilson term ensures that spatial doubler modes are suppressed. In particular the low-momentum excitations show a low-energy particle-like dispersion relation. We do not include a Wilson term for the temporal direction since the doubler modes are suppressed for appropriate initial conditions. This applies if the temporal lattice spacing is much smaller than the spatial lattice spacing, $a_0 \ll a_i$ [28, 76]. In order to simplify the calculation, we use the gauge freedom and set $U_{0,n} = 1$. This is the lattice version of the temporal-axial gauge condition $A_{0,n} = 0$.

4.3.2 Equations of Motion

Using the action $S_G[U] + S_F[\psi, \bar{\psi}, U]$ we obtain discretized equations of motion by varying the dynamical degrees of freedom. For the fermionic fields, these are given

$$\psi_{n+\hat{0}} = \psi_{n-\hat{0}} - 2ia_0 \left(M + \sum_i \frac{1}{a_i} \right) \gamma^0 \psi_n + \sum_i \frac{a_0}{a_i} [(i + \gamma^i) \gamma^0 U_{i,n} \psi_{n+\hat{i}} + (i - \gamma^i) \gamma^0 U_{-i,n} \psi_{n-\hat{i}}], \quad (4.67)$$

where we employed the temporal-axial gauge. Since we wish to calculate the Dirac field $\psi_{n+\hat{0}}$ we have to determine the link $U_{i,n}$ as well as the Dirac field at the two time slices ψ_n and $\psi_{n-\hat{0}}$. This is due to the central derivative discretization of the Dirac action $S_F[\psi, \bar{\psi}, U]$. Hence, we need two initial values for the Dirac field at the two time slices $n_0 = \{0, 1\}$. In an

explicit simulation, we take $\psi_{(0,\mathbf{n})}$ according to the chosen initial condition and perform a free field evolution of this state in order to obtain a consistent value for $\psi_{(1,\mathbf{n})}$. This choice of initial conditions also keeps the temporal doubler mode unexcited [76].

The equations of motion of the gauge sector (4.40) now contain a contribution of the Keldysh two-point function:

$$\Delta_{n,m}^K = \langle [\psi_n, \bar{\psi}_m] \rangle . \quad (4.68)$$

We evaluate this object by mode function expansion as described in Appendix B. Another way to do this is possible using so-called ‘low-cost’ fermions [77]. However, using the former approach the equations of motion (4.67) are essentially equations of motion for the mode functions denoted by $\Phi_{\lambda,n,\mathbf{q}}^u$ and $\Phi_{\lambda,n,\mathbf{q}}^v$.

The Gauss’s law constraint in temporal axial gauge is given by

$$\sum_i \frac{E_{i,n} - E_{i,n-\hat{i}}}{a_i} = -\frac{g}{2} \text{Re tr} \{ \Delta_{n+\hat{0},n}^K \gamma^0 \} , \quad (4.69)$$

and the trace is performed with respect to the Dirac indices. This equation is a constraint and has to be satisfied at each time step. In particular the initial field configuration has to fulfill this condition. This implies that a field configuration which fulfills Gauss’s law at initial times $n_0 = 0$ will respect it at later times $n_0 > 0$.

Finally, in order to obtain a self consistent system of equations the equation of motion of the electric field is determined by

$$\begin{aligned} E_{i,n} &= E_{i,n-\hat{0}} - \frac{a_0}{ga_i} \sum_{j \neq i} \frac{\text{Im}[U_{ij,n} + U_{ji,n-\hat{j}}]}{a_j^2} \\ &+ \frac{ga_0}{2} \text{Re tr} \{ \Delta_{n+\hat{i}}^K (\gamma^i - i) U_{i,n} \} . \end{aligned} \quad (4.70)$$

Note that this equation corresponds to Ampere’s circuit law.

4.3.3 Numerical Algorithm

Now, we want to present a numerical algorithm that can be used to solve the above set of equations:

1. *Initial conditions:*

$$n_0 = 0 : \quad \psi_{(0,\mathbf{n})}, E_{i,(0,\mathbf{n})}, \quad (4.71a)$$

$$n_1 = 0 : \quad \psi_{(1,\mathbf{n})}, U_{i,(1,\mathbf{n})}. \quad (4.71b)$$

2. *Solving the equations of motion:*

2a. *Discretized Dirac equation:* Given ψ_{n-0}, ψ_n and $U_{i,n}$ obtain the Dirac field at ψ_{n+0} according to (4.67).

2b. *Discretized Electric field evolution:* Given $E_{i,n-\hat{0}}, \psi_n$ and $U_{i,n}$ obtain the electric field $E_{i,n}$ according to (4.70).

2c. *Spatial link propagation:* Calculate the temporal plaquette

$$U_{0i,n} = \sqrt{1 - (ga_0a_iE_{i,n})^2} + i ga_0a_iE_{i,n}. \quad (4.72)$$

Obtain the link $U_{i,n+\hat{0}}$ from

$$U_{i,n+\hat{0}} = U_{0i,n}U_{i,n}. \quad (4.73)$$

2d. Reiterate the steps 2a – 2c.

3. *Classical-statistical sampling:*

Reiterate the steps 1 – 2. Average the solutions to determine the observables.

4.3.4 Initial Conditions

Both the fermion sector and the gauge sector need individual initial conditions. We will assume that these two sectors decouple at initial times and consider both sectors as free.

For the fermions, we determine the Dirac vacuum being characterized by the correlation functions

$$\langle \psi_{(0,\mathbf{n})} \rangle = \langle \bar{\psi}_{(0,\mathbf{n})} \rangle = 0, \quad (4.74a)$$

$$\Delta_{(0,\mathbf{n}), (0,\mathbf{m})}^K = \frac{1}{V} \sum_{\mathbf{q} \in \tilde{\Lambda}} \frac{\bar{M} - \gamma^i \bar{p}_i}{\bar{\omega}} e^{i\mathbf{p} \cdot (\mathbf{x}_n - \mathbf{x}_m)}. \quad (4.74b)$$

The details leading to this result can be found in Appendix B.

In the gauge sector the initial state will be modeled by a Gaussian state. Such states are completely characterized by the one-point and two-point correlation functions of the gauge field [78]. Note that we have to choose a gauge condition in order to fix the initial correlations. As mentioned before, we will focus on the temporal-axial gauge, where $A_{0,n} = 0$. On the lattice the temporal axial gauge is given by $U_{0,n} = 1$. There is a remaining residual gauge invariance under time-independent gauge transformations [79]. We will exploit this gauge freedom at initial times $n_0 = 0$ to enforce

$$\sum_i \frac{A_{i,(0,\mathbf{n})} - A_{i,(0,\mathbf{n}-\hat{i})}}{a_i} = 0. \quad (4.75)$$

In order to describe a coherent field with vacuum fluctuations, we fix the one-point correlation functions

$$\langle A_{i,(0,\mathbf{n})} \rangle = \mathcal{A}_i, \quad (4.76a)$$

$$\langle E_{i,(0,\mathbf{n})} \rangle = \mathcal{E}_i, \quad (4.76b)$$

where \mathcal{A}_i and \mathcal{E}_i are the coherent fields. In addition we focus on the two-point correlation functions

$$\langle \{A_{i,(0,\mathbf{n})}, A_{j,(0,\mathbf{m})}\} \rangle_c = \frac{1}{V} \sum_{\mathbf{q} \in \tilde{\Lambda}} \frac{1}{|\tilde{\mathbf{p}}|} \mathcal{P}_{ij} e^{i\mathbf{p} \cdot (\mathbf{x}_n - \mathbf{x}_m)}, \quad (4.77a)$$

$$\langle \{E_{i,(0,\mathbf{n})}, E_{j,(0,\mathbf{m})}\} \rangle_c = \frac{1}{V} \sum_{\mathbf{q} \in \tilde{\Lambda}} |\tilde{\mathbf{p}}| \mathcal{P}_{ij} e^{i\mathbf{p} \cdot (\mathbf{x}_n - \mathbf{x}_m)}, \quad (4.77b)$$

where \mathcal{P}_{ij} is the transverse projector. All the calculational details connected to the initial conditions can be found in Appendix C.

Initially we set the vacuum modes only up to a finite momentum scale. This scale is chosen to be below the ultraviolet cutoff. This choice ensures that the energy density of the vacuum modes is small and will not significantly contribute to the dynamics of the system. We choose this finite momentum scale at $5M$ in the following and verified the independence of the result by additional calculations varying this value.

4.4 Fermion Production in Three Dimensions

As a first application we consider the production of electron-positron pairs by a large coherent field, the so called Schwinger mechanism [10, 80, 81]. In order to quantify the production we define the dimensionless field strength parameter

$$\epsilon_0 = \frac{gE_0}{M^2} . \quad (4.78)$$

In this chapter, the presented numerical results are performed for $g = 0.3$ and $\epsilon_0 = 3$.

In the gauge sector, we will consider the one-point correlation function of the electric field. On the other hand we present results for the total fermion density $N(t)/V$ being the number of electrons per volume. Further we determine the normalized momentum distribution $n(p, t)$.

4.4.1 Schwinger Mechanism

In a first calculation we neglect the back-reaction of the fermion current on the gauge fields (4.70) and the classical-statistical sampling. In this way we can compare to analytically known continuum results. In addition we show that they can be reproduced with our real-time lattice simulations.

We choose the Dirac vacuum as our initial conditions for the fermions. Under all these assumption we only have to evolve the fermion equation of motion (4.67) with a sudden switching-on of the electric field at $n_0 = 0$.

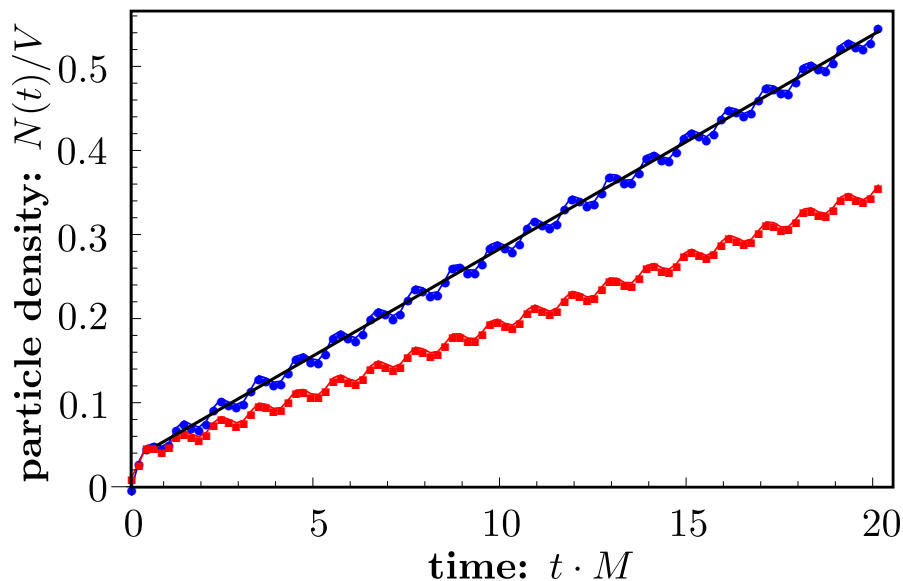


FIGURE 4.6: Time evolution of the total fermion density $N(t)/V$ for $\epsilon_0 = 3$ with lattice parameters $a_0 = 0.002/M$, $a_3 = 0.05/M$, $N_{1,2} = 12$, $N_3 = 40$. Shown is a comparison of the continuum expression (black) with numerical results for $a_{1,2} = 0.75/M$ (red) and $a_{1,2} = 0.25/M$ (blue).

The evolution of the total fermion density, $N(t)/V$ at $\epsilon_0 = 3$ and two sets of different spatial lattice spacings a_i is depicted in Fig. 4.6.

We distinguish between two regimes: At early times ($t_{\text{tr}} \sim 1/M$) we see transient enhanced fermion production. This behavior can be explained by a quench in the electric field. In contrast, at subsequent times, we determined a linear growth of the fermion density. This is expected from the analytic continuum results, which are collected in the Appendix E:

$$\frac{\dot{N}(t)}{V} = \frac{M^4 \epsilon_0^2}{4\pi^3} \exp\left(-\frac{\pi}{\epsilon_0}\right). \quad (4.79)$$

Note that when deriving this analytical result the initial time is sent to $-\infty$ and it will not exhibit the transient/initial regime. The analytic result is given in Fig. 4.6 at times directly after the initial regime. The lattice results for $a_3 = 0.05/M$ and $a_{1,2} = 0.25/M$ coincide with the analytic result whereas the result for $a_{1,2} = 0.75/M$ shows deviations. In this respect the real-time lattice simulations are able to reproduce known results for small spatial lattice spacings. Note that we still observe deviations from the analytic results due to the numerical restriction caused by small lattices. Moreover, the numerical results oscillate around the analytical curve. This is due to the fact that we are not able to fully resolve the momentum space with $N_3 = 40$ grid points.

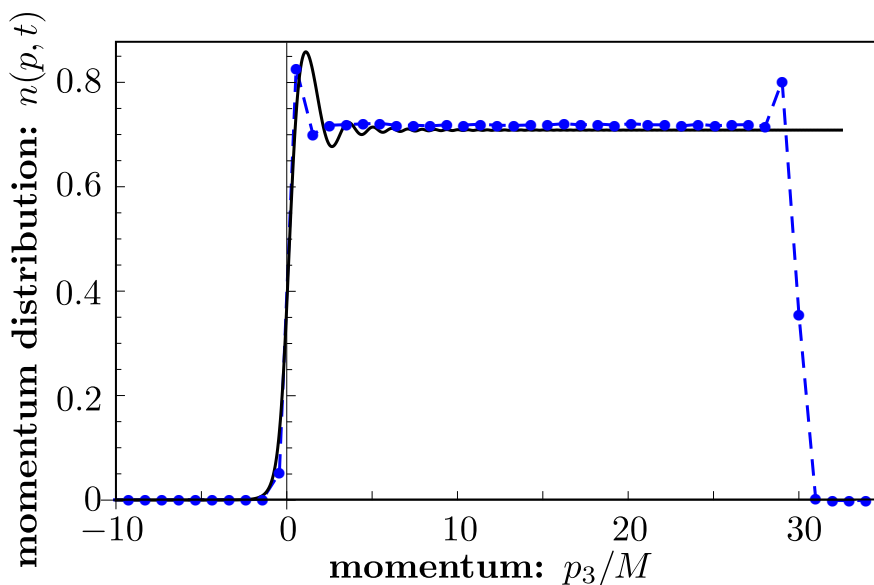


FIGURE 4.7: Comparison of the continuum expression (black) with the normalized momentum distribution $n(p, t)$ (blue) for $\epsilon_0 = 3$ at $p_{1,2} = 0$ and $t = 20/M$. The parameters are $a_0 = 0.001/M$, $a_{1,2} = 0.5/M$, $a_3 = 0.05/M$, $N_{1,2} = 12$, $N_3 = 64$ such that $V = 115.2/M^3$.

The normalized momentum distribution $n(p, t)$ for $\epsilon_0 = 3$, $p_1 = p_2 = 0$ at $t = 20/M$ is depicted in Fig. 4.7. This can be compared to the analytic continuum value $f(p)$, which can be found in Appendix E. The quantity $f(p)$ measures the electric field energy being transformed into virtual electron–positron pairs. This is visible at the distinctive peak around kinetic momenta $p = 0$. Choosing a large field strength, the charged excitations are separated and become real electron–positron pairs. The electric

field will accelerate these real particles since we neglect the back-reaction in this section. In this way the particles gain momentum up to $p \rightarrow \infty$.

There is agreement when comparing the numerical simulation and the analytic result. Nevertheless there is a qualitatively different behavior for large momenta. Note that the analytic result assumes a static electric field such that all momenta up to $p \rightarrow \infty$ are occupied. In the numerical simulation the peak at large momenta is a consequence due to the initial particle production from the vacuum. The quench in the electric field enhances the particle production at early times $t_{\text{tr}} \sim 1/M$. This results in the single peak around $p = 0$ propagating to higher momenta during the time evolution.

4.4.2 Back-reaction and Plasma Oscillations

In this section, we include back-reaction of the fermion current on the gauge fields (4.70) and perform the classical-statistical sampling. As a matter of fact, we find that a very small number of field configurations is needed since the physics is completely determined by the large zero-mode of the electric field. We perform five distinct runs and observe that the individual realizations differ marginally when calculating volume averaged quantities.

We compare the time evolution of the total fermion density $N(t)/V$ for $\epsilon_0 = 3$ with and without including the effect of the fermionic current. This is shown in Fig. 4.8. The particle number grows linearly without including the effect of the produced fermionic current. The picture changes when we consider the fermion density with back-reaction. The particle number of the fermions develops into a staircase structure with decreasing step height.

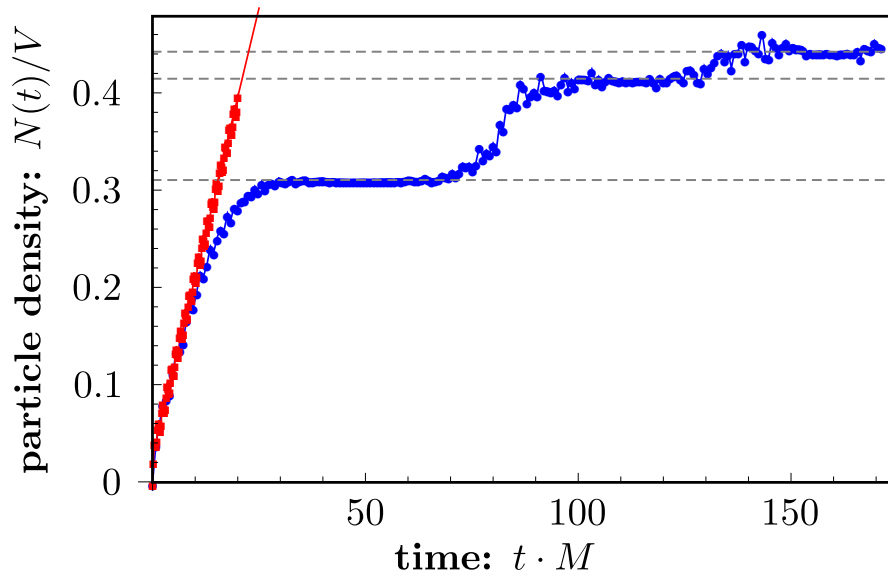


FIGURE 4.8: Time evolution of the total fermion density $N(t)/V$ for $\epsilon_0 = 3$ with lattice parameters $a_0 = 0.002/M$, $a_{1,2} = 0.5/M$, $a_3 = 0.05/M$, $N_{1,2} = 12$, $N_3 = 40$ such that $V = 72/M^3$. The straight line depicts the result without the back-reaction of fermions and the horizontal dashed lines indicate the plateaus in the fermion density.

This qualitative feature is accessible, when considering the volume averaged electric field

$$\langle E_3(t) \rangle = \frac{1}{V} \sum_{\mathbf{n} \in \Lambda} E_{3,n} \quad (4.80)$$

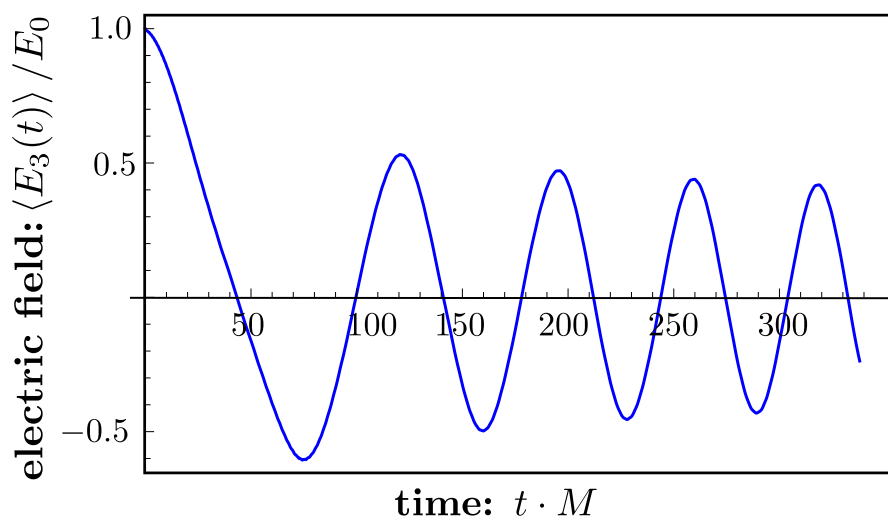


FIGURE 4.9: The volume averaged electric field $\langle E_3(t) \rangle$ as a function of time. The parameters are the same as in Fig. 4.8.

for longer times in Fig. 4.9. The initial state enforces the expectation values of the electric components $\langle E_{1,2}(t) \rangle$ and the magnetic components $\langle B_i(t) \rangle$ to be zero. Initially at $t = 0$ the electron-positron pairs are created and subsequently accelerated. In this way a fermionic current arises. This leads to an electric field counteracting the initial electric field. Note that the electric field changes sign and reaches a first local minimum. The electric field increases again, changes sign, reaches again a local maximum and this continues. These plasma oscillations are in accordance with an alternative investigation [58, 82, 83].

The oscillation of the electric field can also be found in the fermion sector. The particle production terminates when the magnitude of the field strength is too small. This leads to the plateau structure in $N(t)/V$. However, when the electric field reaches a local extremum, the pair production is present again. The envelope of the electric field decreases with time. The oscillation frequency of the electric field increases with the number of produced fermions.

We show the normalized momentum distribution $n(p, t)$ at different times

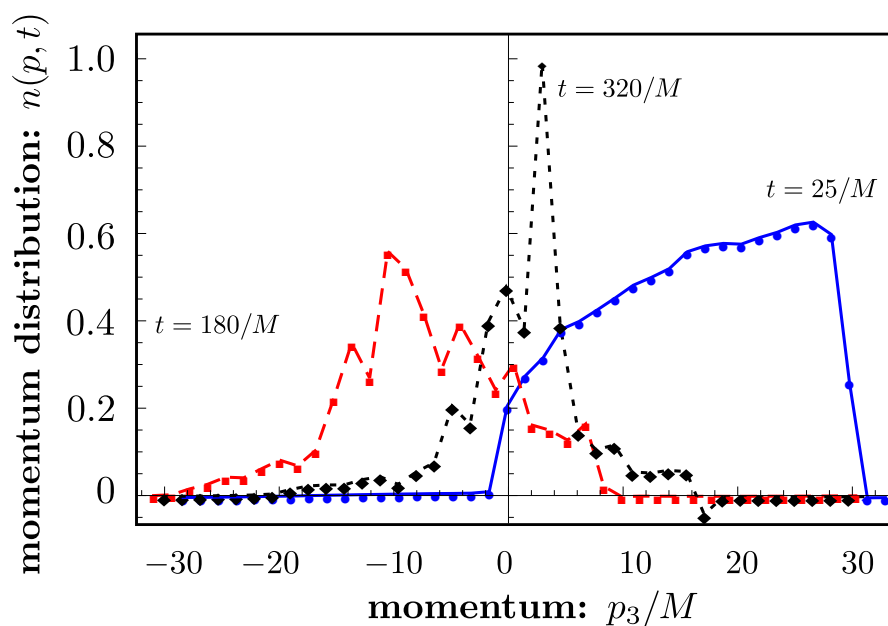


FIGURE 4.10: Normalized momentum distribution $n(p, t)$ for $\epsilon_0 = 3$ at $p_{1,2} = 0$. The parameters are identical to Fig. 4.8.

in Fig. 4.10. For the definition of the momentum distribution see Appendix D. Since the electric field changes its sign in a repetitive manner, the electrons and positrons are accelerated in an oscillatory way in momentum space. This results in a peaked distribution which oscillates around $p = 0$, similar to the electric field. In the next chapter we will use a similar approach to tackle lattice gauge theories built from cold atom systems.

Chapter 5

Strong Field QED with Cold Atoms

In chapter 3 we introduced an experimental setup which can be used to quantum simulate a one-dimensional U(1) gauge theory coupled to fermionic matter. In addition, we elaborated a theoretical approach to study such gauge theories in the classical-statistical regime in chapter 4. Consequently, we will combine the content of both chapters and investigate the non-equilibrium dynamics of gauge theories realized by cold atom systems. In this chapter, we will explore the time evolution of quantum link models in a yet less considered regime and test their ability to depict the physics of strong field QED. Depending on the observable, the realization of a U(1) gauge theory employing coherent many-body states may be preferable in comparison to proposals using single atoms [17–19].

In particular, we plan to study Schwinger pair production in the proposed cold atom experiment of chapter 3. This phenomena has not been observed directly because of the large electric fields [13], but it is a long standing prediction [11, 12] of quantum electrodynamics. The critical field strength $E_c = M^2/g \sim 10^{18} \text{V}/m$ is given by the electron mass M and the absolute value of the electric charge g of QED. However, the pair production phenomenon is determined by the dimensionless ratio $E/E_c \gtrsim 1$, where E is the electric field. Hence, changing the value of M and g in order to make E_c smaller would make the phenomenon more easily accessible. One reason why quantum simulations can be powerful is that

physical systems with vastly different scales can be used to investigate the same phenomena, because dimensionless ratios are identical. The proposed cold atom setup of chapter 3 allows for an investigation of pair production at a completely different scale than strong field QED [43, 84]. This experiment simplifies the realization of a strong electric field as we will show in the following.

When considering a system of ultracold atoms in an optical lattice as a quantum simulator for electron-positron pair production in QED, we will focus again on one spatial dimension. We remind ourselves that the key idea to realize gauge theories with cold atoms was the finite dimensional representation of the links. This allowed us to engineer a cold atom setup with a continuous $U(1)$ gauge invariance. Our experimental proposal has the possibility to directly tune the dimensionality of the local Hilbert spaces, which allows us to tune from a quantum link model to the Kogut-Susskind Hamiltonian [23]. We will always aim for the infinite dimensional Hilbert space of QED and study its approximation by experiments employing Bose-Einstein condensates interacting with fermionic atoms. The functional integral approach developed in the last chapter is a suitable tool to tune from a quantum link model towards the Wilson formulation of lattice gauge theory. In particular we study the necessary particle numbers per link in order to observe the QED phenomena of Schwinger pair production. In previous publications quantum link models were investigated for small dimensional representations of the link variable. This corresponds to using single atoms in order to realize the link. The employed techniques to study such states are diagonalization or matrix-product-states methods [35, 43, 85–87]. Note that the generalization of the functional integral representation to higher spatial dimensions and non-Abelian gauge theories was already presented in chapter 4 and applied in [36], but the aforementioned methods are difficult to use in these more general situations.

5.1 Kogut-Susskind and the Cold Atoms

One main result of chapter 2 was a formulation of lattice QED using the staggered fermion discretization. In particular, it is suitable for numerical simulations and it is a possible starting point for a U(1) gauge theory of a cold atom system [41]. The dynamical variables are the staggered fermion field ψ_n , the link U_n and the electric field E_n . They build the Kogut-Susskind Hamiltonian [21, 22] of QED given by

$$H_{\text{KS}} = \sum_n \left\{ \frac{a_S}{2} E_n^2 + M(-1)^n \psi_n^\dagger \psi_n - \frac{i}{2a_S} \left[\psi_n^\dagger U_n \psi_{n+1} - \psi_{n+1}^\dagger U_n^\dagger \psi_n \right] \right\}, \quad (5.1)$$

where a_S is the lattice spacing, M is the mass and g denotes the gauge coupling, which appears in the link $U_n = \exp(iga_S A_n)$. We discussed how to verify local gauge invariance employing Gauss's law (3.50). The proposed quantum simulator of chapter 3 can be described by the Hamiltonian

$$H_{\text{QL}} = \sum_n \left\{ \frac{g^2 a_S}{2} L_{z,n}^2 + M(-1)^n \psi_n^\dagger \psi_n - \frac{i}{2a_S \sqrt{\ell(\ell+1)}} \left[\psi_n^\dagger L_{+,n} \psi_{n+1} - \psi_{n+1}^\dagger L_{-,n} \psi_n \right] \right\}. \quad (5.2)$$

Both models can be connected by the substitution rule:

$$E_n \rightarrow g L_{z,n}, \quad (5.3)$$

$$U_n \rightarrow [\sqrt{\ell(\ell+1)}]^{-1} L_{+,n}, \quad (5.4)$$

$$U_n^\dagger \rightarrow [\sqrt{\ell(\ell+1)}]^{-1} L_{-,n}. \quad (5.5)$$

The structure of the commutator of link and electric field is not changed by this substitution. Further we force the Hilbert space of the links and the electric field finite to be finite. This is the main difference to the infinite dimensional QED case. The Schwinger boson representation was introduced

in (3.21). Inserting the latter into (5.2) we get the Hamiltonian

$$H_{\text{QL}} = \sum_n \left\{ \frac{g^2 a_S}{4} [b_n^\dagger b_n^\dagger b_n b_n + d_n^\dagger d_n^\dagger d_n d_n] + M(-1)^n \psi_n^\dagger \psi_n \right. \\ \left. - \frac{i}{2a_S \sqrt{\ell(\ell+1)}} \left[\psi_n^\dagger b_n^\dagger d_n \psi_{n+1} - \psi_{n+1}^\dagger d_n^\dagger b_n \psi_n \right] \right\}, \quad (5.6)$$

where we neglected irrelevant constants [23]. We use the density-phase representation for the Schwinger bosons

$$b_n = \sqrt{\ell + \delta\rho_{b,n}} e^{i\theta_{b,n}}, \quad (5.7)$$

$$d_n = \sqrt{\ell + \delta\rho_{d,n}} e^{i\theta_{d,n}}. \quad (5.8)$$

If we expand the square root in the density fluctuation $\delta\rho_{b,n}$ and $\delta\rho_{d,n}$, the connection between H_{KS} and H_{QL} becomes obvious and we observe

$$H_{\text{QL}} = H_{\text{KS}} + \mathcal{O}(\delta\rho/\ell). \quad (5.9)$$

Hence the total number of bosonic atoms per site 2ℓ can control the difference between (5.2) and (5.1).

5.2 Classical-Statistical Approach with Cold Atoms

Before performing the classical-statistical approximation for the Hamiltonian of the quantum simulator, we discuss if this approach can be used to study the strong field physics of QED. The initial electric field is of the order of the critical field strength $E_c = M^2/g$. In the cold atom experiment this corresponds to $|E_c| = g|N_b - N_d|/2 \sim M^2/g$, where N_b and N_d are the number of atoms in the bosonic modes. Considering $N_b, N_d \sim \mathcal{O}(\ell) \gg 1$, the dynamics in this regime can be accurately described using the developed functional integral approach in chapter 4. Similar criteria for the validity of the classical-statistical approximation can be found in [36, 88]. Hence, we can expect that the classical-statistical approximation is valid, when we study strong field QED.

Since the detailed derivation of the classical-statistical approximation was given in chapter 4, we can briefly point out the differences to the gauge theories presented there. We collect the bosonic fields in $\phi_n = (b_n^\dagger, b_n, d_n^\dagger, d_n)$ and define the generating functional in the presence of sources $J_n = (J_{b,n}, J_{b,n}^*, J_{d,n}, J_{d,n}^*)$ by $Z[J] = \text{Tr}\{\rho_0 T_{\mathcal{C}} e^{iJ \cdot \phi}\}$. Here, ρ_0 is the initial density matrix, $J \cdot \phi = \sum_n \int_{t,\mathcal{C}} J_n(t) \cdot \phi_n(t)$ with t the time coordinate along the closed time path \mathcal{C} , and $T_{\mathcal{C}}$ denotes time-ordering along \mathcal{C} . Employing the coherent state basis, the functional integral representation of the generating functional becomes

$$Z[J] = \int [d\phi][d\psi^\dagger d\psi] \langle + | \rho_0 | - \rangle e^{iS+iJ \cdot \phi}, \quad (5.10)$$

with the action

$$S = \int_t \sum_n (\psi_n^\dagger i\partial_t \psi_n + b_n^\dagger i\partial_t b_n + d_n^\dagger i\partial_t d_n) - H_{\text{QL}}, \quad (5.11)$$

and the $|+\rangle$ and $|-\rangle$ are the initial coherent states appearing on the forward and backward path leading to the matrix element of the density operator $\langle + | \rho_0 | - \rangle$, see Fig. 4.1.

Again the fermion degrees of freedom appear quadratically in the exponent. We integrate out the fermions and perform the Keldysh rotation, $\phi_n = \bar{\phi}_n + \text{sgn}_{\mathcal{C}} \tilde{\phi}_n$. Then we expand to first order in the bosonic response fields $\tilde{\phi}_n$. Note that neglecting the higher-order terms is justified in the classical-statistical regime [36]. In our case the corrections will be suppressed by factors of $N_b^{-1}, N_d^{-1} \ll 1$. This leads to the following set of self-consistent equations

$$\begin{aligned} i\partial_t b_n &= \frac{g^2 a_S}{2} b_n^\dagger b_n b_n + i \frac{d_n F_{n+1n}}{4a_S \sqrt{\ell(\ell+1)}}, \\ i\partial_t d_n &= \frac{g^2 a_S}{2} d_n^\dagger d_n d_n - i \frac{b_n F_{nn+1}}{4a_S \sqrt{\ell(\ell+1)}}, \\ i\partial_t F_{nm} &= \sum_{n'} [h_{nn'}^{\text{QL}} F_{n'm} - F_{nn'} h_{n'm}^{\text{QL}}]. \end{aligned} \quad (5.12)$$

Here, $F_{nm} = \langle [\psi_n, \psi_m^\dagger] \rangle$ is the fermion equal-time correlation function, whose evolution is governed by the matrix

$$h_{nm}^{\text{QL}} = \frac{i[d_{n-1}^\dagger b_{n-1} \delta_{n-1,m} - b_n^\dagger d_n \delta_{n+1,m}]}{2a_S \sqrt{\ell(\ell+1)}} + M(-1)^n \delta_{n,m}.$$

The equations of motion (5.12) preserve Gauss's law, i.e. $\partial_t G_n = 0$ at all times. The derivation of the classical-statistical approximation with staggered fermions is similar to the one presented in chapter 4 and leads to

$$\begin{aligned} \partial_t E_n &= \frac{g}{2a_S} \text{Re}[F_{n+1} U_n], \\ \partial_t U_n &= i g a_S E_n U_n, \\ i \partial_t F_{nm} &= \sum_{n'} [h_{nn'}^{\text{KS}} F_{n'm} - F_{nn'} h_{n'm}^{\text{KS}}], \end{aligned} \quad (5.13)$$

with

$$h_{nm}^{\text{KS}} = \frac{i}{2a_S} [U_{n-1}^* \delta_{n-1,m} - U_n \delta_{n+1,m}] + M(-1)^n \delta_{n,m}.$$

By considering the time derivative of $E_n = g(b_n^\dagger b_n - d_n^\dagger d_n)/2$ and $U_n = [\sqrt{\ell(\ell+1)}]^{-1} b_n^\dagger d_n$, insert the density-phase representation, one can show that (5.12) approximates (5.13) up to order $\mathcal{O}(\delta\rho/\ell)$. This implies that both the classical-statistical approximation and the approach towards Wilson's lattice gauge theory are consistent. We remind ourselves that ℓ controls whether essential phenomena of QED can be observed or not.

5.3 Pair Production with Cold Atoms

In a homogeneous electric field E the creation of electron-positron pairs can be interpreted as a process where virtual electron-positron dipoles are separated over a finite distance and become real pairs. The binding energy of these dipoles will be at the order of twice the rest mass energy. This process can also be estimated [11, 12] when neglecting the back-reaction.

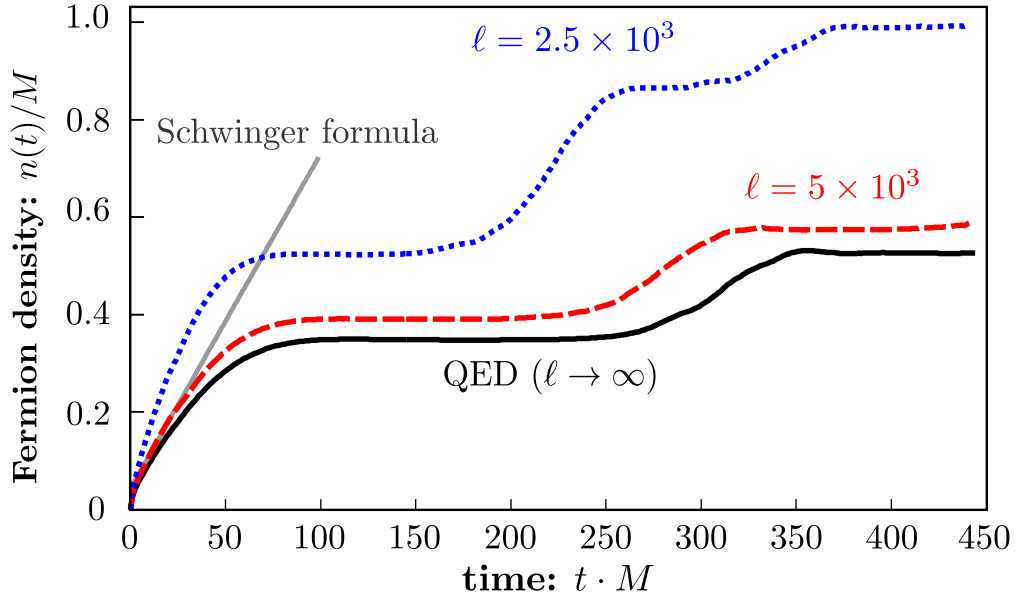


FIGURE 5.1: For different numbers of atoms ℓ per link the fermion number density results in a staircase structure. The Schwinger formula corresponds to the straight line, which neglects the back-reaction. When increasing the number of atoms ℓ per link (blue and red line), we approximate the $\ell \rightarrow \infty$ result.

In one spatial dimension the analytic result for the production-rate is then given by

$$\dot{n} = M^2 E / (2\pi E_c) \exp(-\pi E_c / E) \quad (5.14)$$

and is depicted in Fig. 5.1.

At sufficiently early times we assume that the analytic estimate describes the production rate of the full system and provides a benchmark for the simulation method. The simulated system has a volume of Na_S with periodic boundary conditions. The real-time evolution is performed according to the equations (5.12) with the parameters $g/M = 0.1$ and $a_S \cdot M = 0.005$ in the limit $\ell \rightarrow \infty$ and corresponds to QED described by (5.13). N determines the number of lattice sites, but also denotes the number of fermionic atoms. We checked that the employed lattices with $N = 512$ show no significant volume dependence anymore. Moreover, the results are insensitive to changes in the lattice spacing, i.e. the UV-cutoff, as it was demanded in chapter 4. We use a particle number definition introduced in [36, 77] and Appendix D. The results of the simulation for QED ($\ell = \infty$)

are then given in Fig. 5.1. They agree with the Schwinger formula at early times and show the same qualitative behavior as the three-dimensional system in chapter 4. Again, the constant rate changes at later times and results in a staircase structure [77, 89] with a decreasing step size.

Obviously, the corresponding cold atom system does not produce any particle since the number of atoms is fixed. However, the staggered formulation for fermionic atoms allows the interpretation of two neighboring lattice sites to represent particles and antiparticles. Then pair production is described by the hopping of atoms between even and odd sites in the optical lattice. The time evolution of the correlations describing the corresponding phenomenon of pair production is shown in Fig. 5.1 as well. This figure demonstrates the convergence of the quantum simulator's dynamics to the QED behavior as the number of bosonic atoms per lattice site is increased. For $\ell = 2500$ there are observable deviations from the QED result, whereas the difference almost vanishes for $\ell = 5000$.

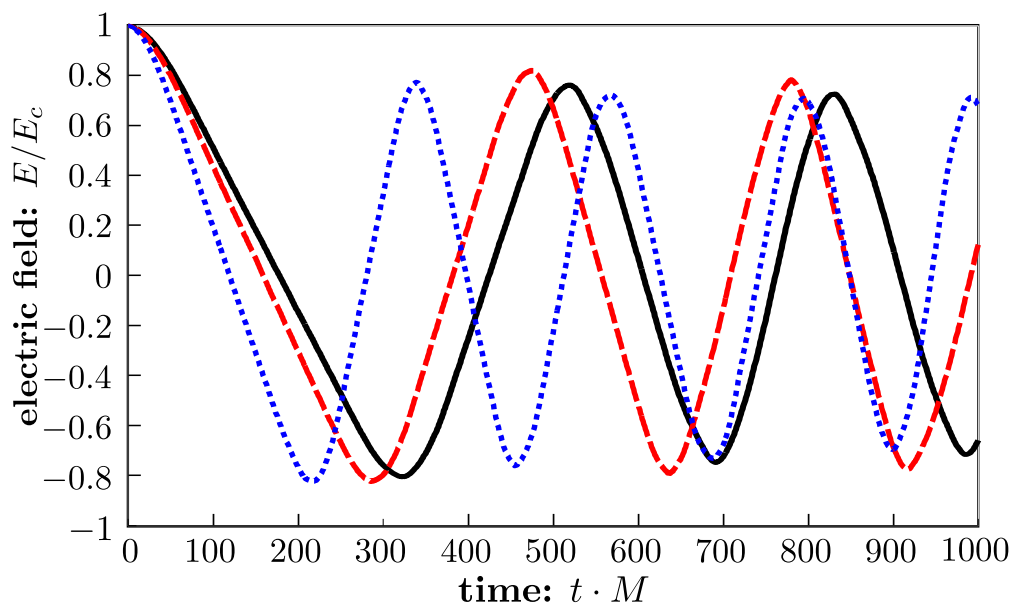


FIGURE 5.2: The dynamics of the electric field and gL_z as represented by the bosonic species population imbalance is shown for different values of ℓ . The color code and the values of ℓ are the same as in Fig. 5.1. The back-reaction of the produced pairs leads again to the plasma oscillations seen in chapter 4.

The time evolution of the electric field in the cold atom system is shown in Fig. 5.2 for different values of ℓ . Note that the electric field is given by

$E = g(N_b - N_d)/2$ and corresponds to the occupation number difference of the two addressed hyperfine states. In Fig. 5.2, we begin with the imbalance $N_b - N_d = 2M^2/g^2 > 0$ being the critical electric field strength in the atomic system. On the other hand, we start with the Dirac vacuum in the fermionic sector (3.50). This state is given by occupying the lowest $N/2$ energy eigenstates. The contrasting juxtaposition of Fig. 5.1 and Fig. 5.2 reveals a decrease of the electric field while the fermion number grows due to pair production. The imbalance of the bosonic species becomes zero because of the correlated hopping process of the fermions. The behavior of the imbalance of the atoms is again the plasma oscillation encountered in chapter 4 and similar in [36, 77, 90]. As soon as the electric field drops below a critical value, the particle creation effectively terminates. This physical situation is reflected in the characteristic plateaus in the particle number density. In this respect three and one dimensions are similar.

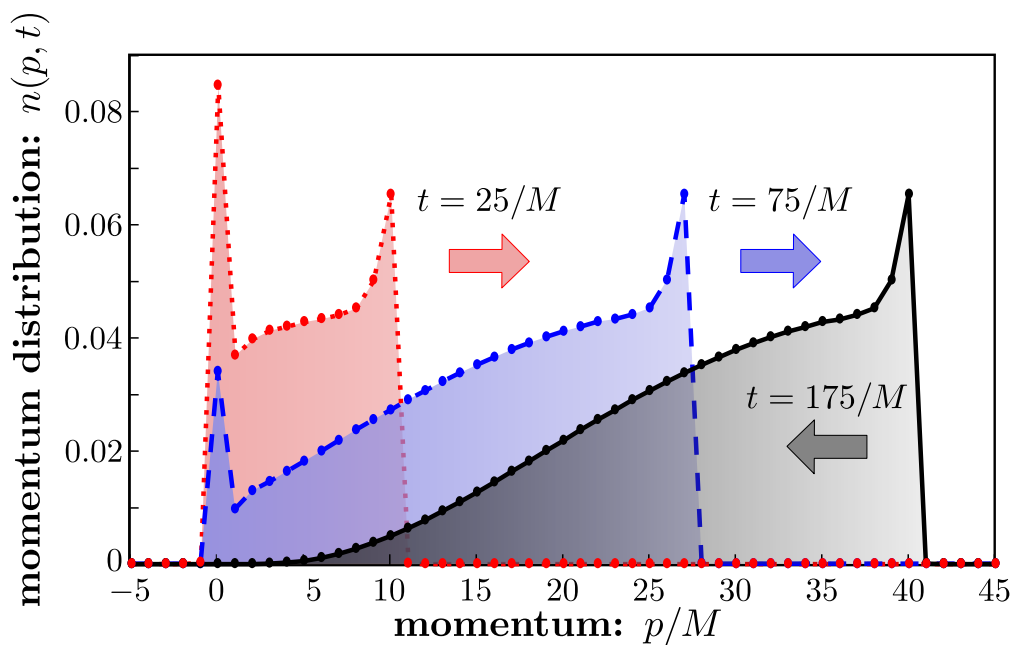


FIGURE 5.3: At three instants of time $t \cdot M = 25$ (red), $t \cdot M = 75$ (blue) and $t \cdot M = 175$ (black) the momentum distribution $n(p, t)$ of the produced fermions for $\ell = 10^4$ is shown. For this value of ℓ we reproduce the QED result and observe the acceleration of the charges.

Moreover, after the production of the electron-positron pair, the particles get accelerated by the electric field. Therefore, we study the momentum

distribution of the fermions [36, 77] in Fig. 5.3 for $\ell = 10^4$ which reproduced the QED results. Due to the homogeneous electric field, the fermions are dominantly produced around zero momentum. In addition, they are accelerated by the electric field to higher momenta at later times. The fermions arrive at their maximum momentum at the same time as the electric field vanishes. Thereafter, the current causes the decrease of the electric field to a negative value and consequently leads to a deceleration of the produced particles.

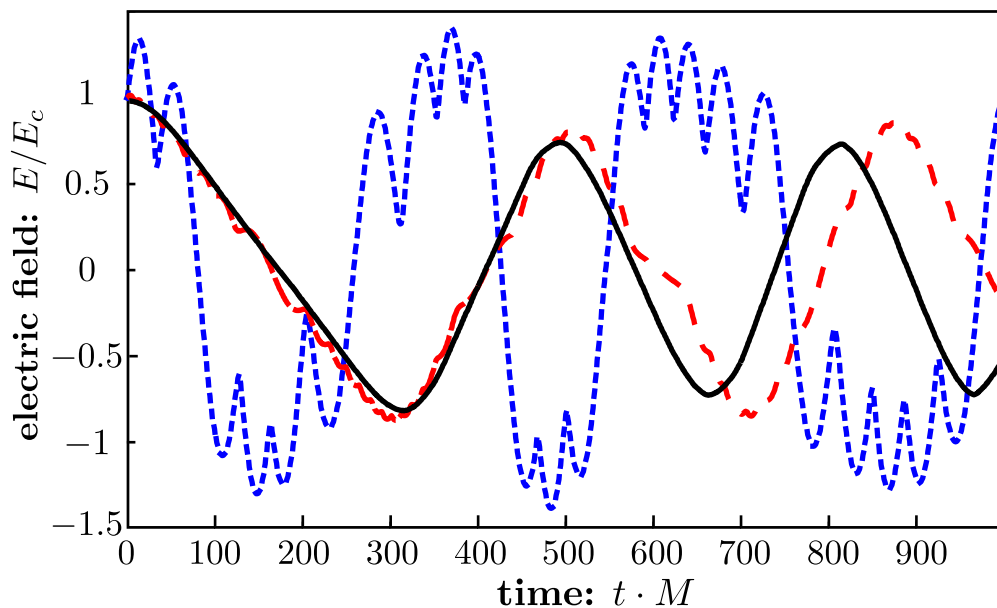


FIGURE 5.4: The dynamics of the electric field for different system sizes $N = 32$ (blue), $N = 128$ (red) and $N = 512$ (black) with $\ell = 10^4$.

The experimental setup is usually restricted in size, therefore we investigate the dependence of the results on the system size N . The electric field for different N with fixed angular momentum $\ell = 10^4$ is shown Fig. 5.4. In order to observe a reasonable approximation to the QED results we need about $N = 128$ for a full oscillation period, but we note deviations at later times. For $N = 512$ we see an accurate descriptions for the time ranges considered in this work.

5.4 String Breaking

The physics of confinement in the theory of quantum chromodynamics (QCD) manifests itself in the formation of a string between two external, static quarks. This confining string can break in theories with dynamical fermions by the production of charged particle-antiparticle pairs which result in a screening of the static sources [91–94]. It is important to note that QED in one spatial dimension shares the intriguing phenomenon of dynamical string breaking. It therefore serves as a popular model for addressing questions which are still too hard to answer in full QCD [89, 95].

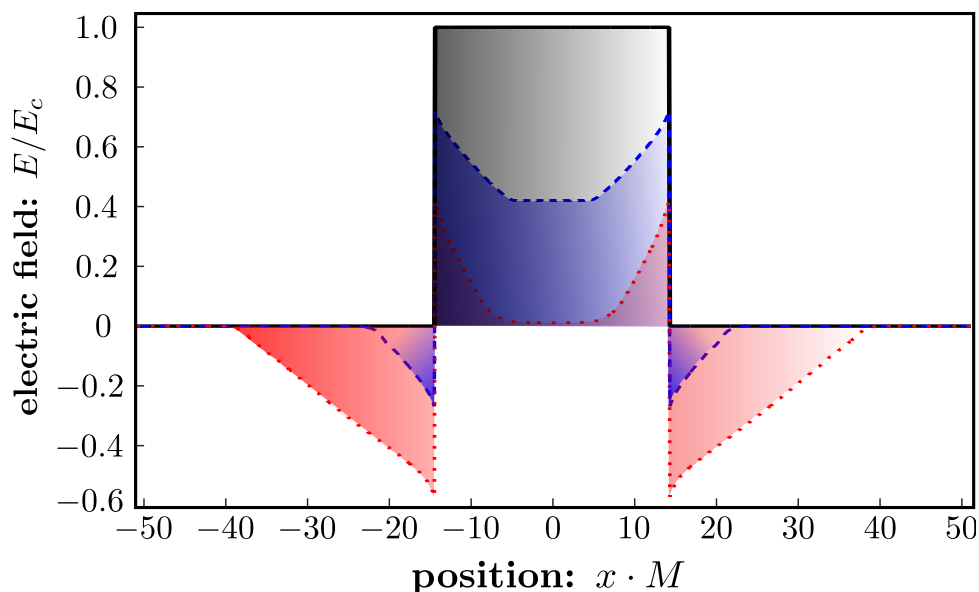


FIGURE 5.5: Dynamical breaking of the string. We consider three instants of time $t_1 \cdot M = 0.0$ (black), $t_2 \cdot M = 8.4$ (blue) and $t_3 \cdot M = 24.9$ (red) for $\ell \rightarrow \infty$.

To study dynamical string breaking in QED in one spatial dimension we prepare two static elementary charges $\pm Q$ located at $\pm d/2$. The corresponding electric field between the charges is given by $E = Q$ whereas it vanishes outside. In the remainder of this section we choose $Q = g$. In the cold-atom setup, this corresponds to a bosonic species imbalance of $N_b - N_d = 2Q/g$ inside the string $|x| < d/2$ whereas it vanishes outside of the charges.

We first make contact to the corresponding QED literature [88, 89] by considering the limit $\ell \rightarrow \infty$ for $g/M = 1.0$, $a_S \cdot M = 0.1$ and $N =$

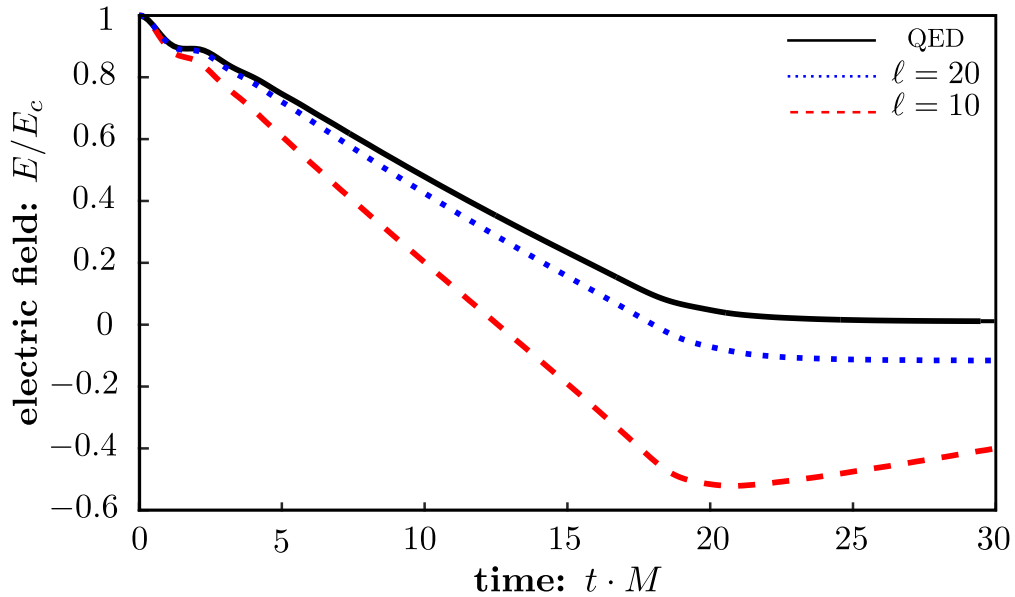


FIGURE 5.6: The electric field E/M in the center of the string breaks due to the dynamical fermion production (black). We also show the results for different atom numbers $\ell = 20$ (blue) and $\ell = 10$ (red), but for the same distance of the static charges. We observe the same behavior in the cold atom setup. However, there is also the onset of an oscillation in the cold atom setup.

1024. To this end, we study the time-evolution of the electric field E_n for $d/a_S = 287$. We chose this particular distance in order to detect clean string breaking as we will explain in the following. We display the electric field for different instances of time in Fig. 5.5.

Starting from the initial field configuration, the field energy is transferred to the fermionic sector by particle-antiparticle production, while the amplitude decreases. The dynamics is such that opposite charges are produced on top of each other and are then accelerated by the electric field. Depending on the value of d , the initial string may or may not contain enough energy to produce the required charges $\pm Q$ to screen the external charges.

In Fig. 5.5 we display the situation where d is chosen such that the produced amount of charge screens the external charges, which we would then attribute to the phenomenon of string breaking. Considering the cold-atom setup, the finite value of ℓ then again introduces deviations from the QED behavior. Most notably, Fig. 5.6 implies that the breaking of the string

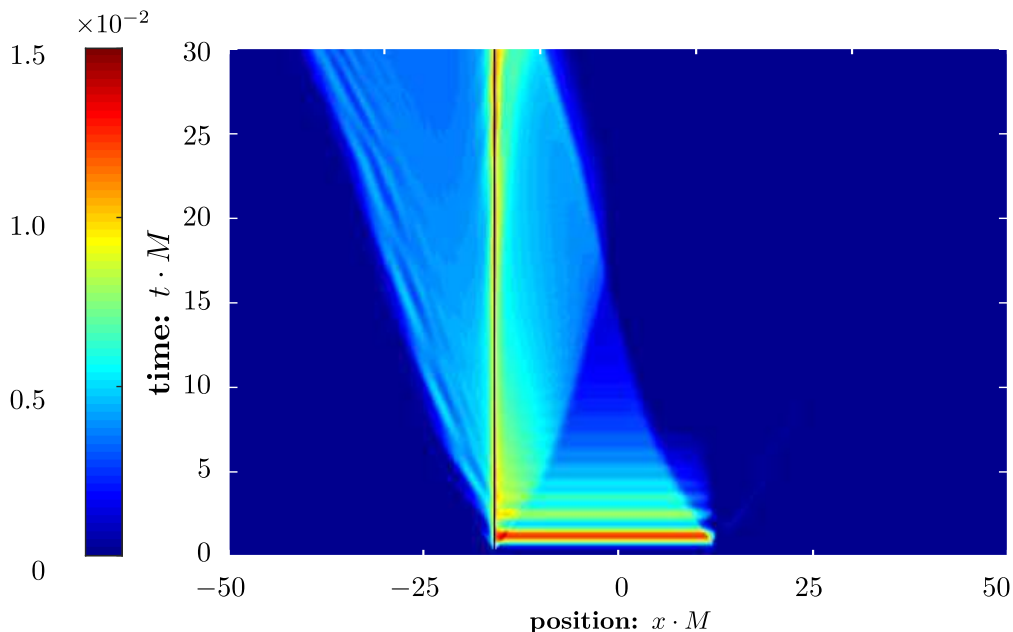


FIGURE 5.7: Positive charge density $\rho(x)/M$ determined by the even sites of the Kogut-Susskind Hamiltonian. We observe that the left negative external charge accumulates positive charge and gets screened.

in the quantum link model needs less energy as the Kogut-Susskind Hamiltonian for the same parameters $g/M = 1.0$, $a_S \cdot M = 0.1$ and $N = 1024$. As expected, we again observe convergence towards the QED results upon increasing the value of ℓ .

Unlike in the Schwinger mechanism for a homogeneous electric field, we directly observe charge separation owing to the spatially inhomogeneous situation. Accordingly, we focus on the charge density ρ_n , which appears as source term in the Gauss's law.

If we rewrite the discretized Gauss's law as

$$(E_n - E_{n-1}) |\text{phys}\rangle = \rho_n |\text{phys}\rangle, \quad (5.15)$$

we can directly extract the charge density from the electric field. In Fig. 5.7 and Fig. 5.8, we display the time evolution of the local charge density for QED and at the same time for the cold-atom setup in Fig. 5.9 and Fig. 5.10. As described previously, the dynamical charges are produced on top of

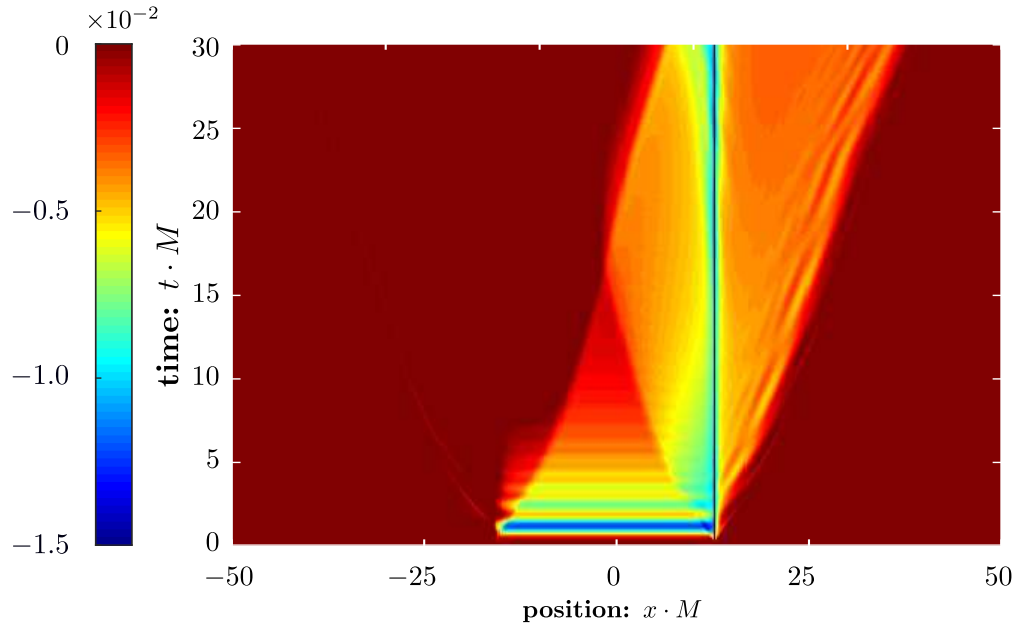


FIGURE 5.8: Negative charge density $\rho(x)/M$ determined by the odd sites in QED. We observe that the right positive external charge accumulates negative charge and gets screened similar to Fig. 5.7.

each other such that the total charge density vanishes initially. The dynamical charges are then separated by the existing field such that positive charges are accelerated towards $-Q$ and negative charge towards $+Q$.

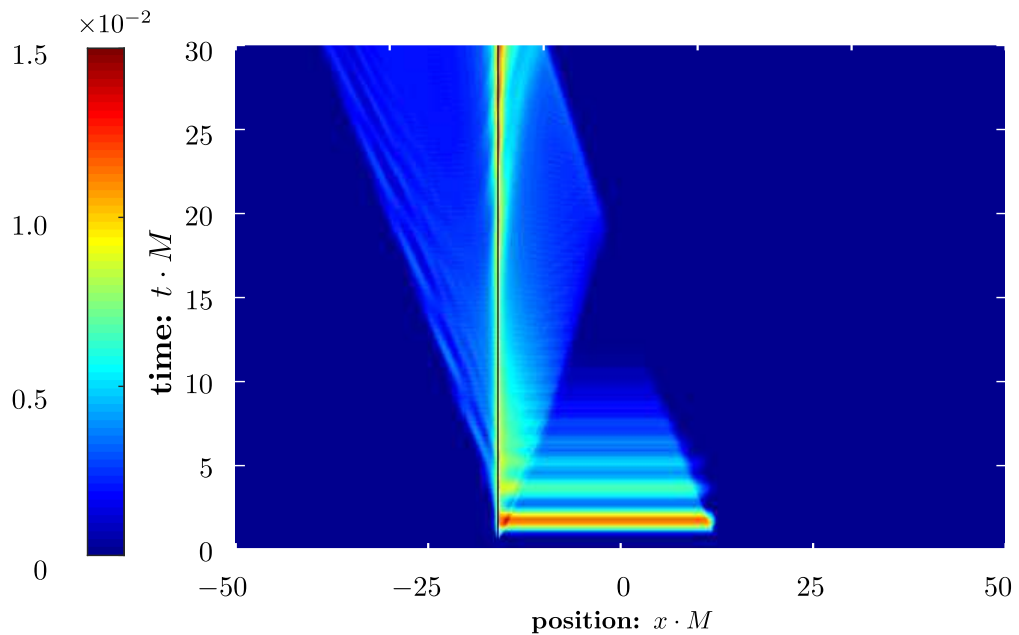


FIGURE 5.9: Positive charge density $\rho(x)/M$ at the even sites in the cold atom gauge theory. We observe the same qualitative behavior as in the QED case. Again the left negative external charge accumulates positive charge and gets screened ($\ell = 20$).

As the dynamical charges cannot be considered as hardcore particles, the charge density spreads beyond the static charges resulting in the outwards directed parts of the charge density. Thus, the external charges are gradually screened and finally result in the breaking of the string. At asymptotic times, the external charges are then supposed to become screened by a cloud of charges, which decays exponentially [88, 96].

The same qualitative behavior can be observed in the cold atom setup. Here, the breaking of the string corresponds to zero imbalance of the bosonic atoms. It is remarkable, that in the case of stronger couplings $g/M = 1$, we need less atoms to see the QED behavior in comparison to the study of the Schwinger mechanism in section 5.3. This is in agreement with studies of the classical-statistical approximation in the strong coupling limit [88]. Hence, we conclude that the number of requested atoms is much smaller in order to observe string breaking at strong coupling.

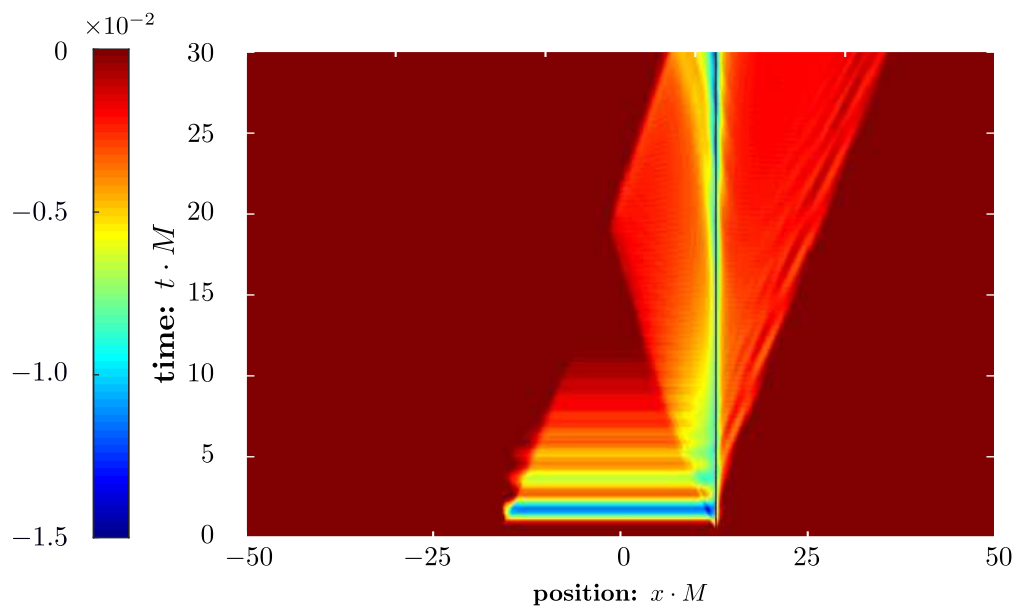


FIGURE 5.10: Negative charge density $\rho(x)/M$ at the odd sites in the cold atom gauge theory. We observe a similar behavior as in Fig. 5.9 except that we focus on the negative charge ($\ell = 20$).

5.5 Correlation Functions of the Schwinger Model

Simulating non-perturbative processes of high energy physics by experiments with ultracold atoms may open the field to resolve fundamental questions in the strong-coupling regime of gauge theories. In the last sections we considered the discretized version of the Schwinger model. In this section, we will show how one can use cold atom experiments to study the continuous Schwinger model in $(1 + 1)$ -dimensions in equilibrium. Therefore, we consider the Euclidean action

$$S_E = \int_0^\beta d\tau \int dz \left[\frac{1}{4} F_{\mu\nu}^2 - \bar{\psi}(z) (\not{\partial} + igA + M) \psi(z) \right] \quad (5.16)$$

of the massive Schwinger model, where ψ is now a two component spinor. Using bosonization techniques [97] we get the massive sine-Gordon model

$$S_E = \int_0^\beta d\tau \int dz \left\{ \frac{1}{2} [\partial_\mu \varphi(z)]^2 + \frac{1}{2} m^2 \varphi^2(z) - \alpha_0 \cos \sqrt{4\pi} \varphi(z) \right\}, \quad (5.17)$$

where we identify the parameters of (5.17) with (5.16) by

$$\alpha_0 = \frac{M\Lambda}{\pi}, \quad m = \frac{g}{\sqrt{\pi}}, \quad (5.18)$$

and Λ is the UV-cutoff. Note that the new dynamical variable is the bosonic field φ .

On the other hand, we find the sine-Gordon model again as a low-energy effective theory of two tunnel-coupled one-dimensional Bose gases. The Hamiltonian is given by

$$H = \int dz \sum_{j=1}^2 \left(\frac{\hbar^2}{2m_b} \frac{\partial \psi_j^\dagger}{\partial z} \frac{\partial \psi_j}{\partial z} + \frac{g}{2} \psi_j^\dagger \psi_j^\dagger \psi_j \psi_j - \mu \psi_j^\dagger \psi_j \right) - \hbar J \int dz \left(\psi_1^\dagger \psi_2 + \psi_2^\dagger \psi_1 \right). \quad (5.19)$$

The bosonic fields are denoted by $\psi_j(t, z)$ and g is the interaction of the bosons, μ is the chemical potential, J is the tunnel-coupling and m_b is the mass of the atoms [98]. Its corresponding Euclidean action is

$$S_E = \int_0^\beta d\tau \int dz \sum_{j=1}^2 \psi_j^\dagger \partial_\tau \psi_j + \int_0^\beta d\tau H. \quad (5.20)$$

The density-phase representation [99] of the bosonic fields is given by

$$\psi_1 = \sqrt{\rho_0 + \delta\rho_1} e^{i\theta_1}, \quad (5.21)$$

$$\psi_2 = \sqrt{\rho_0 + \delta\rho_2} e^{i\theta_2}, \quad (5.22)$$

with the homogeneous background density ρ_0 and the density fluctuations $\delta\rho_1$ and $\delta\rho_2$ and the phases θ_1 and θ_2 .

We define symmetric and anti-symmetric degrees of freedom for the density fluctuations and the phase,

$$\delta\rho_s = \delta\rho_1 + \delta\rho_2, \quad \varphi_s = [\theta_1 + \theta_2]/2, \quad (5.23a)$$

$$\delta\rho_a = [\delta\rho_1 - \delta\rho_2]/2, \quad \varphi_a = \theta_1 - \theta_2. \quad (5.23b)$$

In the quasi-condensate regime the density fluctuations and phase gradients are small. This allows for a systematic expansion in $\delta\rho_i$ and $\nabla\theta_i$ with $i \in \{1, 2\}$. Moreover, terminating the series at second order allows the full Hamiltonian to be separated into an independent sum of symmetric and anti-symmetric degrees of freedom [99].

In the following, we will consider only the anti-symmetric degree of freedom and hence will omit the subscript a . The Hamiltonian becomes [98]

$$H_{\text{SG}} = \int dz \left[g\delta\rho^2 + \frac{\hbar^2 n_{1\text{D}}}{4m_b} (\partial_z \varphi)^2 \right] + \int dz 2\hbar J n_{1\text{D}} \cos \varphi. \quad (5.24)$$

This is the sine-Gordon model in the Hamiltonian formulation. Moving to the action we get

$$S_E = \int_0^\beta d\tau \int dz [\delta\rho (i\partial_\tau\varphi) + H] \quad (5.25)$$

and integrating out the momentum $\delta\rho$ leads to

$$S_E = \int_0^\beta d\tau \int dz \left[\frac{1}{4g} (\partial_\tau\varphi)^2 + \frac{\hbar^2 n_{1D}}{4m_b} (\partial_z\varphi)^2 + 2\hbar J n_{1D} \cos\varphi \right]. \quad (5.26)$$

After a rescaling of the fields and parameters this action is of the same form as the sine-Gordon action given in (5.17) with $m = 0$. This allows the experimental setup to quantum simulate the sine-Gordon model. Such an experiment is already realized [100] and was used to measure higher order correlation functions of the phase difference φ . These correlation functions can be used to identify qualitative different regimes of this interacting theory. We introduce two length scales

$$\lambda_T = 2\hbar^2 n_{1D} / (m_b k_B T), \quad l_J = \sqrt{\hbar / (4m_b J)}, \quad (5.27)$$

which can be independently tuned in the experiment. We define the higher order correlation functions of the phase through the equal-time N -point correlation functions

$$G^{(N)}(\mathbf{z}, \mathbf{z}') = \langle [\varphi(z_1) - \varphi(z'_1)] \dots [\varphi(z_N) - \varphi(z'_N)] \rangle, \quad (5.28)$$

with coordinates $\mathbf{z} = (z_1, \dots, z_N)$ and $\mathbf{z}' = (z'_1, \dots, z'_N)$ along the length of the Bose gases. Note that Fig. 5.11 depicts the full correlation function, the connected part as well as the disconnected part of the correlation function $G^{(4)}$ [97, 100]. We observe that in box A of Fig. 5.11 there is no connected part and conclude that the equal time correlation functions can be described by a quadratic theory for $q = 0$ and $q = 14.7$.

Further, we identify a connected part in B of Fig. 5.11 and we conclude

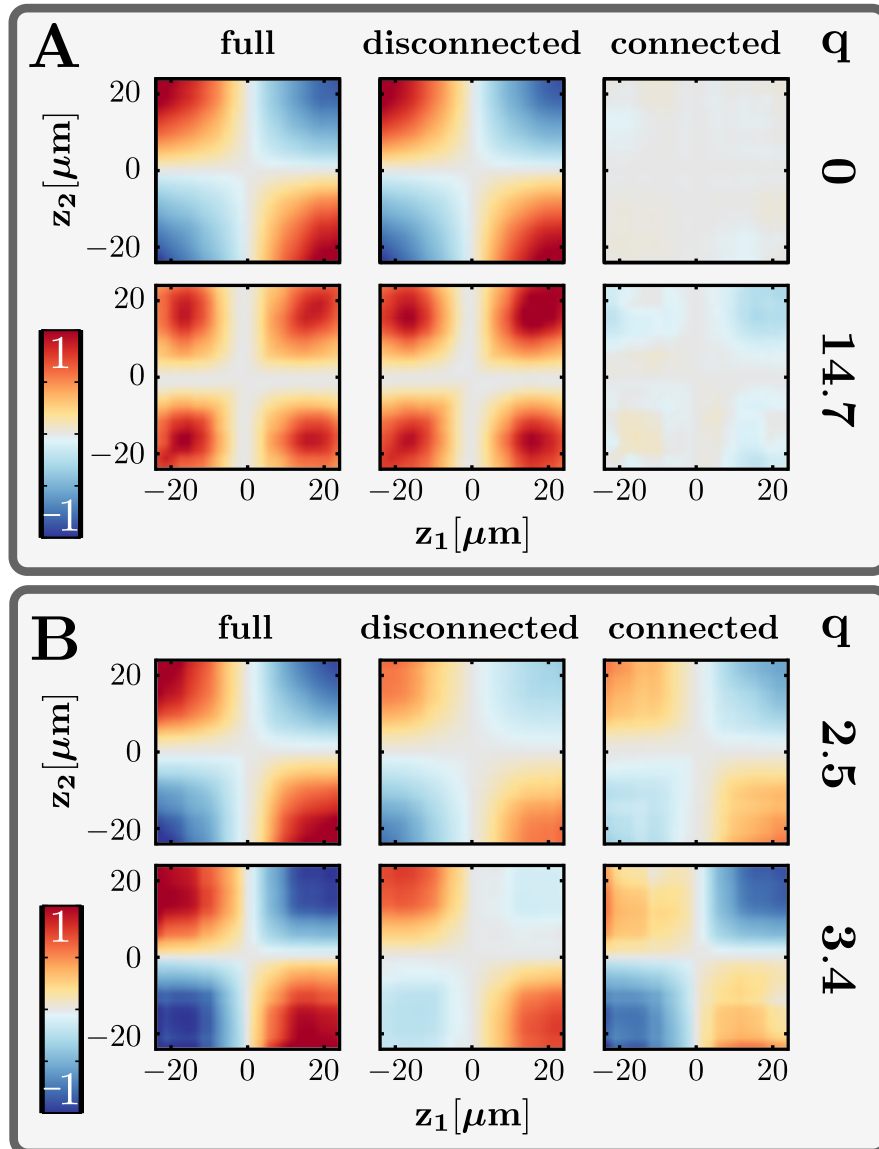


FIGURE 5.11: The dimensionless ratio $q = l_J/\lambda_T$ distinguishes the regime **A** and **B**. The 4-point phase correlation function $G^{(N)}(\mathbf{z}, \mathbf{z}')$ is high dimensional, thus we choose $z_3 = -z_4 = 15\mu\text{m}$ and $\mathbf{z}' = 0$. This leads to symmetric crosses with a vanishing correlation function. The color bar is normalized to the maximum value of the depicted correlation function. The entire experiment is described in [100].

that the underlying theory cannot be quadratic in the phase. Thus, the experiment is able to identify qualitative different regimes of an interacting theory and can be regarded as a quantum simulator of the Schwinger model.

Chapter 6

Conclusion and Outlook

In this section, we summarize the main results [36, 49, 100] of this thesis and we will give an overview of future perspectives concerning the quantum simulation of lattice gauge theories [101]. In particular, we will focus on the prospects to investigate the non-equilibrium dynamics of quantum simulators for fundamental gauge theories. We emphasize that one of the most important goals is to understand the long-time behavior of gauge theories coupled to matter. The present work is a step towards a detailed and deep theoretical understanding of quantum simulators of gauge theories. Future experiments will offer the possibility to study the non-equilibrium physics of gauge theories in cold-atom setups. One may even envisage the realization of the Standard Model as a table top experiment.

This thesis gives an explicit proposal for an experiment, realizing a quantum simulator of a one-dimensional $U(1)$ gauge theory, that is coupled to dynamical fermionic matter using cold atoms. There are two major conceptual steps behind the proposed experiments: First, using an optical periodic potential, one is able to imprint a lattice structure on a gas of bosonic and fermionic atoms. This is a very convenient way to model the underlying system by discrete degrees of freedom. Moreover, from a theoretical point of view, a description by discretized degrees of freedom, naturally points to lattice gauge theories. The second step is to restrict the amount of interactions by exploiting conservation laws and suppressing

unwanted processes in order to engineer a system with local gauge invariance. Realizing such a system may give researchers the unique chance to interpolate from the weak to the strong coupling limit of a gauge theory. This is an experimental situation which is very difficult to achieve in high energy physics and makes quantum simulators an outstanding tool [102].

In fact, the prospects resulting from an Abelian one-dimensional gauge theory are far-reaching and will be explained in the following. A future possibility could be an implementation of a non-Abelian gauge group or the generalization of the quantum simulators to higher dimensions [18, 23, 103]. Quantum link models already offer a promising theoretical framework to formulate non-Abelian links on a finite dimensional Hilbert-space and in higher dimensions.

Similarly, these more complicated theories can be realized utilizing the ideas put forward in chapter 3. Again, we can imprint the lattice structure by an external optical potential. However, the precise engineering of the interactions in order to obtain non-Abelian gauge invariance will become extremely challenging. Indeed, there is no present experimental setup, which realizes a dynamical non-Abelian gauge field coupled to matter. Using alkaline-earth atoms [104] may provide a possibility to simplify the experimental setups. Indeed, there are already proposals, how one could be able to realize non-Abelian links exploiting these atoms [18].

Apart from the non-Abelian gauge groups, also higher dimensions are of generic interest. An experiment in $(3 + 1)$ -dimensions with a $U(1)$ gauge group would realize quantum electrodynamics as it is used to formulate the Standard Model of particle physics. One main difference to one spatial dimension is the presence of purely spatial plaquette terms or equivalently ring exchange terms [105]. These interactions are very intricate objects since they contain more link variables. If one realizes the link by two bosons, one ends up with an interaction involving four initial bosonic states and four final bosonic states. One current theoretical approach is to use higher order perturbation theory in order to generate such terms [23].

Proposals using this idea, produce the plaquette term at the fourth order of such a perturbative series and one has to suppress the first, second and third order in order to realize the desired Kogut-Susskind Hamiltonian [73].

It is an intriguing question if the design of the plaquette term is always a necessary ingredient for planned quantum simulators. As explained in the last paragraph, a Hamiltonian with gauge invariant interactions but without a plaquette at the microscopic level can effectively create a ring exchange through higher order processes. Assume, we are interested in observables, which test the large distance properties of the quantum simulator. Then the effective theory describing the large distance behavior will include an effectively created plaquette term. Note that this effective theory will still be a gauge theory. Moreover, universality states that certain observables are insensitive to the microscopic details of the theory. In this respect, one should still be able to study universal properties of gauge theories even in the absence of the plaquette term at the microscopic level.

However, not only the gauge fields are challenging objects. The fermion doubling problem will also play a crucial role in higher dimensions. While the staggered fermions in one spatial dimension in the Hamiltonian formulation will not suffer from the doubling problem, it is still present in higher dimensions [106]. A solution to a doubler free implementation of chiral fermions on a lattice is given by domain wall fermions [74]. By introducing an extra dimension one is able to achieve both: chiral fermions and no doubling. Extra dimensions are conceptually no problem in cold-atom systems since any quantum number or index of the quantum fields can be considered as a candidate for a spatial dimension. This idea is usually summarized in the concept of artificial or synthetic dimensions [107] and was already used to implement static gauge fields in higher dimensions [108].

Currently, the proposed quantum simulators focus on coupling gauge fields to fermionic matter. However, there are important theories, where

the gauge field is coupled to a bosonic degree of freedom [109]. One famous example are SU(2) gauge fields coupled to a Higgs sector. Already, the $(1 + 1)$ -dimensional Abelian Higgs model possesses a topological degenerate ground state. This model allows for sphaleron transitions being thermal activated ‘hopping’ processes from one degenerate ground-state to another ground state. Sphalerons become again of interest in the context of the chiral magnetic effect out of equilibrium [110].

A future experiment should aim towards the clean realization of a gauge invariant Hamiltonian. However, most likely non-gauge invariant terms can appear in the process of a clean realization of the desired Hamiltonian. An easy example for such a situation would be an unwanted interaction between bosonic and fermionic atoms in the quantum simulator presented in this thesis. However, there are claims that gauge invariance may be a robust property [111] in certain situations. This would be highly relevant for the experimental realization. Hence, this deserves further investigation and may lead to improved setups for quantum simulators.

Note that our original motivation was the study of the long-time behavior of gauge theories from first principles. This is a challenging theoretical task. In particular, so far there is no theoretical framework being able to study the equilibration of strongly coupled non-Abelian gauge theories interacting with matter from first principles. However, this thesis outlines a possibility to get theoretical insight for short- and intermediate-times. The main idea consists in mapping particular classes of quantum problems onto a classical-statistical ensemble. We used this approach to elaborate the contributing quantum processes when studying the dynamics of Abelian and non-Abelian gauge theories. We could identify them by analyzing the diagrammatic contributions of quantum effects and investigated the range of validity of this classical-statistical approach.

Consequently, we used this method to compare the dynamics of Wilson’s formulation of QED with the atomic quantum simulator proposed in this thesis. We studied in detail the two important phenomena of Schwinger

pair production and string breaking. These two effects are very important, because the Schwinger effect has not been observed so far and string breaking is of great importance in QCD. Using the classical-statistical approach, we were able to determine experimental parameters in order to get the same results in both theories. Hence, there is the prospect, that both phenomena can be studied in an upcoming experiment.

The immediate next step concerning the classical-statistical approximation involving fermions should be the study of the next order in the quantum corrections. In this way, one has the ability to improve the classical-statistical method. Similar ideas were partially studied for purely bosonic systems [31], but have not been used for fermions. However, this approach will not be enough to study gauge fields, which are strongly interacting with fermions. Such problems need new ideas, because the 2PI $1/N$ re-summation is not able to tackle $SU(N)$ gauge invariant theories [112]. Hence, one is in need for new theoretical ideas.

Finally, the idea of quantum simulation of lattice gauge theories goes far beyond the study of non-equilibrium situations. It will allow for the precise measurement of the phase structure of the simulated lattice gauge theories. This is relevant for QCD, but also for high temperature superconductors, where $SU(2)$ gauge theories emerge as effective field theories. In quantum information, Z_2 gauge theories are a promising framework for quantum computation [113]. The quantum simulation of lattice gauge theory will have an incredible potential to control the parameters of these gauge theories and henceforth deepen our understanding of nature.

Appendix A

Overlap Integrals

We assume that the radial and longitudinal direction of the wavefunction of the atoms decouple. Further the bosonic and fermionic atoms are in the ground state with respect to the radial direction. Since the potential can be approximated by a harmonic potential the wave functions introduced in (3.9) are given by the ground state of the harmonic oscillator

$$\varphi_b(y) = (\pi a_{b\perp}^2)^{-1/4} e^{-\frac{1}{2}(y/a_{b\perp})^2}, \quad (\text{A.1a})$$

$$\varphi_f(y) = (\pi a_{f\perp}^2)^{-1/4} e^{-\frac{1}{2}(y/a_{f\perp})^2}. \quad (\text{A.1b})$$

Here we introduce the length scale of the harmonic oscillator as

$$a_{f\perp} = \sqrt{\frac{\hbar}{M_f \omega_{f\perp}}}, \quad a_{b\perp} = \sqrt{\frac{\hbar}{M_b \omega_{b\perp}}}. \quad (\text{A.2})$$

The expressions for $\varphi_b(z)$ and $\varphi_f(z)$ are given by substituting y by z in the above equation. We assumed that the ground state wave functions are independent of the magnetic quantum number.

In order to determine the Wannier functions we approximate the optical lattice by a harmonic oscillator at each minimum of the optical lattice potential

$$V_{\parallel}^s(x) = V_1^s \cos^2(kx) + V_2^s \sin^2(2kx), \quad (\text{A.3})$$

with $s \in \{b, f\}$, $V_1^b = -V_1^f$, $V_2^b = -V_2^f$ and $k = \pi/a$.

We will first focus on the bosons and later on the fermions. The minima of the potential for the bosons are

$$x_{b,2n} = \frac{n\pi}{k} - \frac{1}{2k} \arccos \frac{V_1}{4V_2} \quad (\text{A.4})$$

at the even sites and at the odd sites they are given by

$$x_{b,2n+1} = \frac{n\pi}{k} + \frac{1}{2k} \arccos \frac{V_1}{4V_2} \quad (\text{A.5})$$

with n being an integer, see Fig. 3.2. The minima of the bosonic potential can be determined from the equation

$$\cos(2kx) = \frac{V_1^b}{4V_2^b}. \quad (\text{A.6})$$

Because of parity symmetry it will be enough to consider one minimum. We choose

$$x_{b,1} = \frac{1}{2k} \arccos \frac{V_1}{4V_2}, \quad (\text{A.7})$$

which corresponds to site 1 in Fig. 3.2. For the bosons we approximate the potential as

$$\begin{aligned} V_b(x) = & -V_2^b - \frac{(V_1^b)^2}{16V_2^b} - \frac{V_1^b}{2} \\ & + \frac{1}{2} \left(-\frac{k^2(V_1^b)^2}{2V_2^b} + 8V_2^b k^2 \right) (x - x_{b,1})^2. \end{aligned} \quad (\text{A.8})$$

Now, we focus on the fermions. The minima of the fermionic potential are given by

$$x_{f,2n} = n\frac{\pi}{k} + \frac{\pi}{2k}; \quad x_{f,2n+1} = n\frac{\pi}{k}. \quad (\text{A.9})$$

For the fermionic atoms it is enough to Taylor expand the optical potential around $x_{f,1} = 0$ to second order leading to

$$V_f(x) = V_1^f + \left(4V_2^f k^2 - V_1^f k^2\right) x^2 + \dots, \quad (\text{A.10})$$

and the Taylor expansion around $x_{f,0} = \pi/(2k)$ results in

$$V_f(x) = \left(V_1^f k^2 + 4V_2^f k^2\right) \left(x - \frac{\pi}{2k}\right)^2 + \dots. \quad (\text{A.11})$$

Then we can identify the following frequencies of the harmonic oscillators

$$\frac{1}{2}M_b\omega_{b\parallel}^2 \equiv \frac{1}{2} \left(-\frac{k^2(V_1^b)^2}{2V_2^b} + 8V_2^b k^2 \right), \quad (\text{A.12})$$

$$\frac{1}{2}M_f\omega_{f\parallel L}^2 \equiv \left(V_1^f k^2 + 4V_2^f k^2 \right), \quad (\text{A.13})$$

$$\frac{1}{2}M_f\omega_{f\parallel R}^2 \equiv \left(4V_2^f k^2 - V_1^f k^2 \right). \quad (\text{A.14})$$

In the experiment we will choose V_1^s and V_2^s such that this results in positive expressions of $\omega_{b\parallel}^2$, $\omega_{f\parallel L}^2$ and $\omega_{f\parallel R}^2$. We have two frequencies for the fermions, whereas the bosons only have one frequency due to parity symmetry. The frequencies again define length scales for the harmonic oscillator

$$a_{b\parallel} = \sqrt{\frac{\hbar}{M_b\omega_{b\parallel}}}, a_{f\parallel L} = \sqrt{\frac{\hbar}{M_f\omega_{f\parallel L}}}, a_{f\parallel R} = \sqrt{\frac{\hbar}{M_f\omega_{f\parallel R}}}. \quad (\text{A.15})$$

Then the Wannier functions for the bosons and fermions are approximated by the ground state of the local harmonic oscillators

$$w_{2n}^b(x) = (\pi a_{b\parallel}^2)^{-1/4} e^{-\frac{1}{2} \left(\frac{x-x_{b,2n}}{a_{b\parallel}} \right)^2}, \quad (\text{A.16a})$$

$$w_{2n+1}^b(x) = (\pi a_{b\parallel}^2)^{-1/4} e^{-\frac{1}{2} \left(\frac{x-x_{b,2n+1}}{a_{b\parallel}} \right)^2}, \quad (\text{A.16b})$$

$$w_{2n}^f(x) = (\pi a_{f\parallel}^2)^{-1/4} e^{-\frac{1}{2} \left(\frac{x-x_{f,2n}}{a_{f\parallel L}} \right)^2}, \quad (\text{A.16c})$$

$$w_{2n+1}^f(x) = (\pi a_{f\parallel}^2)^{-1/4} e^{-\frac{1}{2} \left(\frac{x-x_{f,2n+1}}{a_{f\parallel R}} \right)^2}, \quad (\text{A.16d})$$

where we assumed again the independence of the wave functions on the magnetic state, i.e. $w_n^b(x) = w_{\alpha,n}^b(x)$ and $w_n^f(x) = w_{\alpha,n}^f(x)$, and n is the site label. Since every site has one Wannier function we do not need the parity label in (3.11). The dimensional reduction and the change of basis to the Wannier functions introduces the following overlap integrals in the interaction term

$$U_{\mathbf{n}}^b = \int dy |\varphi_b(y)|^4 \int dz |\varphi_b(z)|^4 \times \int dx [w_{n_1}^b(x) w_{n_2}^b(x)]^* w_{n_3}^b(x) w_{n_4}^b(x) \quad (\text{A.17a})$$

$$U_{\mathbf{n}}^f = \int dy |\varphi_f(y)|^4 \int dz |\varphi_f(z)|^4 \times \int dx [w_{n_1}^f(x) w_{n_2}^f(x)]^* w_{n_3}^f(x) w_{n_4}^f(x) \quad (\text{A.17b})$$

$$U_{\mathbf{n}}^{bf} = \int dy |\varphi_b(y) \varphi_f(y)|^2 \int dz |\varphi_b(z) \varphi_f(z)|^2 \times \int dx [w_{n_1}^f(x) w_{n_2}^b(x)]^* w_{n_3}^b(x) w_{n_4}^f(x), \quad (\text{A.17c})$$

with n_1, n_2, n_3 and n_4 being integers and denoting the sites. All these integrals can now be performed since they are gaussian.

Appendix B

Mode Functions for Fermions

The Dirac field operator can be expressed in terms of time-dependent mode functions $\Phi_{\lambda,n,\mathbf{q}}^u$, $\Phi_{\lambda,n,\mathbf{q}}^v$ and corresponding time-independent creation or annihilation operators $b_{\lambda,\mathbf{q}}$ and $d_{\lambda,\mathbf{q}}^\dagger$. This leads to

$$\psi_n = \frac{1}{V} \sum_{\mathbf{q} \in \tilde{\Lambda}} \sum_{\lambda} \left[\Phi_{\lambda,n,\mathbf{q}}^u b_{\lambda,\mathbf{q}} + \Phi_{\lambda,n,\mathbf{q}}^v d_{\lambda,\mathbf{q}}^\dagger \right], \quad (\text{B.1})$$

with the total volume $V = \prod_i N_i a_i$ and the spin index $\lambda \in \{1, 2\}$. We define the conjugate lattice $\tilde{\Lambda}$ as

$$\tilde{\Lambda} = \left\{ \mathbf{q} \left| q_i = \frac{N_i a_i p_i}{2\pi} \in \frac{N_i}{2}, \dots, \frac{N_i}{2} - 1 \right. \right\}, \quad (\text{B.2})$$

and we assume periodic boundary conditions in the spatial directions. The creation and annihilation operators obey the canonical anti-commutator relations

$$\{b_{\lambda,\mathbf{q}}, b_{\lambda',\mathbf{q}'}^\dagger\} = \{d_{\lambda,\mathbf{q}}, d_{\lambda',\mathbf{q}'}^\dagger\} = V \delta_{\lambda,\lambda'} \delta_{\mathbf{q},\mathbf{q}'}. \quad (\text{B.3})$$

The fermion occupation numbers are given by

$$\langle b_{\lambda,\mathbf{q}}^\dagger b_{\lambda,\mathbf{q}} \rangle = V n_{\lambda,\mathbf{q}}^u, \quad (\text{B.4a})$$

$$\langle d_{\lambda,\mathbf{q}}^\dagger d_{\lambda,\mathbf{q}} \rangle = V n_{\lambda,\mathbf{q}}^v. \quad (\text{B.4b})$$

Note that we assumed an initial decoupling of the fermion and the gauge sector at $n_0 = 0$. This leads to

$$\Phi_{\lambda,(0,\mathbf{n}),\mathbf{q}}^u = u_{\lambda,\mathbf{q}} e^{i\mathbf{p}\cdot\mathbf{x}_n}, \quad (\text{B.5a})$$

$$\Phi_{\lambda,(0,\mathbf{n}),\mathbf{q}}^v = v_{\lambda,\mathbf{q}} e^{-i\mathbf{p}\cdot\mathbf{x}_n}. \quad (\text{B.5b})$$

Here, the vectors are $\mathbf{x}_n = (a_1 n_1, a_2 n_2, a_3 n_3)$ and $\mathbf{p} = (p_1, p_2, p_3)$, where we defined p_i already in (B.2). The Dirac representation of the γ -matrices is given by

$$\gamma^0 = \begin{pmatrix} \mathbb{1} & 0 \\ 0 & -\mathbb{1} \end{pmatrix}, \quad \gamma^i = \begin{pmatrix} 0 & \sigma^i \\ -\sigma^i & 0 \end{pmatrix}. \quad (\text{B.6})$$

An explicit expression of the spinors $u_{\lambda,\mathbf{q}}$ and $v_{\lambda,\mathbf{p}}$ is

$$u_{1,\mathbf{q}} = \sqrt{\frac{\bar{\omega} + \bar{M}}{2\bar{\omega}}} \begin{pmatrix} 1 & 0 & \frac{\bar{p}_3}{\bar{\omega} + \bar{M}} & \frac{\bar{p}_1 + i\bar{p}_2}{\bar{\omega} + \bar{M}} \end{pmatrix}^T, \quad (\text{B.7a})$$

$$u_{2,\mathbf{q}} = \sqrt{\frac{\bar{\omega} + \bar{M}}{2\bar{\omega}}} \begin{pmatrix} 0 & 1 & \frac{\bar{p}_1 - i\bar{p}_2}{\bar{\omega} + \bar{M}} & \frac{-\bar{p}_3}{\bar{\omega} + \bar{M}} \end{pmatrix}^T, \quad (\text{B.7b})$$

$$v_{1,\mathbf{q}} = \sqrt{\frac{\bar{\omega} + \bar{M}}{2\bar{\omega}}} \begin{pmatrix} \frac{\bar{p}_3}{\bar{\omega} + \bar{M}} & \frac{\bar{p}_1 + i\bar{p}_2}{\bar{\omega} + \bar{M}} & 1 & 0 \end{pmatrix}^T, \quad (\text{B.7c})$$

$$v_{2,\mathbf{q}} = \sqrt{\frac{\bar{\omega} + \bar{M}}{2\bar{\omega}}} \begin{pmatrix} \frac{\bar{p}_1 - i\bar{p}_2}{\bar{\omega} + \bar{M}} & \frac{-\bar{p}_3}{\bar{\omega} + \bar{M}} & 0 & 1 \end{pmatrix}^T, \quad (\text{B.7d})$$

where we introduced

$$\bar{p}_i = \frac{1}{a_i} \sin\left(\frac{2\pi q_i}{N_i}\right), \quad (\text{B.8a})$$

$$\bar{M} = M + \sum_i \frac{2}{a_i} \sin^2\left(\frac{\pi q_i}{N_i}\right), \quad (\text{B.8b})$$

$$\bar{\omega} = \sqrt{\bar{M}^2 + \bar{p}_1^2 + \bar{p}_2^2 + \bar{p}_3^2}. \quad (\text{B.8c})$$

For later times $n_0, m_0 > 0$ the Keldysh Green's function is determined according to

$$\Delta_{n,m}^K = \frac{1}{V} \sum_{\mathbf{q} \in \tilde{\Lambda}} \sum_{\lambda} [\Phi_{\lambda,n,\mathbf{q}}^u \bar{\Phi}_{\lambda,m,\mathbf{q}}^u (1 - 2n_{\lambda,\mathbf{q}}^u) - \Phi_{\lambda,n,\mathbf{q}}^v \bar{\Phi}_{\lambda,m,\mathbf{q}}^v (1 - 2n_{\lambda,\mathbf{q}}^v)] , \quad (\text{B.9})$$

with the mode functions obeying the equation of motion (4.67) and $\bar{\Phi} = \Phi^\dagger \gamma^0$. The vacuum corresponds to $n_{\lambda,\mathbf{q}}^u = n_{\lambda,\mathbf{q}}^v = 0$ and is specified by the following one-point correlation functions and the Keldysh Green's function

$$\langle \psi_{(0,\mathbf{n})} \rangle = \langle \bar{\psi}_{(0,\mathbf{n})} \rangle = 0 , \quad (\text{B.10a})$$

$$\Delta_{(0,\mathbf{n}), (0,\mathbf{m})}^K = \frac{1}{V} \sum_{\mathbf{q} \in \tilde{\Lambda}} \frac{\bar{M} - \gamma^i \bar{p}_i}{\bar{\omega}} e^{i\mathbf{p} \cdot (\mathbf{x}_n - \mathbf{x}_m)} , \quad (\text{B.10b})$$

where we employed that the one-point function vanishes meaning $\langle b_{\lambda,\mathbf{q}} \rangle = \langle d_{\lambda,\mathbf{q}} \rangle = 0$.

Appendix C

Mode Functions for Gauge Fields

We have to fulfill the Gauss law for the initial state given by the Dirac vacuum (4.69). Further we wish to fulfill the residual gauge condition (4.75), therefore we perform a discrete Fourier transformation

$$E_{i,(0,\mathbf{n})} \equiv \mathcal{E}_i + \frac{1}{V} \sum_{\mathbf{q} \in \Lambda^*} e^{i\mathbf{p} \cdot \mathbf{x}_n} E_{i,\mathbf{q}}, \quad (\text{C.1})$$

and similarly for $A_{i,(0,\mathbf{n})}$. Here, \mathcal{E}_i denotes the coherent field in the zero-momentum mode. Accordingly, the transversality condition in conjugate space reads

$$\sum_i \tilde{p}_i E_{i,\mathbf{q}} = 0 = \sum_i \tilde{p}_i A_{i,\mathbf{q}}, \quad (\text{C.2})$$

with

$$\tilde{p}_i = \frac{2}{a_i} e^{-i\pi q_i / N_i} \sin\left(\frac{\pi q_i}{N_i}\right), \quad (\text{C.3a})$$

$$|\tilde{\mathbf{p}}| = \sqrt{\tilde{p}_1^2 + \tilde{p}_2^2 + \tilde{p}_3^2}. \quad (\text{C.3b})$$

We solve (C.2) via the mode function expansion given by

$$A_{i,\mathbf{q}} = \frac{1}{\sqrt{2|\tilde{\mathbf{p}}|}} \sum_{\lambda} [a_{\lambda,\mathbf{q}} \epsilon_{i,\lambda,\mathbf{q}} + a_{\lambda,-\mathbf{q}}^{\dagger} \epsilon_{i,\lambda,-\mathbf{q}}^*], \quad (\text{C.4a})$$

$$E_{i,\mathbf{q}} = i\sqrt{\frac{|\tilde{\mathbf{p}}|}{2}} \sum_{\lambda} [a_{\lambda,\mathbf{q}} \epsilon_{i,\lambda,\mathbf{q}} - a_{\lambda,-\mathbf{q}}^{\dagger} \epsilon_{i,\lambda,-\mathbf{q}}^*], \quad (\text{C.4b})$$

with the polarization vectors $\epsilon_{\lambda,\mathbf{q}}$ and index of polarization $\lambda \in \{1, 2\}$. The creation and annihilation operators have to fulfill the commutation relation

$$[a_{\lambda,\mathbf{q}}, a_{\lambda',\mathbf{q}'}^{\dagger}] = V \delta_{\lambda\lambda'} \delta_{\mathbf{q}\mathbf{q}'}. \quad (\text{C.5})$$

The occupation number of the photonic modes is determined by

$$\langle a_{\lambda,\mathbf{q}}^{\dagger} a_{\lambda,\mathbf{q}} \rangle = V n_{\lambda,\mathbf{q}}. \quad (\text{C.6})$$

The transversality (C.2) condition is fulfilled for the following choice of polarization vectors

$$\tilde{\mathbf{p}} \cdot \epsilon_{\lambda,\mathbf{q}} = 0, \quad (\text{C.7a})$$

$$\epsilon_{\lambda,\mathbf{q}}^* \cdot \epsilon_{\lambda',\mathbf{q}} = \delta_{\lambda\lambda'}. \quad (\text{C.7b})$$

We give an explicit representation for the polarization vectors. For $q_1 \neq 0$ we use

$$\epsilon_{1,\mathbf{q}} = \frac{1}{\sqrt{|\tilde{p}_1|^2 + |\tilde{p}_2|^2}} \begin{pmatrix} -\tilde{p}_2 \\ \tilde{p}_1 \\ 0 \end{pmatrix}, \quad (\text{C.8a})$$

$$\epsilon_{2,\mathbf{q}} = \frac{1}{|\tilde{\mathbf{p}}| \sqrt{|\tilde{p}_1|^2 + |\tilde{p}_2|^2}} \begin{pmatrix} \tilde{p}_1^* \tilde{p}_3 \\ \tilde{p}_2^* \tilde{p}_3 \\ -|\tilde{p}_1|^2 - |\tilde{p}_2|^2 \end{pmatrix}, \quad (\text{C.8b})$$

and for the case $q_1 = 0$ we choose

$$\boldsymbol{\epsilon}_{1,\mathbf{q}} = \frac{1}{\sqrt{|\tilde{p}_2|^2 + |\tilde{p}_3|^2}} \begin{pmatrix} 0 \\ \tilde{p}_3 \\ -\tilde{p}_2 \end{pmatrix}, \quad \boldsymbol{\epsilon}_{2,\mathbf{q}} = \begin{pmatrix} 1 \\ 0 \\ 0 \end{pmatrix}. \quad (\text{C.9})$$

Then the polarization vectors fulfill

$$\boldsymbol{\epsilon}_{1,-\mathbf{q}}^* = -\boldsymbol{\epsilon}_{1,\mathbf{q}}, \quad (\text{C.10a})$$

$$\boldsymbol{\epsilon}_{2,-\mathbf{q}}^* = \boldsymbol{\epsilon}_{2,\mathbf{q}} \quad (\text{C.10b})$$

and the transverse projector \mathcal{P} is given by

$$\mathcal{P}_{ij} = \sum_{\lambda} \epsilon_{i,\lambda,\mathbf{q}} \epsilon_{j,\lambda,\mathbf{q}}^* = \delta_{ij} - \frac{\tilde{p}_i \tilde{p}_j^*}{|\tilde{\mathbf{p}}|^2}. \quad (\text{C.11})$$

Gaussian initial states are specified in terms of the one-point correlation functions, corresponding to coherent background fields

$$\langle A_{i,(0,\mathbf{n})} \rangle = \mathcal{A}_i, \quad (\text{C.12a})$$

$$\langle E_{i,(0,\mathbf{n})} \rangle = \mathcal{E}_i, \quad (\text{C.12b})$$

where we used $\langle a_{\lambda,\mathbf{q}} \rangle = 0$, and the connected two-point correlation functions

$$\frac{1}{2} \langle \{A_{i,(0,\mathbf{n})}, A_{j,(0,\mathbf{m})}\} \rangle - \langle A_{i,(0,\mathbf{n})} \rangle \langle A_{j,(0,\mathbf{m})} \rangle, \quad (\text{C.13a})$$

$$\frac{1}{2} \langle \{A_{i,(0,\mathbf{n})}, E_{j,(0,\mathbf{m})}\} \rangle - \langle A_{i,(0,\mathbf{n})} \rangle \langle E_{j,(0,\mathbf{m})} \rangle, \quad (\text{C.13b})$$

$$\frac{1}{2} \langle \{E_{i,(0,\mathbf{n})}, E_{j,(0,\mathbf{m})}\} \rangle - \langle E_{i,(0,\mathbf{n})} \rangle \langle E_{j,(0,\mathbf{m})} \rangle. \quad (\text{C.13c})$$

The discrete Fourier series (C.1) and the assumption $n_{1,\mathbf{q}} = n_{2,\mathbf{q}} \equiv n_{\mathbf{q}}$ leads to

$$\frac{1}{2} \langle \{A_{i,\mathbf{q}}, A_{j,\mathbf{q}}\} \rangle = \frac{V}{|\tilde{\mathbf{p}}|} \left(\frac{1}{2} + n_{\mathbf{q}} \right) \mathcal{P}_{ij}, \quad (\text{C.14a})$$

$$\frac{1}{2} \langle \{A_{i,\mathbf{q}}, E_{j,\mathbf{q}}\} \rangle = 0, \quad (\text{C.14b})$$

$$\frac{1}{2} \langle \{E_{i,\mathbf{q}}, E_{j,\mathbf{q}}\} \rangle = V|\tilde{\mathbf{p}}| \left(\frac{1}{2} + n_{\mathbf{q}} \right) \mathcal{P}_{ij}. \quad (\text{C.14c})$$

The vacuum initial conditions containing quantum fluctuations are determined by $n_{\mathbf{q}} = 0$.

Appendix D

Fermionic Observables

The mode function expansion of the Dirac field operators and the vacuum initial conditions $n_{\lambda,\mathbf{q}}^u = n_{\lambda,\mathbf{q}}^v = 0$, can be used to determine the energy density ϵ_n according to

$$\epsilon_n = -\frac{1}{2} \sum_{m \in \Lambda} \text{tr}\{\mathcal{H}_{n,m} \Delta_{m,n}^K\}. \quad (\text{D.1})$$

The trace is performed with respect to Dirac indices, and the lattice Hamiltonian includes the spatial Wilson term determined by

$$\begin{aligned} \mathcal{H}_{n,m} = \delta_{n_0,m_0} & \left[\left(M + \sum_i \frac{1}{a_i} \right) \delta_{\mathbf{n},\mathbf{m}} - \sum_i \frac{1}{2a_i} (i\gamma^i + 1) U_{i,n} \delta_{\mathbf{n}+\hat{i},\mathbf{m}} \right. \\ & \left. + \sum_i \frac{1}{2a_i} (i\gamma^i - 1) U_{-i,n} \delta_{\mathbf{n}-\hat{i},\mathbf{m}} \right]. \end{aligned} \quad (\text{D.2})$$

The energy density can be expressed in terms of the mode functions

$$\begin{aligned} \epsilon_n = \frac{1}{2V} \sum_{m \in \Lambda} \sum_{\mathbf{q} \in \bar{\Lambda}} \sum_{\lambda} \\ \left[\bar{\Phi}_{\lambda,n,\mathbf{q}}^v \mathcal{H}_{n,m} \Phi_{\lambda,m,\mathbf{q}}^v - \bar{\Phi}_{\lambda,n,\mathbf{q}}^u \mathcal{H}_{n,m} \Phi_{\lambda,m,\mathbf{q}}^u \right]. \end{aligned} \quad (\text{D.3})$$

We define a momentum distribution by discrete Fourier transformation of the mode functions

$$\Phi_{\lambda,(m_0,\mathbf{m}),\mathbf{q}}^{u/v} \equiv \frac{1}{V} \sum_{\tilde{\mathbf{q}} \in \tilde{\Lambda}} e^{i\tilde{\mathbf{p}} \cdot \mathbf{x}_m} \Phi_{\lambda,\tilde{\mathbf{q}},\mathbf{q}}^{u/v}, \quad (\text{D.4})$$

with $\tilde{p}_i = 2\pi\tilde{q}_i/N_i a_i$ for $i \in \{1, 2, 3\}$. We interpret this as a discrete phase-space energy density of

$$\begin{aligned} \epsilon_{n,\tilde{\mathbf{q}}} = & \frac{1}{2V^2} \sum_{m \in \Lambda} e^{i\tilde{\mathbf{p}} \cdot \mathbf{x}_m} \sum_{\mathbf{q} \in \tilde{\Lambda}} \sum_{\lambda} \\ & [\bar{\Phi}_{\lambda,n,\mathbf{q}}^v \mathcal{H}_{n,m} \Phi_{\lambda,\tilde{\mathbf{q}},\mathbf{q}}^v - \bar{\Phi}_{\lambda,n,\mathbf{q}}^u \mathcal{H}_{n,m} \Phi_{\lambda,\tilde{\mathbf{q}},\mathbf{q}}^u] \end{aligned} \quad (\text{D.5})$$

and observe

$$\epsilon_n = \sum_{\tilde{\mathbf{q}} \in \tilde{\Lambda}} \epsilon_{n,\tilde{\mathbf{q}}}. \quad (\text{D.6})$$

The discrete phase-space particle number density is then given by the total energy density divided by twice the single-particle energy density

$$N_{n,\tilde{\mathbf{q}}} \equiv \frac{\epsilon_{n,\tilde{\mathbf{q}}}}{2\omega_{n,\tilde{\mathbf{q}}}}. \quad (\text{D.7})$$

The single-particle energy density can be computed from the lattice dispersion relation

$$\omega_{n,\tilde{\mathbf{q}}} = \sqrt{\bar{M}^2 + \bar{p}_1^2 + \bar{p}_2^2 + \bar{p}_3^2}, \quad (\text{D.8})$$

and

$$\bar{p}_i = \frac{i}{2a_i} \left[U_{-i,n} e^{-\frac{2\pi i \tilde{q}_i}{N_i}} - U_{i,n} e^{\frac{2\pi i \tilde{q}_i}{N_i}} \right], \quad (\text{D.9a})$$

$$\bar{M} = M + \sum_i \frac{1}{2a_i} \left[2 - U_{i,n} e^{\frac{2\pi i \tilde{q}_i}{N_i}} - U_{-i,n} e^{-\frac{2\pi i \tilde{q}_i}{N_i}} \right]. \quad (\text{D.9b})$$

These expressions coincide with (B.8) for the free field theory. The normalized momentum distribution $N_{n_0,\tilde{\mathbf{q}}}$ – in chapter 4 denoted as $n(p, t)$ –

is then defined by

$$n(p, t) \equiv N_{n_0, \tilde{\mathbf{q}}} = a_1 a_2 a_3 \sum_{\mathbf{n} \in \Lambda} N_{n, \tilde{\mathbf{q}}}. \quad (\text{D.10})$$

The total fermion density N_{n_0} - in chapter 4 denoted as $N(t)/V$ can be obtained from

$$N(t)/V \equiv N_{n_0} = \frac{1}{N_1 N_2 N_3} \sum_{\mathbf{n} \in \Lambda} \sum_{\tilde{\mathbf{q}} \in \tilde{\Lambda}} N_{n, \tilde{\mathbf{q}}}. \quad (\text{D.11})$$

Appendix E

Continuum Results for the Schwinger effect

There are analytic results for the Schwinger effect in a static background field [114]. The Dirac equation for the homogeneous background field E_0 is analytically solvable in terms of parabolic cylinder functions $D_\nu(z)$. We define $\epsilon_0 = gE_0/m^2$, $\epsilon_\perp^2 = m^2 + p_1^2 + p_2^2$ such that $\omega^2(p) = \epsilon_\perp^2 + p_3^2$ and $\eta = \epsilon_\perp^2/gE_0$. Then the analytic solution for the momentum distribution $f(p)$ is given by

$$f(p) = e^{-\pi\eta/4} \left[\frac{\eta}{2} \left(1 - \frac{p_3}{\omega(p)} \right) \mathcal{D}_1(p) + \left(1 + \frac{p_3}{\omega(p)} \right) \mathcal{D}_2(p) - \sqrt{\frac{\epsilon_0\eta^2}{2}} \frac{m}{\omega(p)} \mathcal{D}_3(p) \right], \quad (\text{E.1})$$

with

$$\mathcal{D}_1(p) = |D_{-1+i\eta/2}(\hat{p})|^2, \quad (\text{E.2a})$$

$$\mathcal{D}_2(p) = |D_{i\eta/2}(\hat{p})|^2, \quad (\text{E.2b})$$

$$\mathcal{D}_3(p) = e^{i\pi/4} D_{i\eta/2}(\hat{p}) D_{-1-i\eta/2}(\hat{p}^*) + c.c., \quad (\text{E.2c})$$

for

$$\hat{p} = -\sqrt{\frac{2}{\epsilon_0} \frac{p_3}{m}} e^{-i\pi/4}. \quad (\text{E.3})$$

The momentum distribution $f(p)$ vanishes for kinetic momenta $p_3 \rightarrow -\infty$ and approaches a non-vanishing constant for large kinetic momenta $p_3 \rightarrow \infty$, i.e.

$$\lim_{p_3 \rightarrow -\infty} f(p) = 0 \quad , \quad \lim_{p_3 \rightarrow \infty} f(p) = 2e^{-\pi\eta}. \quad (\text{E.4})$$

The production rate of electrons and positrons is a constant. Hence, the total number ΔN of electrons and positrons, which are created per volume V during a time interval T , is determined by

$$\frac{\dot{N}}{V} = \frac{(gE_0)^2}{4\pi^3} \exp\left(-\frac{\pi m^2}{gE_0}\right) = \frac{m^4 \epsilon_0^2}{4\pi^3} \exp\left(-\frac{\pi}{\epsilon_0}\right). \quad (\text{E.5})$$

Bibliography

- [1] P. A. Lee, N. Nagaosa, and X.-G. Wen, [Reviews of Modern Physics](#) **78**, 17 (2006).
- [2] S. Weinberg, [The European Physical Journal C - Particles and Fields](#) **34**, 5 (2004).
- [3] S. Tomonaga, [Progress of Theoretical Physics](#) **1**, 27 (1946).
- [4] J. Schwinger, [Physical Review](#) **74**, 1439 (1948).
- [5] R. P. Feynman, [Physical Review](#) **76**, 769 (1949).
- [6] M. Creutz, L. Jacobs, and C. Rebbi, [Physical Review Letters](#) **42**, 1390 (1979).
- [7] M. Gring, M. Kuhnert, T. Langen, T. Kitagawa, B. Rauer, M. Schreitl, I. Mazets, D. A. Smith, E. Demler, and J. Schmiedmayer, [Science](#) **337**, 1318 (2012).
- [8] J. Berges, S. Borsányi, and C. Wetterich, [Physical Review Letters](#) **93**, 142002 (2004).
- [9] J. Berges, [Phys. Rev. D](#) **70**, 105010 (2004).
- [10] F. Sauter, [Zeitschrift für Physik](#) **69**, 742 (1931).
- [11] W. Heisenberg and H. Euler, [Zeitschrift für Physik](#) **98**, 714 (1936).
- [12] J. Schwinger, [Physical Review](#) **82**, 664 (1951).
- [13] <http://www.eli-laser.eu>, “Eli Delivery Consortium,” (2015).

- [14] F. Gelis, E. Iancu, J. Jalilian-Marian, and R. Venugopalan, [Annual Review of Nuclear and Particle Science](#) **60**, 463 (2010).
- [15] R. P. Feynman, [International Journal of Theoretical Physics](#) **21**, 467 (1982).
- [16] M. Greiner, O. Mandel, T. Esslinger, T. W. Hänsch, and I. Bloch, [Nature](#) **415**, 39 (2002).
- [17] E. Zohar, J. I. Cirac, and B. Reznik, [Physical Review Letters](#) **109**, 125302 (2012).
- [18] D. Banerjee, M. Bögli, M. Dalmonte, E. Rico, P. Stebler, U.-J. Wiese, and P. Zoller, [Physical Review Letters](#) **110**, 125303 (2013).
- [19] L. Tagliacozzo, A. Celi, A. Zamora, and M. Lewenstein, [Annals of Physics](#) **330**, 160 (2013).
- [20] P. Orland and D. Rohrlich, [Nuclear Physics B](#) **338**, 647 (1990).
- [21] J. S. Schwinger, [Physical Review](#) **128**, 2425 (1962).
- [22] J. Kogut and L. Susskind, [Phys. Rev. D](#) **11**, 395 (1975).
- [23] E. Zohar, J. I. Cirac, and B. Reznik, [Phys. Rev. A](#) **88**, 023617 (2013).
- [24] M. Troyer and U.-J. Wiese, [Physical Review Letters](#) **94**, 170201 (2005).
- [25] D. T. Son, (1996), [arXiv:hep-ph/9601377](#) .
- [26] S. Y. Khlebnikov and I. I. Tkachev, [Physical Review Letters](#) **77**, 219 (1996).
- [27] T. Prokopec and T. G. Roos, [Phys. Rev. D](#) **55**, 3768 (1997).
- [28] G. Aarts and J. Smit, [Nuclear Physics B](#) **555**, 355 (1999).
- [29] F. Gelis and N. Tanji, [Phys. Rev. D](#) **87**, 125035 (2013).
- [30] G. Aarts and J. Berges, [Physical Review Letters](#) **88**, 041603 (2002).
- [31] A. Polkovnikov, [Phys. Rev. A](#) **68**, 053604 (2003).

- [32] A. Arrizabalaga, J. Smit, and A. Tranberg, *Journal of High Energy Physics* **10**, 017 (2004).
- [33] J. Berges and T. Gasenzer, *Phys. Rev. A* **76**, 033604 (2007).
- [34] J. Berges, A. Rothkopf, and J. Schmidt, *Physical Review Letters* **101**, 041603 (2008).
- [35] S. Kühn, J. I. Cirac, and M. Bañuls, *Phys. Rev. A* **90**, 042305 (2014).
- [36] V. Kasper, F. Hebenstreit, and J. Berges, *Phys. Rev. D* **90**, 025016 (2014).
- [37] H. J. Rothe, *Lattice Gauge Theories: An Introduction*, 4th ed. (World Scientific Publishing Co, New Jersey, 2012).
- [38] I. Montvay and G. Münster, *Quantum Fields on a Lattice* (Cambridge University Press, Cambridge, 1997).
- [39] M. Creutz, *Annals of Physics* **117**, 471 (1979).
- [40] J. J. Sakurai and J. Napolitano, *Modern Quantum Mechanics*, 2nd ed. (Pearson, Harlow, 2014).
- [41] U.-J. Wiese, *Annalen der Physik* **525**, 777 (2013).
- [42] F. Schwabl, *Quantenmechanik (QM I)* (Springer-Verlag, Berlin, 2007).
- [43] D. Banerjee, M. Dalmonte, M. Müller, E. Rico, P. Stebler, U.-J. Wiese, and P. Zoller, *Physical Review Letters* **109**, 175302 (2012).
- [44] M. Lewenstein, A. Sanpera, and V. Ahufinger, *Ultracold Atoms in Optical Lattices: Simulating Quantum Many-Body Systems* (OUP, Oxford, 2012).
- [45] Y. Kawaguchi and M. Ueda, *Physics Reports* **520**, 253 (2012).
- [46] S. Fölling, *Probing Strongly Correlated States of Ultracold Atoms in Optical Lattices*, *Ph.D. thesis*, Johannes Gutenberg-Universität Mainz (2008).

- [47] W. Müssel, *Scalable Spin Squeezing for Quantum-Enhanced Magnetometry with Bose-Einstein Condensates*, [Ph.D. thesis](#), Ruprecht-Karls-Universität Heidelberg (2014).
- [48] A. Auerbach, *Interacting Electrons and Quantum Magnetism* (Springer Science & Business Media, New York, 2012).
- [49] V. Kasper, F. Hebenstreit, M. Oberthaler, and J. Berges, (2015), [arXiv:1506.01238](#).
- [50] J. Berges, D. Gelfand, and J. Pruschke, [Physical Review Letters](#) **107**, 061301 (2011).
- [51] J. Berges, D. Gelfand, and D. Sexty, [Phys. Rev. D](#) **89**, 025001 (2014).
- [52] A. H. Mueller and D. T. Son, [Physics Letters B](#) **582**, 279 (2004).
- [53] S. Jeon, [Phys. Rev. C](#) **72**, 014907 (2005).
- [54] V. Mathieu, A. H. Mueller, and D. N. Triantafyllopoulos, [European Physical Journal C](#) **74**, 2873 (2014).
- [55] J. Berges, K. Boguslavski, S. Schlichting, and R. Venugopalan, [Phys. Rev. D](#) **89**, 074011 (2014).
- [56] J. Berges, K. Boguslavski, S. Schlichting, and R. Venugopalan, [Phys. Rev. D](#) **89**, 114007 (2014).
- [57] M. C. Abraao York, A. Kurkela, E. Lu, and G. D. Moore, [Phys. Rev. D](#) **89**, 074036 (2014).
- [58] F. Hebenstreit, J. Berges, and D. Gelfand, [Phys. Rev. D](#) **87**, 105006 (2013).
- [59] J. Schwinger, [Journal of Mathematical Physics](#) **2**, 407 (1961).
- [60] L. Keldysh, [Sov. Phys. JETP](#) **20**, 1018 (1965).
- [61] J. Ambjørn, T. Askgaard, H. Porter, and M. E. Shaposhnikov, [Nuclear Physics B](#) **353**, 346 (1991).

- [62] J. Berges, S. Scheffler, and D. Sexty, *Phys. Rev. D* **77**, 034504 (2008).
- [63] J. Berges, in *American Institute of Physics Conference Series*, American Institute of Physics Conference Series, Vol. 739, edited by M. E. Bracco, M. Chiapparini, E. Ferreira, and T. Kodama (2004) pp. 3–62.
- [64] H. Kawai, R. Nakayama, and K. Seo, *Nuclear Physics B* **189**, 40 (1981).
- [65] P. Danielewicz, *Annals of Physics* **152**, 305 (1984).
- [66] R. L. Kobes, G. W. Semenoff, and N. Weiss, *Zeitschrift für Physik C Particles and Fields* **29**, 371 (1985).
- [67] F. Cooper, S. Habib, Y. Kluger, E. Mottola, J. P. Paz, and P. R. Anderson, *Phys. Rev. D* **50**, 2848 (1994).
- [68] W. H. Furry, *Physical Review* **51**, 125 (1937).
- [69] J. Berges, K. Boguslavski, S. Schlichting, and R. Venugopalan, *Journal of High Energy Physics* **5**, 54 (2014).
- [70] N. Tanji, (2015), [arXiv:1506.08442](https://arxiv.org/abs/1506.08442) .
- [71] H. B. Nielsen and M. Ninomiya, *Physics Letters B* **105**, 219 (1981).
- [72] K. G. Wilson, *Phys. Rev. D* **10**, 2445 (1974).
- [73] J. Kogut and L. Susskind, *Phys. Rev. D* **11**, 395 (1975).
- [74] D. B. Kaplan, *Physics Letters B* **288**, 342 (1992).
- [75] R. Frezzotti, P. A. Grassi, S. Sint, and P. Weisz, (2001), [hep-lat/0101001](https://arxiv.org/abs/hep-lat/0101001) .
- [76] Z.-G. Mou, P. M. Saffin, and A. Tranberg, *Journal of High Energy Physics* **11**, 97 (2013).
- [77] F. Hebenstreit, J. Berges, and D. Gelfand, *Phys. Rev. D* **87**, 105006 (2013).
- [78] F. Cooper, S. Habib, Y. Kluger, and E. Mottola, *Phys. Rev. D* **55**, 6471 (1997).

- [79] G. Leibbrandt, [Reviews of Modern Physics](#) **59**, 1067 (1987).
- [80] W. Heisenberg and H. Euler, [Zeitschrift für Physik](#) **98**, 714 (1936).
- [81] J. Schwinger, [Physical Review](#) **82**, 664 (1951).
- [82] Y. Kluger, J. M. Eisenberg, B. Svetitsky, F. Cooper, and E. Mottola, [Phys. Rev. D](#) **45**, 4659 (1992).
- [83] J. C. R. Bloch, V. A. Mizerny, A. V. Prozorkevich, C. D. Roberts, S. M. Schmidt, S. A. Smolyansky, and D. V. Vinnik, [Phys. Rev. D](#) **60**, 116011 (1999).
- [84] N. Szpak and R. Schützhold, [New J. Phys](#) **14**, 035001 (2012).
- [85] B. Buyens, J. Haegeman, K. Van Acoleyen, H. Verschelde, and F. Verstraete, [Physical Review Letters](#) **113**, 091601 (2014).
- [86] M. Banuls, K. Cichy, J. Cirac, and K. Jansen, [Journal of High Energy Physics](#) **2013**, 158 (2013).
- [87] T. Pichler, M. Dalmonte, E. Rico, P. Zoller, and S. Montangero, (2015), [arXiv:1505.04440](#) .
- [88] F. Hebenstreit and J. Berges, [Phys. Rev. D](#) **90**, 045034 (2014).
- [89] F. Hebenstreit, J. Berges, and D. Gelfand, [Physical Review Letters](#) **111**, 201601 (2013).
- [90] Y. Kluger, J. M. Eisenberg, B. Svetitsky, F. Cooper, and E. Mottola, [Phys. Rev. D](#) **45**, 4659 (1992).
- [91] W. Bock, H. G. Evertz, K. Jansen, J. Jersák, K. Kanaya, H. A. Kastrup, D. P. Landau, T. Neuhaus, and J. L. Xu, [Zeitschrift für Physik C Particles and Fields](#) **45**, 597 (1990).
- [92] F. Knechtli and R. Sommer, [Physics Letters B](#) **440**, 345 (1998).
- [93] O. Philipsen and H. Wittig, [Physical Review Letters](#) **81**, 4056 (1998).
- [94] M. Pepe and U.-J. Wiese, [Physical Review Letters](#) **102**, 191601 (2009).

- [95] C.-Y. Wong, R. C. Wang, and C. C. Shih, [Phys. Rev. D **44**, 257 \(1991\)](#).
- [96] S. Iso and H. Murayama, [Progress of Theoretical Physics **84**, 142 \(1990\)](#).
- [97] J. Zinn-Justin, [Quantum Field Theory and Critical Phenomena](#) (Clarendon Press, Oxford, 1996).
- [98] V. Gritsev, A. Polkovnikov, and E. Demler, [Phys. Rev. B **75**, 174511 \(2007\)](#).
- [99] N. K. Whitlock and I. Bouchoule, [Phys. Rev. A **68**, 053609 \(2003\)](#).
- [100] T. Schweigler, V. Kasper, S. Erne, B. Rauer, T. Langen, T. Gasenzer, J. Berges, and J. Schmiedmayer, (2015), [arXiv:1505.03126](#) .
- [101] E. Zohar, J. I. Cirac, and B. Reznik, (2015), [arXiv:1503.02312](#) .
- [102] K. A. Olive *et al.* (Particle Data Group), [Chin. Phys. **C38**, 090001 \(2014\)](#).
- [103] E. Zohar, J. I. Cirac, and B. Reznik, [Physical Review Letters **110**, 125304 \(2013\)](#).
- [104] A. V. Gorshkov, M. Hermele, V. Gurarie, C. Xu, P. S. Julienne, J. Ye, P. Zoller, E. Demler, M. D. Lukin, and A. M. Rey, [Nature Physics **6**, 289 \(2010\)](#).
- [105] H. P. Büchler, M. Hermele, S. D. Huber, M. P. Fisher, and P. Zoller, [Physical Review Letters **95**, 040402 \(2005\)](#).
- [106] L. Susskind, [Phys. Rev. D **16**, 3031 \(1977\)](#).
- [107] A. Celi, P. Massignan, J. Ruseckas, N. Goldman, I. B. Spielman, G. Juzeliunas, and M. Lewenstein, [Physical Review Letters **112**, 043001 \(2014\)](#).
- [108] M. Mancini, G. Pagano, G. Cappellini, L. Livi, M. Rider, J. Catani, C. Sias, P. Zoller, M. Inguscio, M. Dalmonte, and L. Fallani, [Science **349**, 1510 \(2015\)](#).

-
- [109] A. Bazavov, Y. Meurice, S.-W. Tsai, J. Unmuth-Yockey, and J. Zhang, [Phys. Rev. D **92**, 076003 \(2015\)](#).
- [110] K. Fukushima, D. E. Kharzeev, and H. J. Warringa, [Phys. Rev. D **78**, 074033 \(2008\)](#).
- [111] D. Foerster, H. B. Nielsen, and M. Ninomiya, [Physics Letters B **94**, 135 \(1980\)](#).
- [112] G. 't Hooft, [Nuclear Physics B **72**, 461 \(1974\)](#).
- [113] A. Kitaev, [Annals of Physics **321**, 2 \(2006\)](#).
- [114] F. Hebenstreit, R. Alkofer, and H. Gies, [Phys. Rev. D **82**, 105026 \(2010\)](#).

Acknowledgements

Mein ganz besonderer, ausdrücklicher und herzlicher Dank gilt Prof. Jürgen Berges, unter dessen Betreuung diese Arbeit entstanden ist. Des Weiteren bedanke ich mich sehr bei Priv.-Doz. Dr. Jörg Evers für das Übernehmen des Zweitgutachtens.

Für sehr wertvolle Diskussionen und die Zusammenarbeit möchte ich mich besonders bei Prof. Thomas Gasenzer, Prof. Fred Jendrzejewski, Prof. Markus Oberthaler, Prof. Jörg Schmiedmayer, Dr. Tim Langen, Sebastian Erne, Bernhard Rauer und Thomas Schweigler bedanken.

Eine Sonderstellung nimmt Dr. Florian Hebenstreit ein. Danke!

Folgenden Physikern möchte ich sehr für die mir vermittelten Einsichten und ihre Unterstützung danken: Prof. Ehud Altman, Prof. Eugene Demler, Prof. Selim Jochim, Prof. Christoph Keitel, Prof. Maciej Lewenstein, Prof. Jan Pawlowski, Prof. Anatoli Polkovnikov, Prof. Christof Wetterich, Prof. Uwe-Jens Wiese, Prof. Peter Zoller, Dr. Marcello Dalmondo und Dr. Antonino Di Piazza .

Ich habe sehr viel von den folgenden Postdocs und Wissenschaftlern gelernt und danke Ihnen sehr herzlich an dieser Stelle: Dr. Michael Buchhold, Dr. Daniil Gelfand, Dr. Fabian Grusdt, Dr. Pjotrs Grisins, Dr. Philipp Hauke, Marton Kanász-Nagy, Dr. David Mestehazy, Dr. Letícia F. Palhares, Dr. Yulia Schandilova, Dr. Sören Schlichting, Dr. Richard Schmidt, Dr. Dénes Sexty.

Meiner Arbeitsgruppe und folgenden Physikern gilt ein überaus freudiger Dank: Kirill Boguslavski, Shainen Davidson, Andreas Elben, Anna Frishman, Markus Karl, Niklas Müller, Asier Piñeiro Orioli, Dr. Alexander Rothkopf, Jan Stockemer, Dr. Naoto Tanji und Benjamin Wallisch.